Title:

Consequences of Extreme Precipitation for the Deterioration of Road Constructions

(Danish): Konsekvenser af Ekstremregnhændelser for Vejkonstruktioners Nedbrydningsforløb.

Theme:

Master Thesis 4th semester. Transportation Engineering.

Project period

February 2013 - June 2013

Produced by:

René Brodersen

Thesis supervisor

Benjamin Nordahl Nielsen

Circulation: 4

Pages: 88

Appendix pages: 49

Handed in: June 6th. 2013

René Brodersen

Preface

This Master's Thesis "Consequences of Extreme Precipitation for the Deterioration of Road Constructions" accounts for 30 ECTS and was carried out from february - june 2013 at the Department of Civil Engineering Aalborg University under the study of Transportation Engineering.

Through the last decade, events of heavy precipitation are observed beyond what have been usual. When estimating residual life of road constructions a modelling approach, considering environmental factors affecting the design life, is used. This modelling approach does not consider the future effects of heavy precipitation. Episodes of heavy rainfall may result in a flooding of some low-lying roads since it will be impossible to ensure proper draining during these events. When a road is flooded by a heavy rainfall the strength of the unbound layers will be affected by the presence of water and hence influence the residual life of the construction. Expectations for the future indicate that the rate of these heavy rainfall events, can be expected to increase and thereby causing an accelerated deterioration of the road constructions, which will result in a considerable socio-economic loss.

The project was inspired by The Danish Road Directorate who are currently having a major focus on the consequences of road construction deterioration when roads are inundated by water when events of heavy precipitation occurs.

This project aims at investigating how the road construction's structurel performance is affected by these heavy rainfalls and considers the effects in a long-term perspective. This will allow taking effects into the long-term consideration when road constructions residual lifes are modelled, and their deterioration processes are estimated.

Reading Guide
This thesis consists of two main parts. The first part consists of two articles; the first article is a litterature review dealing with how the events of extreme precipitation are expected to affect a road construction and the second article presents a field study performed in order to investigate the effect of having a watertable within a road construction.

The second part contains appendices which should be seen as addendum to the articles. Appendices *A* - *D* have their reference to the litterature review in article 1, and appendices *E* - *K* have their reference to the field study presented in article 2.

References are treated using the Harvard Method. These are marked with brackets; *(Author Year)*. Additional information is available at the end of each article. For the second part a complete list of references, for all appendices, is given at the end.

A CD-ROM, with raw field and laboratory data is attached the thesis and can be found at the back of the report.

Figures and tables not listed with references are produced by the author.

The author would like to thank Susanne Baltzer at The Danish Road Directorate for inspiration of relevant project themes. Further, Poul-Erik Jakobsen at Grontmij deserves a grattitude for always lending a helping hand and displaying interest within the topic chosen. Finally, the author wish to thank supervisor Benjamin Nordahl Nielsen and the staff at the Department of Civil Engineering for help in regard of conducting the field study.

Front page figure:

Heavy rainfall floods main road "Lyngbyvejen" in Copenhagen. August 2010.
Found at: http://www.vandibyer.dk/30115. *Accessed 2013-05-08*.

Summary

This Master Thesis treats the issue of dealing with water in road constructions. The report consists of two articles and a part consisting of appendices.

The first article is a litterature review presenting relevant topics and issues when considering water affecting the unbound layers in road constructions. Initially, the litterature review focuses on how the climate is changing in regard of increased precipitation levels and expectations to the future scenarios. A focus of how the water enters and thereby affects the strength of the construction are considered. Several laboratory and field test results found in the litterature, made in order to understand the effects of water to the strength of the unbound layers, are represented and it is discussed which effects are to be considered, when road constructions are exposed to high amounts of water.

The main focus is on the bearing capacity (E-moduli) of the unbound layers. This is due to its importance when modelling the residual life of the construction. The Mathematical Modelling Of Pavement Performance (MMOPP) approaches the climatic effects when modelling the residual life by considering a reduction in E-values due to temperature changes. No considerations are made with regard to inundation caused by heavy rainfalls.

The second article represents a series of field tests performed at Aalborg University. The test series aims at investigating one cycle of rising/lowering a water table within a road construction at controlled steps allowing to correlate E-values and water table. The water table was determined with a sounding device at positions coincedent with E-values.

It is examined how the E-values are affected and to see if any permanent reduction is observed. The tests were performed on 30 cm of subbase sand and 20 cm of base gravel standard road construction materials on top of a limestone subgrade. E-values were determined by using the non-destructive Prima 100 light weight deflectometer. Test field was constructed with drainage pipes allowing inlet/outlet of water to be determined at controlled steps.

The reduction in E-values of the unbound layers will affect the maximum allowable stresses, according to the dansih guideline for designing road constructions leading to an accelerated deterioration if precautions are not made. One way of compensating for bearing capacity reduction, due to a water table inside the unbound layers, could be to increase the thickness of the upper layer reducing the stresses on the lower unbound layer affected by water.

Main results of the field tests series:

- E-values of unbound layers reduces linearly to ≈60% of its origin due to complete saturation when the water table reaches the surface level.
- The same linear trend was observed for both the reducing and the recovering of E-values when construction was later drained.
- A bearing capacity 'loss' of approximately 5-10% was observed when water table was lowered and hence raised for one cycle.

On the basis of the results it is suggested that:

- Future events of extreme precipitation should be considered when designing and maintaining road constructions.
- This could be implemented by increasing the upper layer's thickness on road locations vulnerable to inundation.
- Setting up some simple modelling of water tables for standard cross sections estimating the water table inside the construction at any given time during an extreme event, could be used to estimate the time span of bearing capacity loss and thereby determine the time horizon for road closure or narrowing.

Resumé (danish)

Dette kandidatspeciale omhandler problemstillingen vedrørende vand i vejkonstruktioner. Rapporten består af to artikler og en del med appendiks.

Den første artikel er et litteraturstudie der præsenterer relevante emner og problemstillinger vedrørende vand i veje. Indledningsvist fokuseres der, i litteraturstudiet, på hvorledes klimaet ændrer sig, med særlig vægt på øgede nedbørsmængder samt hvilke forventninger der er i forhold til fremtiden. Der præsenteres en teoretisk ramme for hvordan vandet kan trænge ind i konstruktionen og hvilke styrkemæssige effekter dette kan give anledning til. Flere studier, omhandlednde vandets indflydelse på ubundne materialers styrkeegenskaber, er præsenteret og det er diskuteret hvilke effekter, der bør overvejes når vejkonstruktioner udsættes for større mængder vand.

Det primære fokus er på den strukturelle bæreevne (E-modulen) af de ubundne lag. Dette er med henvisning til denne egenskabs relative store betydning for modellering af konstruktionens samlede levetid. Ved brug af modelleringsværktøjet Mathemathical Modelling Of Pavement Performance (MMOPP) (Matematisk Modellerng Af Vejkonstruktioners Ydeevne), kan levetiden betragtes ved, blandt andet, at benytte en model der beskriver E-modulens klimatiske variation med baggrund i temperaturændringer. Ingen model beskriver den strukturelle nedbrydning som konsekvens af oversvømmelse der opstår på baggrund af en ekstremregnhændelse.

Den anden artikel præsenter et feltforsøg udført ved Aalborg Universitet. Formålet med dette studie var, at undersøge en cyklus af et ændret vandspejl i en vejkonstruktion. Vandspejlet blev ændret i kontrollerede intervaller, hvilket muliggjorde, at sammenholde E-værdier og vandspejl. Pejlerør blev brugt til at bestemme vandspejlet og var placeret i samme punkter som målingerne for E-værdier.

Det er undersøgt i hvilket omfang E-modulen påvirkes og om der eventuelt kan ses en permanent reduktion af E-modulen. Forsøgene blev udført på standard materialer for vejkonstruktioner i Danmark. 30 cm bundsikringslag og 20 cm stabilgrus lag konstrueret oven på en kalkstens underbund. E-værdier er målt ved hjælp af ikke-destruktive deflektionsmålinger udført med Prima 100 minifaldlod. Testfeltet blev konstrueret med drænrør således, at det derved var muligt at hæve/sænke vandspejlet med kontrollerede niveauændringer.

Reduktionen i E-værdier for de ubundne lag vil påvirke de maksimalt tilladelige spændinger på de enkelte lag, som kan beregnes efter den danske vejregel for dimensionering af vejkonstruktioner. Dette vil medføre et accelereret nedbrydningsforløb hvis ikke der foretages de nødvendige foranstaltninger. En måde at kompensere for dette vil være at øge tykkelsen af det øverste asfalt lag og på den måde reducere spændingerne på de ubundne lag.

Hovedresultaterne fra feltforsøget:

- E-værdier af de ubundne lag udviser en lineær reduktion indtil 60% af udgangspunktet når vandspejlet når overfladeniveau.
- Samme lineær tendens kan observeres for både reduction og genvinding af styrke i takt med at vandspejlet i konstruktionen hæves/sænkes.
- Et 'tab' i E-værdi kan observeres efter én cyklus af hæve/sænke vandspejlet på ca 5 - 10 %.

På baggrund af resultaterne fra feltforsøget gives der fremadrettet følgende anbefalinger

- Fremtidige ekstremregnhændelser bør overvejes i forbindelse med design og vedligehold af vejkonstruktioner.
- Dette kan opnås ved at forøge tykkelsen af det øverste (typisk asfalt lag) på vejsektioner som måtte være særlig udsat for oversvømmelser.
- Ved at opstille simple modeller for vandspejlet for standard tværprofiler udsat for oversvømmelse, vil det være muligt at estimere vandspejlet til enhver tid i løbet af en ekstremregnhændelse. Dette kan således bruges til at vurdere den tidsmæssige udstrækning hvormed bæreevnen kan forventes reduceret og dermed angive perioden for en evt. vejlukning eller indsnævring af kørebanen.

Table of Contents

Part One - Articles

Aalborg University
School of Engineering and Science
Transportation Engineering

Article 1 - Consequences of Extreme Precipitation for the Deterioration of Road Constructions - litterature review

René Brodersen

June 2013

Scientific Publications at the Department of Civil Engineering

Technical Reports are published for timely dissemination of research results and scientific work carried out at the Department of Civil Engineering (DCE) at Aalborg University. This medium allows publication of more detailed explanations and results than typically allowed in scientific journals.

Technical Memoranda are produced to enable the preliminary dissemination of scientific work by the personnel of the DCE where such release is deemed to be appropriate. Documents of this kind may be incomplete or temporary versions of papers—or part of continuing work. This should be kept in mind when references are given to publications of this kind.

Contract Reports are produced to report scientific work carried out under contract. Publications of this kind contain confidential matter and are reserved for the sponsors and the DCE. Therefore, Contract Reports are generally not available for public circulation.

Lecture Notes contain material produced by the lecturers at the DCE for educational purposes. This may be scientific notes, lecture books, example problems or manuals for laboratory work, or computer programs developed at the DCE.Theses are monograms or collections of papers published to report the scientific work carried out at the DCE to obtain a degree as either PhD or Doctor of Technology. The thesis is publicly available after the defence of the degree.

Latest News is published to enable rapid communication of information about scientific work carried out at the DCE. This includes the status of research projects, developments in the laboratories, information about collaborative work and recent research results.

Published 2013 by
Aalborg University ©
Department of Civil Engineering
Sohngaardsholmsvej 57,
DK-9000 Aalborg, Denmark

Printed in Aalborg at Aalborg University

Consequences of Extreme Precipitation for the Deterioration of Road Constructions

-litterature review

Brodersen R.[i]

June 2013.

Abstract: This litterature review was made in order to investigate how the climatic changes, in terms of higher precipitation levels will affect the unbound layers of road constructions, and hence the design life of the entire construction. Initially, it is examined how the climate is changing in Denmark. Higher levels of annual precipitation as well as an increased frequency of extreme precipitation events can be expected. This means, that more water will need to be drained from the road network. Since the design of drainage constructions allow occasionally innundation, more water is expected to infiltrate the road constructions in the future. It is a well known fact, that water affects the strength of unbound materials and should hence be considered when making life-cycle analysis of road constructions determining the residual life for a specific site. When designing by means of simulation in regard of the Mathematical Modelling Of Pavement Performance (MMOPP) futuristic scenarios, due to increased events of extreme precipitation, is not considered. Experience is needed on how the water will affect the bearing capacity and thereby the accelerated deterioration of future road constructions.

Keywords: Extreme precipitation, Climatic Changes, Water in Road Constructions, Bearing Capacity, MMOPP, Pavment Management System.

[i]Graduate Student. Department of Planning and Development. School of Engineering and Science. Aalborg University.

Introduction

According to Intergovernmental Panel on Climate Change (IPCC) the world climate is changing. The increase of greenhouse gas emissions will give rise to different environmental changes during the next 100 years. These changes will include higher temperatures, increased amount of precipitation, the sea-water level will rise as a result of ice melting at the poles and the wind gust forces will increase (Nakicenovic et al. 2000).

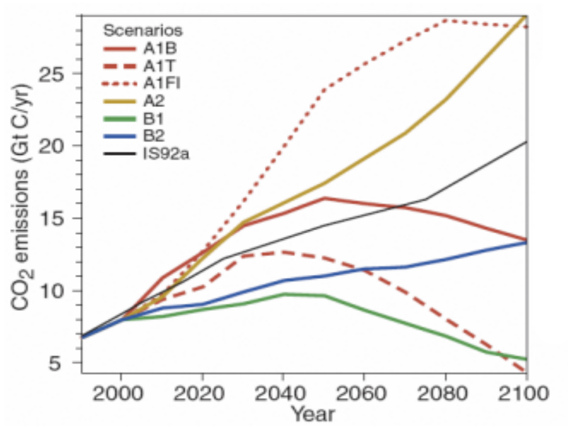

Figure 1: CO2 - emissions due to different scenarios according to IPCC. (Jørgensen 2008).

Since the climatic changes depend on human behaviour, the climatic models have been compiled with different scenarios describing human behaviour. Figure 1 illustrates CO_2 emissions due to the different scenarios.

Precipitation in DK

In Denmark the climatic changes will result in higher air temperature which are able to contain more water. Precipitation will thus increase in the winther and decrease during the summer. The intensity, though, of future rainfall are predicted markedly higher than present for the summer period (GEUS 2010). Generally, the precipitation has increased in all of Denmark. Figure 2 shows the development of precipitation in Denmark from 1874 - 2009.

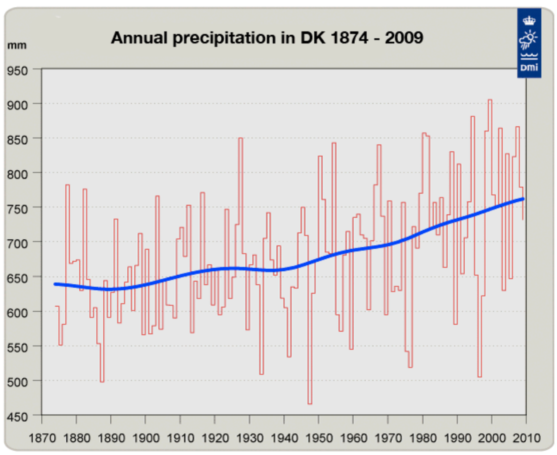

Figure 2: Annual precipitation in Denmark (1874 - 2009) (Cappelen, Scharling 2010).

Since 1990, the average annual precipitation has been 750 mm which is about 100 mm more when measurements were started back in 1874. What could also be noticed is that the deviation has increased as well (Cappelen, Scharling 2010).

Extreme Precipitation

Episodes of extreme precipitations are likewise expected to show an increase. Measurements for the last 50 years has shown that the area in wich extreme precipitation has occured, is increased by 2%. This is illustrated in Figure 3. No climatological explanation can be found in regard of when a rainfall can be characterized as an extreme event. The Danish Meteorological Institute (DMI) has defined extreme precipitation as more than 60 mm rain within an hour. The limit is chosen, since it has not happened to often (Cappelen, Scharling 2010).

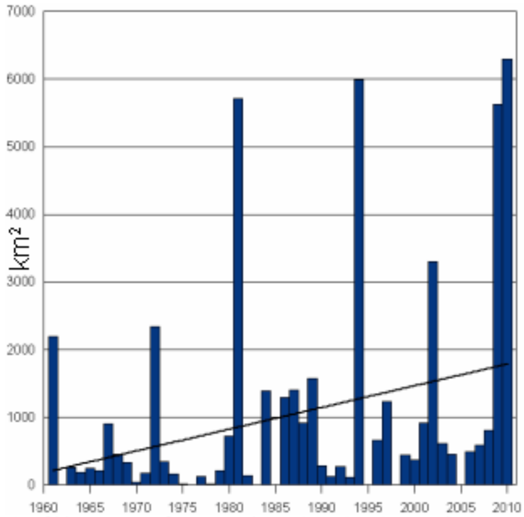

Figure 3: Area in DK, where precipitation has been at least 60 mm within 24 hours. (1961 - 2010). (Cappelen, Scharling 2010).

An examination of the trend i extreme precipitation in Denmark was carried out in order to evaluate the following variables: (Arnbjerg-Nielsen 2003).

- 10 min. intensity
- 360 min. intensity
- Total volume of event

Based on a 22 year observation period, 41 series of precipitation levels on the basis of the danish Wastewater Committee rain gauges were evaluated. The study found a significant trend in the 10 min. intensity towards more intense and more frequently precipitation, even though a substantial number of series showed the opposite trend. The trend was more severe for Sealand than for Jutland. For the 360 min intensity precipitation and total volume variable no significant trend was observed.

Calculations on the basis of a co-ordination of DMI's climatic model (estimated on the basis of the IPCC-report/predictions A2 and B2, see Figure 1) with GEUS' hydrological model have shown that the climatic changes will have significant impact on the water balance in Denmark. The average anual precipitation is dependent on location, and will increase as much as 22 - 27% for Vestjutland and Sealand, respectively, for the B2 scenario. The increase is expected to be 13-14% for the A2 scenario. Increased precipitation affects the formation of groundwater, which will increase as well. For Vestjutland the increase will be significant up to 0.25 m above present for 50% of the area and up to 1 m for 10% of the area.

The effects of climatic changes in Sealand will primarily consists of an increased watercourse-runoff due to the mere clayey subsoil. More precipitation will thus slightly affect the ground-water formation.

Risks of inundations will likewise increase due to the frequent occurence of extreme precipitation. (Sonnenborg et al. 2006).

Considering these changes when designing drainage constructions a regional climatic model HIRHAM4 has been used for predicting the development of extreme precipitation in the future for DK. The simulations were based on scenario A2, according to IPCC. This has led to the implemantation of a climatic factor ($k_{T,d,\Delta t}$), which describes the relationship between the expected precipitation for the future and the current precipitation level, see Eq. 1.

$$k_{T,d,\Delta t} = \frac{i_{T,d,t+\Delta t}}{i_{T,d,t}} \qquad \textbf{\textit{Eq. 1}}$$

where,

i: is the intensity of precipitation used for current design.

t: is present time

Δt: is time period of scenario uncertainty

The correction is thus dependent upon period of repitition, duration of precipitation and the time horizon. Correction to provide for climatic changes increases with increasing period of repitition and decreases with the duration of the precipitation event. Period of repitition is most significant. Based on this period the following factors can be used according to (Arnbjerg-Nielsen 2008).

Table 1: Proposals for factor taking into account the climatic changes produced by (Arnbjerg-Nielsen 2008).

Period of repitition	2 yr.	10 yr.	100 yr.
Climatic factor	1.2	1.3	1.4

For the future scenario an upward adjustment should be applied in regard of intensity in precipitation. The reason for this is that the events of extreme precipitation occurs more frequently and that they on average has become more intense. Futher, an increase in the amount (volumes) of precipitation has increased for the events of high intensity, that occurs with a frequency less than every 10th year. The increase is additionally more significant for duration of precipitation between 60 min. and 3 hours. Which is the durations particularly crucial to innundation in urban areas. (Arnbjerg-Nielsen, Madsen & Mikkelsen 2006).

Water in Road Constructions

The design principle of a typical standard road construction in Denmark is illustrated in Figure 4.

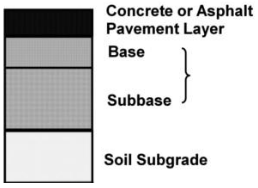

Figure 4: Typical layered cnstruction consists of base and subbase layer on top of a subgrade.

It consists, beside the top asphalt or concrete layer, of a base and a subbase layer on top of a soil subgrade. For this article, this construction principle will serve as point of reference.

Water infiltrating the road construction may come from different sources, the main sources are listed below (Dawson 2008):

1. Surface water
2. Hinterland water
3. Remote water

The surface water refers to the runoff from the top of the pavement and is determined by the amount of precipitation. Hinterland water arises from the surrounding environment, (eg. slope, when pavement is designed in cut) and are also affected by amount of precipitation. The remote water can be recharged far away from the road and may have impact on the construction, (eg. groundwater flow across the road).

Water balance.

The relationship between water and the road construction is achieved by setting up a water balance of the system. The system is shown in Figure 6.

The generel water balance equation of the system can be expressed as shown in Eq. 2 and Eq. 3.

$$P = R - ETR + IR \qquad \textit{Eq. 2}$$

or

$$P = R - ETR + G + \Delta S \qquad \textit{Eq. 3}$$

Where, P is the precipitation, R is the surface runoff, ETR represents the evapotranspiration, IR is the infiltration from the surface and equals G+ΔS, which describes the deep percolation or groundwater recharge plus the water storage change ($\Delta S = q_{out} - q_{in}$). In the case of some external inflow (eg. hinterland or remote waters) The equation is changed to Eq. 4.

$$P + q_{ext} = R - ETR + G + \Delta S \qquad \textit{Eq. 4}$$

which includes this external inflow (q_{ext}).

Water movement in road constructions

As described by (Lay 2009) the water movement within a pavement can be considered as consisting of three phases:

1. Entry phase
2. A redistribution phase
3. An evaporative phase

The entry phase describes the relatively rapid phase when the water enters the road construction. This is possible through severel entries as illustrated in Figure 5. Problems of water entering the road construction in an inappropriate way can be observed due to different types of maintainance related problems as discussed by (NCC 2001, Berntsen, Saarenketo 2005), which include problems relating to melting snow and poorly working drainage constructions, but also potholes and pavement cracking will influence ingression in the entry phase. It is not only the surface water that will affect the construction, but attention should also be made towards seepage from higher ground or the upward movement of the ground-water table. The latter is a recent issue in Denmark. Increased precipitation and rise of sea-water level entails higher water levels in the watercourses. The gradient of the watercourses is hence significantly affected by a sea-water level rise. When the water is prevented from entering the sea-water, it will find its way to the underground contributing to a higher ground-water level. When the climatic changes entails more frequent and heavier precipitation combined with the relatively flat topographi in DK it will result in a markedly increase in groundwater level. (Kristiansen 2009, Kristiansen 2010).

The redistribution phase describes the water movement within the construction. This could either be due to soil suction or gravity. For the case

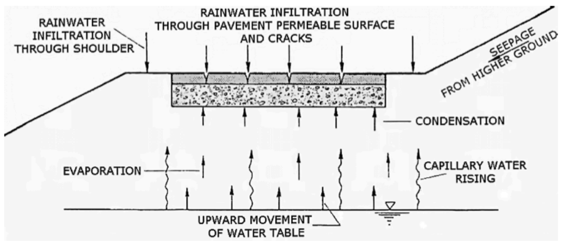

Figure 5: Possible water movements into the pavement zone. (Lay 2009).

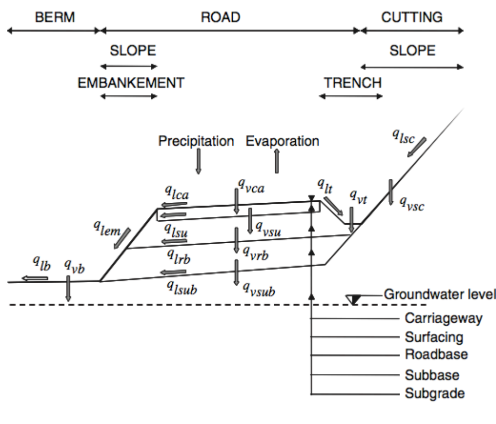

Figure 6: Conceptual model of water balance on pavement - embankment. v=vertical, l=lateral, ca=carriageway, su=surfacing, rb=roadbase, sub=sub-base, sc=slope/cutting, t=trench, This water balance depends on the roads geometry and to the fact that the roads tracé is interacting with multiple different surroundings. This makes is complex to set up a generel waterbalance model for a specific road, but must be divided into smaller sections. em=embankment, b=berm. (Dawson 2008).

where the surface layer consists of a asphalt or concrete layer, it can be considered as impermable. The other layers, though, consisting of sand or gravel, are permable layers in which flow of fluid can take place. The water flow (Q) can be described using Darcy's Law (Eq. 5).

$$Q = k \cdot A \cdot \frac{dh}{dl} \qquad \textit{Eq. 5}$$

where, k is the hydraulic conductivity, A is the cross-sectional area of the specimen and dh/dl is the hydraulic gradient describing the head loss in the direction of flow. The hydraulic conductivity depends on the viscosity of the media flowing through the soil. Eq. 6 shows the relationship between the hydraulic conductivity (k) and permability (K).

$$k = K\frac{\gamma_W}{\eta} \qquad \textit{Eq. 6}$$

where, γ_W and η is the specific gravity and dynamic viscosity of the water. The permability is affected by the porosity (n) of the material which could be expressed in terms of the pore number (e) according to Eq. 7.

$$n = \frac{e}{1+e} \qquad \textit{Eq. 7}$$

The porosity describes the total amount for a given volume that can be filled with water. The pore number depends on factors such as grain size distribution, size segregation and density. The particle grading affects the materials permability the most. The segregation of particle will increase permability. Increasing densitiy will result in lower permability (Ovesen, Fuglsang & Bagge 2009).

The latter evaporative phase is when the water, as vapour, leaves or moves to another layer. Water vapour can occur when temperature gradient is inside the construction and the water moves from a warm to a cool place where it will condense.

The water movement within a road construction will not only rely on the materials of the specific site but also the level and intensity of precipitation. Hence, an extreme event is therefore not necessarily the worst event since the permability will control the rate of redistribution. The event of a heavy rainfall within an hour may not be as crucial as a long event of low intensity, since the amount of water accumulated within the construction may be higher under the latter conditions. (Yoder, Witczak 1975).

Water content variations in pavements

Figure 7 shows an overview of water content in a road construction connected to rainfall on a specific location. It illustrates that water levels in the different layers, in the road construction is completely coincident with time of rainfall. The water level in the subgrade is lower in periods without rain than in the Unbound Granular Material (UGM) but enhances to a level above the UGM when rainfall occurs. Furthermore, it shows that water level is highest near the edge than near pavement centerline (Dawson 2008).

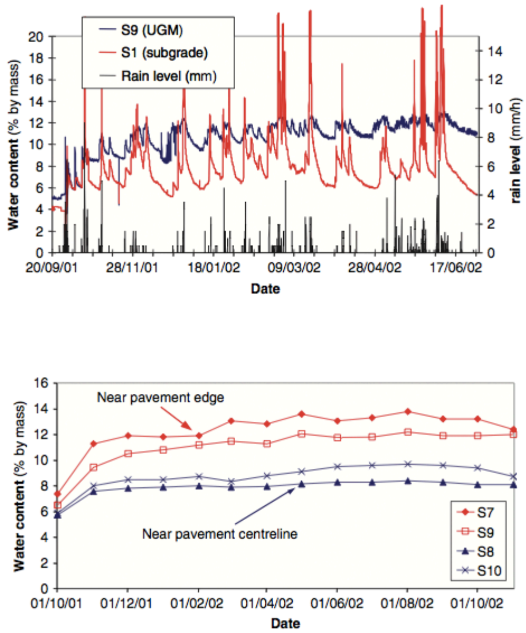

Figure 7: Observed water content in a road construction connected to rainfall. From (Dawson 2008).

Drainage

Drainage systems are designed to fulfill the water balance with respect to the surface water and, to some extend, the hinterland and remote waters. Drainage can be conducted in different ways.

Drainage systems are allowed to extend its limits for some period of repitition. An extreme event, where surface and hinterland waters are no longer able to find its way by the drainage systems carriageway could lead to inundation of the road with a considerable economic loss.

Base and subbase drainage

The danish procurement regulation for designing drainage constructions for roads placed in open land sets up the following design principles for the cross section of the construction (Vejregelrådet 2009).

The bottom of the berm should be located 0.1 - 0.2 m below shoulder edge (see Figure 8) The berm construction has a width of approximately 2 - 3 m. The drainage is normally placed 0.5 m below planum. The ditch is typically 0.5 m deep relative to the surroundings.

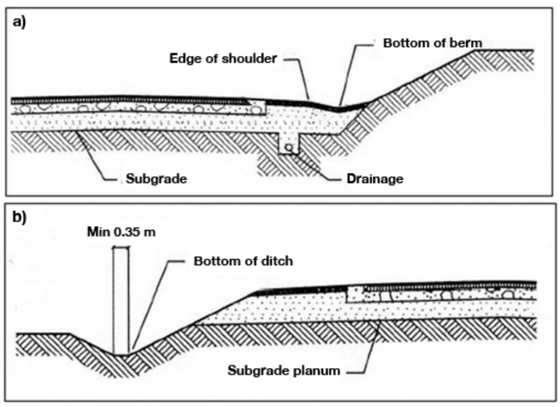

Figure 8: Design principles of drainage systems for roads in open land a) Road in cut with berm b) Road in fill with ditch. Source: (Vejregelrådet 2009) (Own translation editing).

The width of the ditch is normally 0.35 m and if the ditch is used for drainage of the subgrade it should be placed at least 0.3 m below planum (Vejregelrådet 2009).

This means that the water infiltrated in the construction (the unbound layers) must travel through the layers in order to reach the draniage system or the ditch construction. In the case of a berm, water contained in the berm storage will slowly find its way to the drainage depending on the permability and size of the infiltrated material.

This could hence be a problem if drainage systems are allowed to exceed its limits even at a low regularity. Unbound layers can thus be expected to be infiltrated with water at a higher level and intensity than at present.

Bearing capacity

The structural and long term performance of the road is based on its bearing capacity (e.g. E-moduli) and are related to the mechanical behaviour of the material.

When a moving wheel passes on the surface every soil element in the construction are affected by the stress regime shown in Figure 9.

Every element in the layers is subjected to vertical- , horisontal- and shear stresses. Since the vertical and horisontal stresses are positive and that the shear stresses are reversed the axes of principal stresses will rotate, as a wheel passes the surface. This stress regime leads to a deformation of the material, which can be deduced to a result of three mechanisms:

1) Consolidation (dilatation)
2) Distortion
3) Attrition

The first comes from a change in shape and compressibility. Distortion is caused by bending, sliding and rolling of particles and attrition occurs when the particles undergo stresses that exceeds the strenght of the particles thus leading to breakage of the particles (Lekarp, Isaccson 2000).

The deformation of the material caused by the the moving wheel is not fully recoverable but consists of a resilient and a permanent part as illustrated in Figure 10.

These deformation characteristics will be highly affected by the presence of water.

Water and resilient response

Adding water to a soil specimen could affect the resilient response in two ways depending on the specific soil and the amount of water. Partly saturated soils will be likely to show an increase in strength if negative pore pressure occurs and when increasing water content a reduction can be observed.

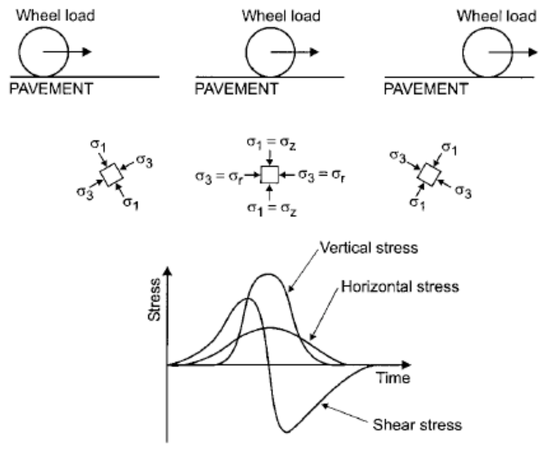

Figure 9: Stress regime in a soil element due to a single wheel load. Source: (Lekarp, Isaccson 2000).

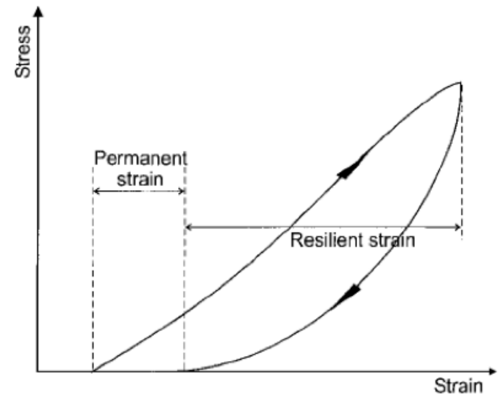

Figure 10: Hysteresis loop outlining the resilient and permanent strain response of unbound materials subjected to loading (Lekarp, Isaccson 2000).

In an early study the resilient response due to degree of saturation was investigated on a crushed and a partially crushed aggregate, used as base course materials in Illinois. The materials were compacted at a relative density ranging from 80-90% and three different levels of saturation (dry, 65-68% saturation, and fully saturated). The results showed a decrease in resilient modulus when saturating the material and increasing confining pressure. The reduction in resilient modulus was dependend upon fines content and the aggregate containing the highest level of fines content showed the largest reduction. The test results were derived on the basis of total stresses, but when derived from effective stresses the resilient modulus only decreased slightly (Hicks 1970).

In another study a large scale cyclic loading triaxial testing facility was used to evaluate different types of coarse grained gravel and rock aggregates and determine which factors affected the materials resilient modulus. When investigating the effect of moisture the effect was also most pronounced for material having the highest fines content (Figure 11). This result was consistent for other well graded materials. For the more poorly-graded materials nearly any effect of moisture could be seen which was believed to be due to the more open structure and that the fine fractions which could be affected by the negative pore pressure were negligible.

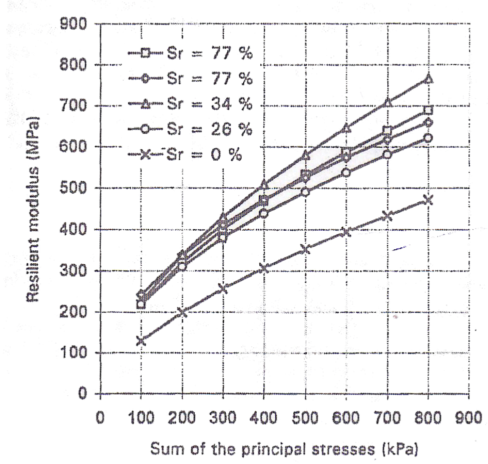

Figure 11: Resilient modulus values of well-graded test material with relatively high fines content at different moisture contents. γ_d *= 2200 kg/m³. (Kolisoja 1994).*

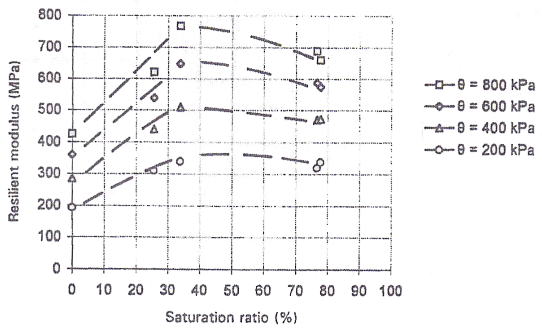

Figure 12: Resilient modulus as function of saturation ratio for well-graded material with relatively high fines content. (Kolisoja 1994).

The material were tested in totally dry and almost completely saturated conditions and for two intermidiate water contents. Material showed the highest value of resilient modulus at saturation level at 34% (Kolisoja 1994) (See Figure 11 and Figure 12).

Figure 13 shows the result for repeated load triaxial tests for a course and a fine-grained soil. Three saturating procedures were used. [i] Evaluating resilient response due to increasing moisture content the following was observed. For the coarse-grained soil (soil 3) a reduction in resilient modulus can be seen of approximately 20% whereas the reduction of resilient modulus for the fine-grained soils (soil 7) were of 50 - 75%. Additionally, a difference in moduli-moisture correlation is influenced by the way the water is imbided into the soil. Using vacuum saturation the most drastic reductions were observed. (Thadkamalla, George 1995).

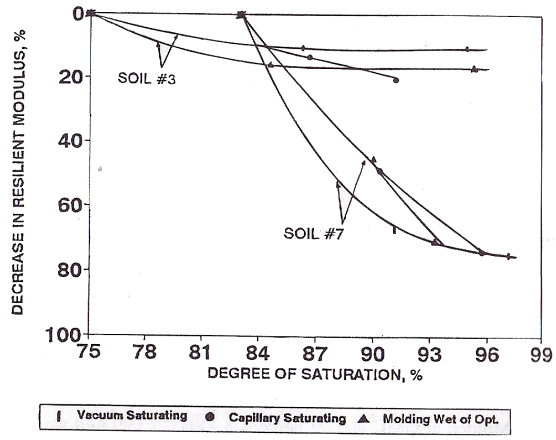

Figure 13: Decrease in resilient modulus due to the degree of saturation for different saturation methods. (Thadkamalla, George 1995)

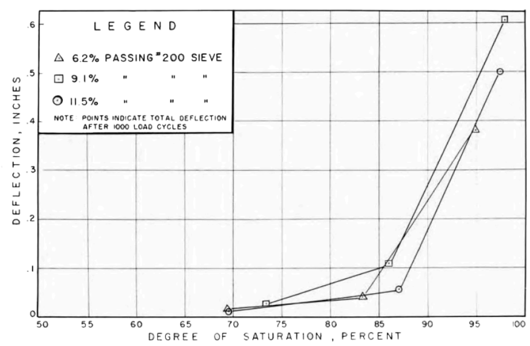

Figure 14: Variation of deflection with saturation level for gravel aterial. From: (Haynes 1961).

The rate at which the degree of saturation becomes critical was also examined with the use of triaxial tests performed on a gravel base material. The rate of the resilient response significantly decreased when saturation increased beyond 85% limit. See Figure 14 (Haynes 1961).

Different base and subbase granular materials from senegal were also tested with the triaxial apparatus: Red quartzite from Bakel (GRB), Basalt from Diac (BAS), and Limestone from Bandia (BAN) (Triax results are only shoved for (GRB) and (BAS). Materials were compacted to 98% of maximum dryunit weight. Each sample were compacted at different moisture contents (W_{opt}, , W_{opt}-2, W_{opt}+1.5), but with the same compaction energy. Results from repeated load triaxial tests are shown in Figure 15. The spread in the data for a constant confining pressure represents the resilient modulus at different deviator stresses. Curve fitting is based upon power dependence on confinement. For the materials GRB and BAS the resilient modulus increased between 10 - 40% when the water content decreases from W_{OPT}+1.5 to W_{OPT} -2.

The results show the importance of moisture content when material is compacted. It was concluded that the effect of water content is more significant in the dry side of the compaction curve than in the wet.

[i] 1) Vacuum: In accordance with AASHTO T 274-82

2) Capillary saturation under 0.914 (3 ft.) of water suction

3) Molding samples at equilibrium or other predetermined moisture.

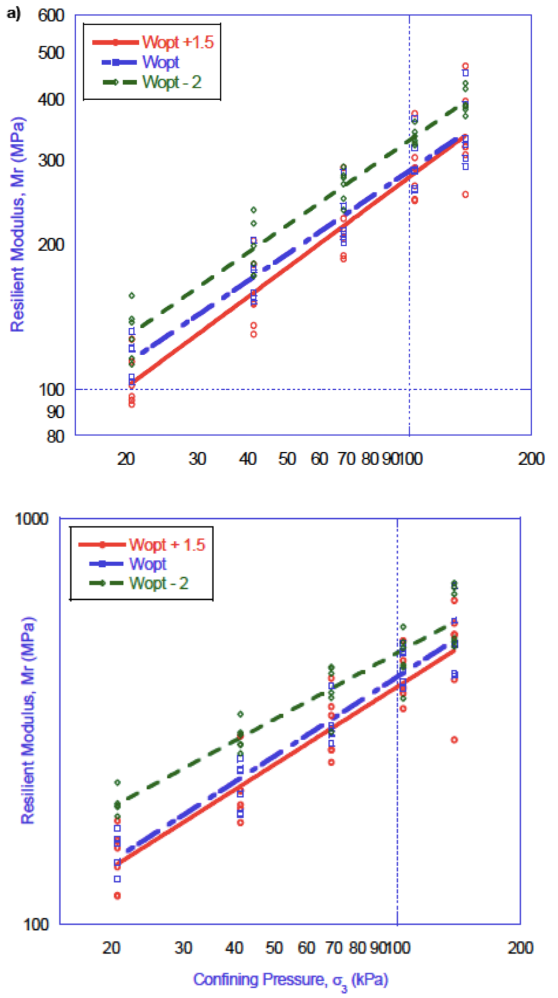

Figure 15: Mr vs. confining pressure tested for different water contents. a) GRB; b) BAS. Source: (Ba et al. 2012).

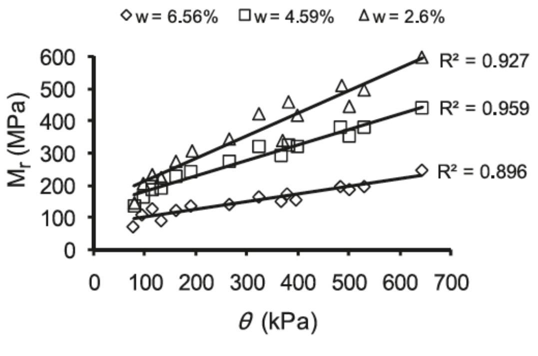

Figure 16: Bulk stress sensitivity of Mr for granular material. OMC=4.61. From: (Stolle, Guo & Liu 2009).

These results were similar to tets series performed on 36 different aggregate types typically used in Ontario. Materials were installed in the resilient modulus test apparatus and fabricated with water content corresponding to $w_{opt.}$, +/- 2%. An example of the bulk stress sensitivity and water content are shown in Figure 16.

OMC was found using the proctor compaction method. A decrease in resilient modulus was thus obtained when increasing moisture content above OMC.

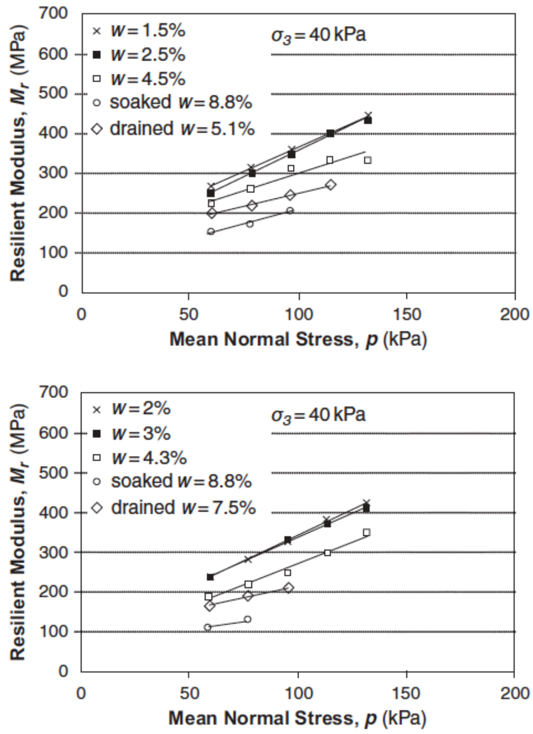

Figure 17: Resilient properties of a coarsed-grained granular material splitted into different gradings (Grading parameter n=0.4 and 0.3 respectively). (Ekblad 2007).

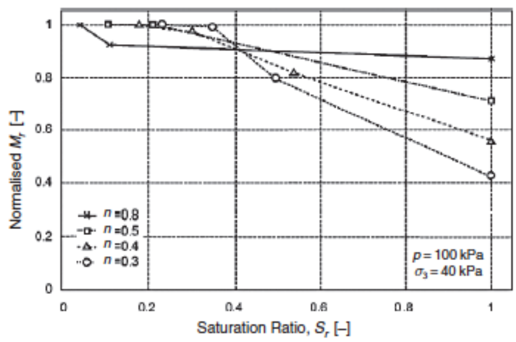

Figure 18: Normalized resilient modulus as a function of degree of saturation. (Ekblad 2007).

It was also stated that coarser grained material was not able to contain moisture at higher levels. The amount of fines content was thereby noted to have significant influence of obtained resilient modulus in regard of capability to a higher level of moisture content.

Difference between resilient modulus and moisture content, was thus very dependent upon gradation curves. The reduction observed in resilient modulus, when subjecting granular materials to repeated load triaxial tests, was more significant for well-graded material with a higher amount of fines content. For the coarser grained materials reduction in resilient modulus was not so distinct and the value regained quickly when drainage were performed (Stolle, Guo & Liu 2009).

Triaxial tests were also performed in another study to examine the influence of water on resilient response. The material used was a coarse unbound granular material with maximum particle size of 90mm. The material was split into different gradings to investigaste the influence of gradation curves. A confining pressure of 40kPa and different mean normal stresses were applied. See Figure 17. The materials saturation level was increased from a low state to a fully saturated (soaked) condition and subsequently allowed to drain freely. Afterwords the resilient response at a mean normal stress of 100kPa and confining pressure of 40kPa was calculated as a function of the degree of saturation as shown in Figure 18. This clearly shows the importance of fines content when considering resilient resoponse at for different saturation levels. For relatively higher fines content (lower grading parameter) a higher reduction in resilient response can be observed. It can thus be stated that the influence of saturation due to resilient response i highly affected by the degree of fines content. Increasing fines content will have a negative effect on the resilient response for same degree of saturation (Ekblad 2007).

Road Testing Machine (RTM)

In a danish study, using the RTM the correlation between bearing capacity and water content were sought on a typical danish pavement construction. The bearing capacity was tasted with the Falling Weight Deflectometer (FWD) and a significant drop in E-moduli due to increased moisture content, for the three layers was observed (Figure 19). The construction was build in a test tank and consisted of a 6 cm asphalt layer on top of a 14 cm granular layer (SG II 0/32) and a 42 cm subbase sand layer on top of a 100 cm subgrade sandy till. Heavy rainfall situations were simulated by spraying water on an open shoulder for entrance. This resulted in positive pore pressure in all the unbound layers. Results showed a significant decrease of the E-values of the unbound layers to 60% of the values obtained after one month when full drainage was accomplaished. When simulating an increased groundwater level E-values of the unbound layers showed a reduction of 40% when groundwater level was placed at the basecourse/subbase interface Figure 19 and Figure 20 shows the correlation between E-values, positive, and negative pore pressures, respectively. E-moduli of the lower unbound layer materials was observed to decrease during the period of varying water tables. It was believed that this was due to the presence of water lubricating the granular material, an issue earlier discussed by (Thom, Brown 1987) for the case of a limestone aggregate used as road base. The variability among the different specimens tested was, for Thom and Brown considerable, but increasing moisture resulted in a stiffness decrease for all tests due to 'lubricating' of the particles.

Figure 21 shows an example of the correlation between suction and degree of saturation. The suction measurements were performed at depths corresponding to these specific layers. These measurements showed a rather significant relationship between these parameters corresponding to the retention curves for the materiels tested. The plots in Figure 21 are time series and not scattered data points. Saturation levels varired during the tests and the curve can hence be followed from left to right and back in order to follow the time series of the performed tests. The base layer (blue lines) were not able to contain the same amount of water than the subbase sand layer (green lines).

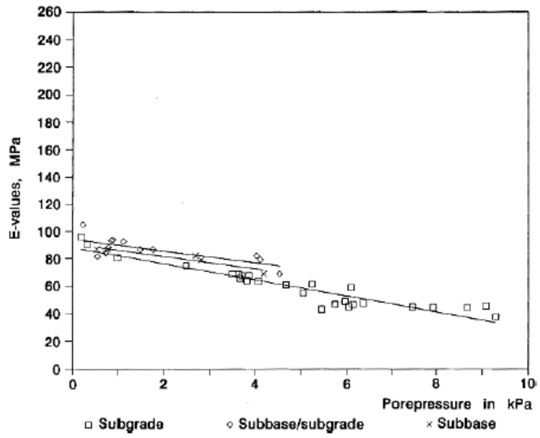

Figure 19: Variations in E-value due to different pore pressures for the different layers. From (Krarup 1995).

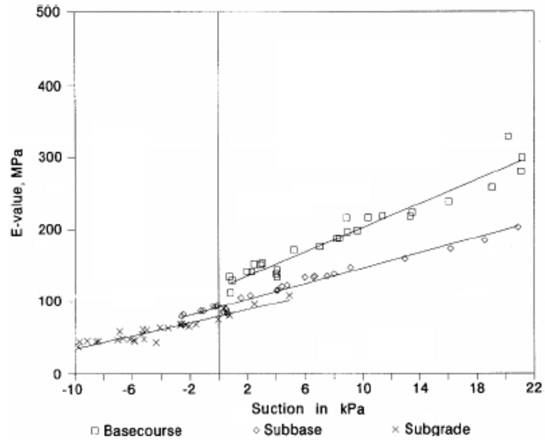

Figure 20: E-moduli for different suction levels. All values measured when fully soaked materials where allowed to drin freely. From (Krarup 1995).

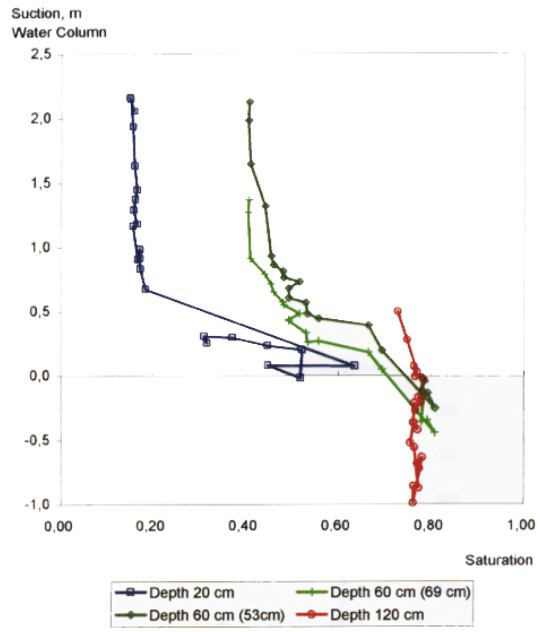

Figure 21: Soil suction measured with tensiometers and saturation measured with moisture/density probe. Blue line: Granular base layer. Green lines: Subbase sand layer at different depths. Red line: Sandy subgrade. From (Krarup 1995).

Similar suction values were obtained for the two materials. Naturel water content was determined to be (% saturation) 0.7 for the subgrade, 0.15-0.35 for the subbase, and 0.15 for the base layer. The degree of saturation changed from a level between 15 and 20% to 60 and 70 % when ground water table was raised to the bottom of the base course layer which was due to capillary effects in the base course layer. Since the base material was more well-graded and had a lower permability the basecourse should then posses a pore size distribution with smaller pore diameters than the subbase and consequently a stonger capillary force.

This was also argued by (Kolisoja 1997). He stated that the approximated value of the resultant force acting on a particle, due to the capillary effcts, decreases as a function of the particle radius. The number of particle contacts will increase as the radii of the particles decreases, which entail a higher suction potential.

Water and permanent response

Positive pore water pressure may built up as a result of repated loadings. This could result in diminishing permanent deformation resistance of the material. The progress can be observed to vary with stress state and water content. One way of reducing this permanent strain development is to ensure proper draining. (Figure 22). In a triaxial testing study, with a granular material, the permanent strain development was showned to proceed at as lower intensity when draining conditions were established. (Lekarp, Isaccson 2000).

Investingating permanent defomation could be performed with the use of the Heavy Vehicle Simulator (HVS), which is capable of testing pavements in their 'as-built' conditions. Figure 23 shows results from testings of different granular materials tested with the HVS and the rut progression. Remarkable is it to observe that rutting increases markedly when water is ingressed. The rut progression further continues with the same trend even after water is removed (Brown 1996).

This was also examined by (Wiman 2003) who used the HVS-nordic to accelerated pavement testings investigating rut progression when applying different load levels. Rut progression continued almost linearly even after increasing load and tire pressure after 1.000.000 passes. But when water was added and load and tire pressure levels were adjusted back to the origin, rut progression increased further (Figure 24).

Seasonal variations

An issue which could be related to the problem concerning water in road constructions is frost heave and hence spring thaw. The mechanics of frost heave are very complex and not completely simlar to those of water ingression. It will include the following factors:

1. Frost-susceptible soil
2. Slowly depressed air temperature
3. Supply of water

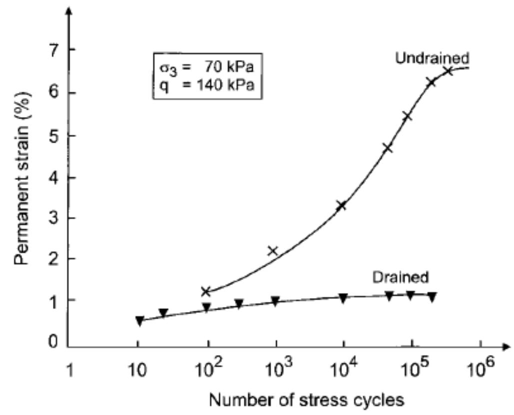

Figure 22: Influence of drainage on the permanent strain development. Source: (Dawson 1990). From: (Lekarp, Isaccson 2000).

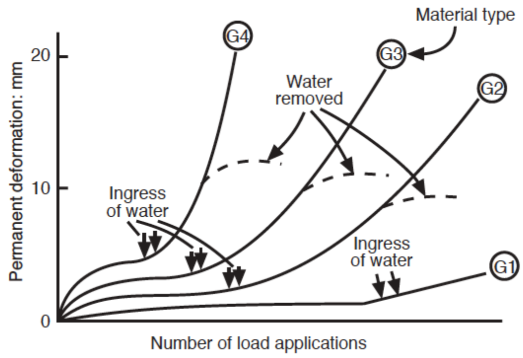

Figure 23: Correlation of no. of load applications and permanent strain for four different qualities of granular layer. From (Brown 1996).

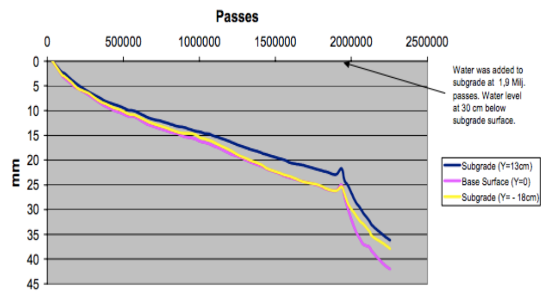

Figure 24: Rut depth propagation during the tests. (Wiman 2003).

When a soil specimen is subjected to cooling temperatures the water in the soils pore spaces will cool until freezing takes place forming ice crystals. If the soil is susceptible to capilary action the ice crystals would continue to grow until ice lenses are formed (Yoder, Witczak 1975).

Water expand approximately 9% percent when reaching temperatures below 0°C which results in a heave of the road construction due to the formation of ice lenses. At spring time when ice lenses melts a major reduction in bearing capacity can be observed according to Figure 25.

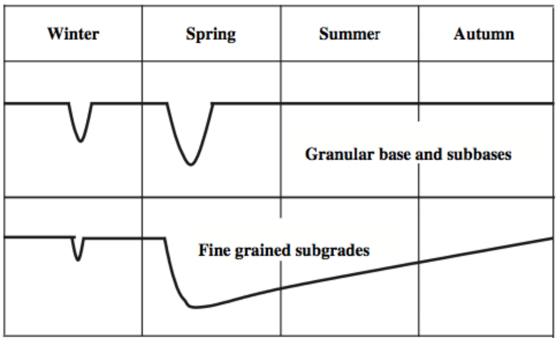

Figure 25: Schematic overview of the variation in stiffness. Source: (Dawson 2008).

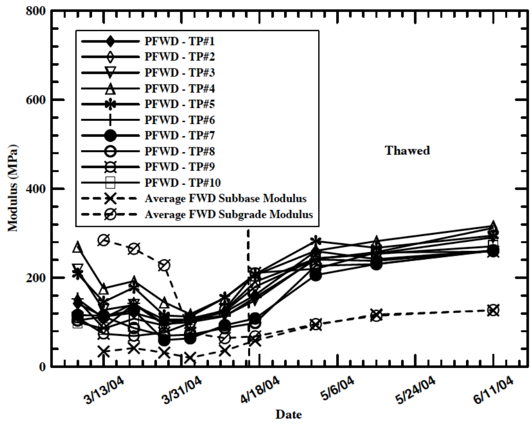

Figure 26: Stiffness variations at Knapp Airport Lot, Berlin, Vermont. Source (Steinert, Humphrey & Kestler 2006):

The bearing capacity of the road construction will vary during the year. Especially spring thaw may soften the subgrade or subbase/base layers.

In the winther, a minor stiffness reduction can be observed due to any short thawing period. The main problem, though, is when spring thaw begins where a major reduction in bearing capacity is observable. Further remarkeble is it that the strenght is not immidiately recovered, but will vary depending on the soil characteristics.

When tracking seasonal changes (Steinert, Humphrey & Kestler 2006) used the Portable Light Weight Deflectometer (PFWD) and concluded that PFWD trends were similar to that of the Falling Weight Deflectometer (FWD) and could hence be used for evaluating the loss of stiffness in asphalt surfaced roads during the year. The result for a specific roadside is shown in Figure 26. What is interesting, though, is that pattern shows that the bearing capacity recovers at a slowly rate and it is not fully recovered until 3 months after spring thaw.

Similar examples can be found in the results presented by (Savard et al. 2005) when comparing water content in subgrade and deflection curves the results shown in Figure 27 were obtained. It is quite noticeable to observe how the deflection and water curves only follow the same trends for the initial phase. Water content is rapidly removed, but the deflection and thus the bearing capacity is regained more slowly.

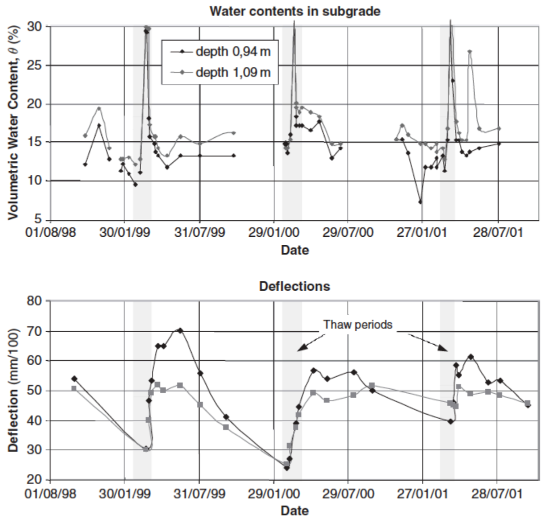

Figure 27: Deflection and water content comparisons. From: (Savard et al. 2005).

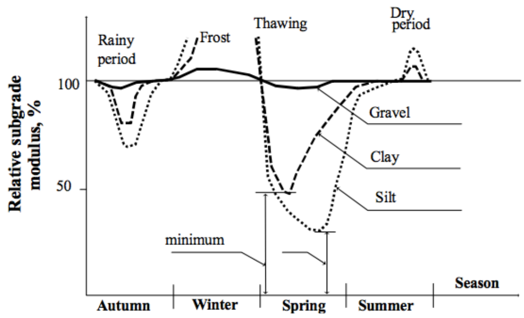

Figure 28: Seasonal changes of subgrade E-moduli used for construction design in Finland (From (Hovli 2000)).

According to the finish design system for road constructions periods of rainfall are taken into account as illustrated in Figure 28. This principle takes into account the relative reduction in subgrade modulus as a consequence of a rainy period.

Based on experience 80% of the deterioration (e.g. rutting or roughness) during a year will take place during the thaw period despite its short extend (Sundahl, Hede 2000).

This was also discussed by (Roy et al. 1992) who performed a field study of two road sections in during a freeze-thaw cycle. Instrumentations at the sites included i.a. temperature and precipitation. These measurements were compared with deflection tests carried out with the benkelman beam (Figure 29). Figure 30 shows the daily recorded precipitation levels. Roy et.al concluded that the deflections depends on the moisture content of the thawed zone. What is noticable, though, is that markedly rainfall occured in the spring (april, may). This fact could have affected the results of deflection obtained with the benkelman beam. Water was thus observed to have significant influence on the deflections.

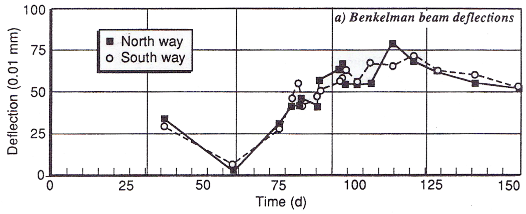

Figure 29: Deflections measured with the Benkelmann Beam at the two locations evaluaeted in (Roy et al. 1992).

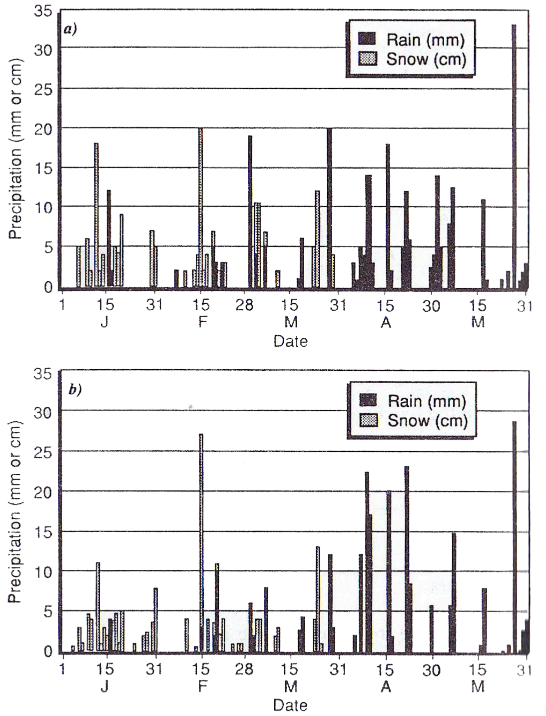

Figure 30: Level of precipitation for the two locations of (Roy et al. 1992).

Modelling Climatic Changes

The danish method for determine the design of a road construction is based on the regulation: Design of Pavements and Pavement Reinforcements (Vejregelrådet 2007).

The design can be approached by means of simulation. Considering climatic or environmental impacts a model determining the the E-value variations due to different temperature levels is used. The values are adopted from the Swedish road regulations and climatic parameters are obtained at Skåne. (Vejregel Arbejdsgruppe p.21 2011) The matrix is based on a slightly modified version of the Swedish approach, one extra day of heat wave has been added in order to provide for deterioration of asphalt layers. E-values are thus adjusted in accordance with factors presented in Table 2. No correction is made for the presence of water during a heavy rainfall.

The table thus summarizes for how many days this temperature can be expected which will finally lead to a summation of the deterioration expected through the constructions service life. During the summer and autumn the E-moduli is thus expected unchanged for the unbound materials.

Table 2: Factors considering the variations in E-moduli due to different temperatures. (E_1 - asphalt, E_2 - base, E_3- subbase, E_m - subgrade)

Period	Day	Temp	E_1	E_2	E_3	E_m
-	-	°C	-	-	-	-
Winter	49	-2	4	4.2	10	20
Winter (thaw)	10	1	3.7	0.3	10	20
Spring (thaw)	15	1	3.7	0.7	0.7	0.6
Late spring	46	4	3.1	1.0	0.8	0.8
Summer	143	20	1.0	1.0	1.0	1.0
Heat wave	10	50	0.3	1.0	1.0	1.0
Autumn	92	7	2.6	1.0	1.0	1.0

During the winther the E-moduli of the unbound layers is expected to increase as much as 20 times and decreases to 60% of its origin during spring thaw.

Sensitivity analysis MMOPP

A sensitivity analysis to the calculated road construction life-cycles based on seasonal variations of E-moduli in MMOPP was made by (COWI A/S 2009). The analysis were performed under influence of different estimated traffic loadings and varying subgrade E-moduli of 20 and 40 MPa.

It was concluded that halving the bearing capacity of the subbase sand layer for the non-frozen scenarios (in relation to Table 2) would reduce the roads life-cycle of approximately 20%. An additionally similar reduction in the granular base layer showed a lifetime reduction of approximately 60%.

On a contrary, halving the increased E-moduli values expected in the unbound layers during the winther showed an insigninficant change in life-cycle, while a complete removal of the higher E-values due to freezing temperatures only shortened the roads life-time by approximately 10%.

The lifetime of a road construction is merely affected by the reduction in E-values due to softening of the unbound layers than the positive hardening effect during the freezing period.

The opposite effect was shown by (Kristiansen 2007) when performing FWD measurements at specific locations on a poorly maintained road network as part of an implementtion of a Pavement Management System (PMS). Influence of groundwater level was examined. Additionally, other registrations were made e.g. visual inspection and thickness measurement. At one location it was decided to lower the groundwater level, surprisingly resulting in a negative effect of the bearing capacity of the section and thereby a markedly decrease in the residuel life of the pavement.

At another location, with a considerably varying groundwater level, the residual life were found to increase.

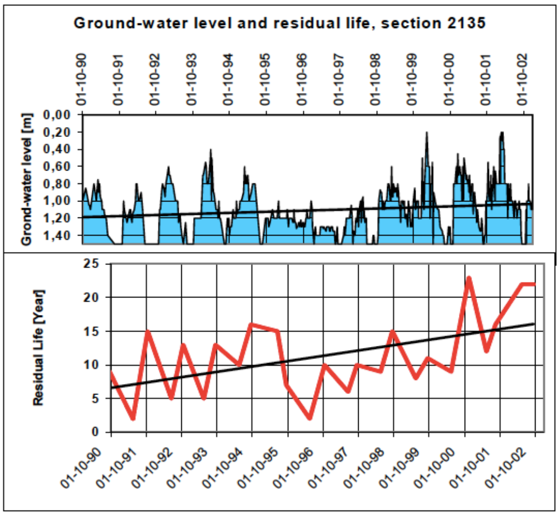

Figure 31: Influence of groundwater level to residual life. From: (Kristiansen 2007).

Figure 31 shows the variaties in the predicted residual life due to FWD-measurements. For specific periods, the groundwater level was only 25 cm below pavement surface. For the last 5 years a relatively rapid distress development was observed. The study concluded that a rebedding of the unbound materials in the road structure might have affected the results.

Conclusion

In the future more water in road constructions can be expected due to higher precipitation levels which will affect the water balance for the road constructions. The majority of road constructions in Denmark are based on the principle consisting of unbound layers highly senstive to water content.

Improper drainage constructions can be found in a great extend since roads are designed and build for long-term horizons. The climatic changes with relation to precipitation levels were not considered to the same extend earlier. For periods where the water is not drained properly, it may find its way into and affect the unbound layers.

When considering the structural performance (e.g. bearing capaciy) of a road construction water in the unbound materials will indeed have its influence on the performance.

The litterature showed a significant reduction in the resilient modulus due to increased moisture content. When exeeding saturation limits of approximately 75%, depending on type of aggregate, a significant decrease in resilient modulus of as much as 75% was observed. The reduction was more distinct for the more fine-grained material than the coarser since the fine grained material are capable of containing more water than the coarser grained which will affect the bearing capacity.

When compacting the materials the litterature showed that compaction with water content lower than optimum resulted in a relatively higher resilient response than if materials were compacted at the wet side of optimum.

At periods with a high amount of water in the construction the bearing capacity reduces immediately but is not regained as quickly.

When observing frost-thaw cycles a significant reduction in bearing capacity can be observed which is considered when designing by means of simulation with relation to the danish design guideline. A similar reduction could be expected when heavy rainfalls innundate low-lying roads and water hence infiltrate the unbound layers. If precipitation levels in the future developes at a frequency higher than present, the accelerated deterioration procces of the road construction can thus be expected to develop at a likely rate.

Sensitivity analysis performed with MMOPP showed a markedly decrease of the life-cycle of different road constructions with different estimated traffic loadings when reducing bearing capacity of the subbase and base layers. The design life reduction was calculated to 20% if bearing capacity was reduced 50% in subbase and 60% life-time reduction was calculated when bearing capacity was reduced 50% in the base layer.

With regard to designing by means of simulation the danish regulations considers roughness and rutting. Threshold values are set determining the design life of the construction. Water in the unbound layers will, indeed, affect the parameters and thus the residual design life.

Future

To include the reduction in bearing capacity and long term performance of the road construction MMOPP should include an *effective stress approach* focusing on increased precipitation levels. There is a need for determining the *effective bearing capacity* of the unbound layers in road construction. The seasonal changes as well as the expectations concerning the increased levels of precipitation in the future should be implemented in the MMOPP software system.

Field tests are needed in order to gather some experience on bearing capacity reduction due to increased water content of the unbound layers for base and subbase materials used as standard in Denmark.

The cyclic behaviour (e.g. reducing/recovering rate) of the bearing capacity should be investigated when unbound layers are subjected to complete saturation due to a heavy rainfall and the reduced bearing capacity and its time horizon should hence be implemented in MMOPP.

References

Arnbjerg-Nielsen, K. 2008, "Forventede ændringer i ekstremregn som følge af klimaændringer", vol. Spildevandskomiteen, IDA; Skrift 29.

Arnbjerg-Nielsen, K. 2003, "Trend i ekstremregn", *Rapport for Spildevandskomiteen.COWI, Lyngby, .*

Arnbjerg-Nielsen, K., Madsen, H. & Mikkelsen, P.S. 2006, *Regional variation af ekstremregn i Danmark: ny bearbejdning (1979-2005),* vol. Spildevandskomiteen, IDA; Skrift 28.

Ba, M., Fall, M., Sall, O.A. & Samb, F. 2012, "Effect of Compaction Moisture Content on the Resilient Modulus of Unbound Aggregates from Senegal (West Africa)", *Geomaterials,* vol. 2, no. 1, pp. 19-23.

Berntsen, G. & Saarenketo, T. 2005, "Drainage on low traffic volume roads", *Roadex report.* *www.roadex.org*, .

Brown, S.F. 1996, "Soil Mechanics in Pavement Engineering", vol. 46, No. 3, no. Géotechnique, pp. 383-426.

Cappelen, J. & Scharling, M. 2010, 30. august 2010-last update, *Mere - og mere intens - regn over Danmark* [Homepage of DMI], [Online]. Available: http://www.dmi.dk/dmi/print/mere_-_og_mere_intens_-_regn_over_danmark [2013, 03/08].

COWI A/S 2009, "Følsomhedsanalyse for MMOPP", , ed. Vejregel Arbejdsgruppe p.21, COWI A/S, Paralelvej 2. 2800 Kongens Lyngby, 5th november.

Dawson, A. 2008, *Water in road structures: movement, drainage & effects,* Springer.

Dawson, A. 1990, "Introduction to Soils and Granular Materials", *Lecture Notes from Residential Course, Bituminous Pavements-Materials, Design and Evaluation,* .

Ekblad, J. 2007, *Influence of water on coarse granular road material properties,* .

GEUS 2010, "Geoviden – Geologi og Geografi", -, vol. 2011, no. 03/08.

Haynes, J.H. 1961, "Effects of repeated loading on gravel and crushed stone base course materials used in the AASHO road test", .

Hicks, R.G. 1970, *Factors Influencing the Resilient Properties of Granular Materials,* University of California, Berkeley.

Hovli, I. 2000, "Vegkonstruktioner og vegbygning. Dagens dimensioneringsmodeller og fremtidig udvikling", *Seminarium: Väger och tunga transporter. Växelverkan mellan väg och fordon.*, ed. NVF-Rapporter. 1/2002, NVF-34, NVF 54., Via Nordica 2000, june, 15th.

Jørgensen, A., K. 2008, 6. maj 2008-last update, *Fremtidens Klima* [Homepage of DMI], [Online]. Available: http://www.dmi.dk/dmi/fremtidens_klima-2.pdf [2013, 03/08].

Kolisoja, P. 1994, "Large Scale Dynamic Triaxial Tests with Coarse Grained Aggregates", *4th International Conference, Bearing Capacity of Roads and Airfields.*

Kolisoja, P. 1997, *Resilient Deformation Characteristics of Granular Materials,* Tampere University of Technology.

Krarup, J. 1995, *Bearing capacity and water: part 3: measured pavement performance.*, Danish Road Institute. Institute of Roads, Transport and Town Planning, -Technical University of Denmark. Report no. 75, Danish Road Directorate. Notat 253.

Kristiansen, J., Riishede 2010, "Grundvandet - En Overset Trussel Mod Infrastrukturen", *Trafik og Veje,* .

Kristiansen, J., Riishede 2009, "Kortlæg Dine Blå Pletter", *Trafik og Veje,* .

Kristiansen, J., Riishede 2007, "Bearing Capacity Development on Low Volume Roads (a 15-Year Case Study)", *Carl Bro Pavement Consultants,* .

Lay, M.G. 2009, *Handbook of road technology,* Taylor & Francis.

Lekarp, F. & Isaccson, U. 2000, "State of the Art. I: Resilient Response of Unbound Aggregates", *Journal of Transportation Engineering,* vol. 126, no. 1, pp. 66.

Nakicenovic, N., Alcamo, J., Davis, G., de Vries, B., Fenhann, J., Gaffin, S., Gregory, K., Grubler, A., Jung, T.Y. & Kram, T. 2000, *Special report on emissions scenarios: a special report of Working Group III of the Intergovernmental Panel on Climate Change,* .

NCC 2001, *Vejbygning. materialer, befæstelser, belægninger,* 3. Edition edn, NCC Danmark A/S, Boisen og Nielsen A/S.

Ovesen, N.K., Fuglsang, L. & Bagge, G. 2009, *Lærebog i Geoteknik,* 1. edition edn, Polyteknisk Forlag, 2800 Lyngby.

Roy, M., Crispin, J., Konrad, J. & Larose, G. 1992, "Field Study of Two Road Sections During a Freeze-Thaw Cycle", *Transportation Research Record,* , no. 1362.

Savard, Y., de Blois, K., Bontonnet, M., Hornych, P. & Manduit, C. 2005, "Analysis of seasonal bearing capacity correlated to pavement deformation in cold regions", *7th Int. Conf. Bearing Capacity Roads, Railways & Airfields.*

Sonnenborg, T.O., Christensen, B.S., van Roosmalen, L. & Henriksen, H.J. 2006, *Klimaændringers betydning for vandkredsløbet i Danmark,* GEUS, Geological Survey of Denmark and Greenland.

Steinert, B.C., Humphrey, D.N. & Kestler, A.M. 2006, "Portable Falling Weight Deflectometers for Tracking Seasonal Stiffness Variations in Asphalt Surfaced Roads", *TRB 2006 Annual Meeting CD-ROM,* , pp. found at: http://docs.trb.org/prp/06-2738.pdf date: 24. sept. 2012.

Stolle, D., Guo, P. & Liu, Y. 2009, "Resilient Modulus Properties of Granular Highway Materials", *NRC Reasearch Press,* vol. 36, no. Can. J. Eng., pp. 639 - 654.

Sundahl, J. & Hede, J. 2000, "Mate ri a l e ka ra k te ri s t i ka ved be l æ g n i n g sd i m e n s i o n e ri n g", *Dansk Vejtidsskrift,* vol. 4, no. 4, pp. 37-40.

Thadkamalla, G.B. & George, K. 1995, "Characterization of subgrade soils at simulated field moisture", *Transportation Research Record,* , no. 1481, pp. 21-27.

Thom, N. & Brown, S.F. 1987, *Effect of moisture on the structural performance of a crushed-limestone road base,* .

Vejregel Arbejdsgruppe p.21 2011, "MMOPP DIMENSIONERINGSPROGRAM FOR VEJBEFÆSTELSER", *ANLÆGSPLANLÆGNING,* .

Vejregelrådet 2009, *Vejkonstruktioner. Afvandingskonstruktioner*, Vejregel edn, Vejdirektoratet.

Vejregelrådet 2007, *Vejregel. Dimensionering af Befæstelser og Forstærkningsbelægninger.*, København: Vejdirektoratet.

Wiman, L.G. 2003, "Accelerated load testing of pavements", *HVS-Nordic tests at VTI Sweden,* vol. 2004.

Yoder, E. & Witczak, M.W. 1975, "MW Witczak Principles of Pavement Design", *John Wiley & Sons, Inc., New York,* .

Aalborg University
School of Engineering and Science
Transportation Engineering

Article 2 - Consequences of Extreme Precipitation for the Deterioration of Road Constructions - field study

René Brodersen

June 2013

Scientific Publications at the Department of Civil Engineering

Technical Reports are published for timely dissemination of research results and scientific work carried out at the Department of Civil Engineering (DCE) at Aalborg University. This medium allows publication of more detailed explanations and results than typically allowed in scientific journals.

Technical Memoranda are produced to enable the preliminary dissemination of scientific work by the personnel of the DCE where such release is deemed to be appropriate. Documents of this kind may be incomplete or temporary versions of papers—or part of continuing work. This should be kept in mind when references are given to publications of this kind.

Contract Reports are produced to report scientific work carried out under contract. Publications of this kind contain confidential matter and are reserved for the sponsors and the DCE. Therefore, Contract Reports are generally not available for public circulation.

Lecture Notes contain material produced by the lecturers at the DCE for educational purposes. This may be scientific notes, lecture books, example problems or manuals for laboratory work, or computer programs developed at the DCE.Theses are monograms or collections of papers published to report the scientific work carried out at the DCE to obtain a degree as either PhD or Doctor of Technology. The thesis is publicly available after the defence of the degree.

Latest News is published to enable rapid communication of information about scientific work carried out at the DCE. This includes the status of research projects, developments in the laboratories, information about collaborative work and recent research results.

Published 2013 by
Aalborg University ©
Department of Civil Engineering
Sohngaardsholmsvej 57,
DK-9000 Aalborg, Denmark

Printed in Aalborg at Aalborg University

Consequences of Extreme Precipitation for the Deterioration of Road Constructions - field study

Brodersen R. [i]

June 2013.

Abstract: The bearing capacity (e.g. E-moduli) of a road constructon is a substantial quantity determining its residual design life. Unbound layers show a high sensitivity towards water. When water is added a change in strength can be observed and hence the bearing capacity will increase or decrease. The climate is changing. Episodes of extreme precipitations can be expected at a higher rate than present and hence more surface water can be expected. If water is not drained properly it will infiltrate the unbound layers and create a temporary water table inside the construction reducing the bearing capacity and thereby the residual life of the construction. Field tests were made in order to investigate this reduction in bearing capacity due to a rising water table. The results showed a significant linear decrease in E-moduli of 40% due to rising the watertable up to the surface level. When lowering the water table the E-moduli were recovered at an almost similar rate but did not fully recover. A bearing capacity 'loss' of ≈ 5-10% was observed due to one cycle of rising/lowering water table. When modelling the residual life for a road construction Mathematical Modelling Of Pavement Performance (MMOPP) is a useful tool but does not consider the future effects for events of extreme precipitation. An approach of increasing asphalt layer thickness is suggested to compensate for reduced bearing capacity of the unbound layers during periods of heavy rainfalls. If this approach is accomplished a socio-economic cost of ≈ 5 - 10 mia. DKK should be invested in order to prepare the danish public road network for the future.

Keywords: Extreme precipitation, Light Weight Deflectometer, Climatic Changes, Water in Road Constructions, Bearing Capacity. Mathematical Modeling Of Pavement Performance.

[i]Graduate Student. Department of Planning and Development. School of Engineering and Science. Aalborg University.

Introduction

The design and maintainance of a road is determined by its functional and structurel properties. (e.g rutting/roughness resistance and bearing capacity). These properties are affected by traffic and environmental impacts but relies further on the properties of the materials used in the construction.

The Mathimatical Model Of Pavement Performance (MMOPP) is widely used in Denmark as an appropriate tool for predicting the life-span of road construction by simulating the accelerated deterioration process. MMOPP takes into account the aforementioned factors. Traffic is determined by a model extrapolating present traffic volume to some future representing the design life of the road. With regard to the environmental effects a climate model adjusting bearing capacity during the year with regard to changing temperatures is used.

It is well known that water affects the unbound layers of a road construction. In future climatic scenarios increasing precipitation levels can be expected and hence more water will affect the unbound layers (Brodersen 2013). MMOPP does not consider this effect.

This article presents the results from a series of field tests made in order to investigate how the bearing capacity (e.g. E-moduli) is affected by the presence of water and hence, any changes in future deterioration due to the presence of water in the construction.

Field Tests

The tests were performed using a standard construction principle consisting of a sand subbase and a gravel basecourse layer on top of a subgrade. The field construction was made in an excavation at Aalborg University. Dimensions of test field was 3 x 4.5 m. The test site can be seen in Figure 1 and Figure 2.

Figure 1: Excavated test field. Limestone subgrade.

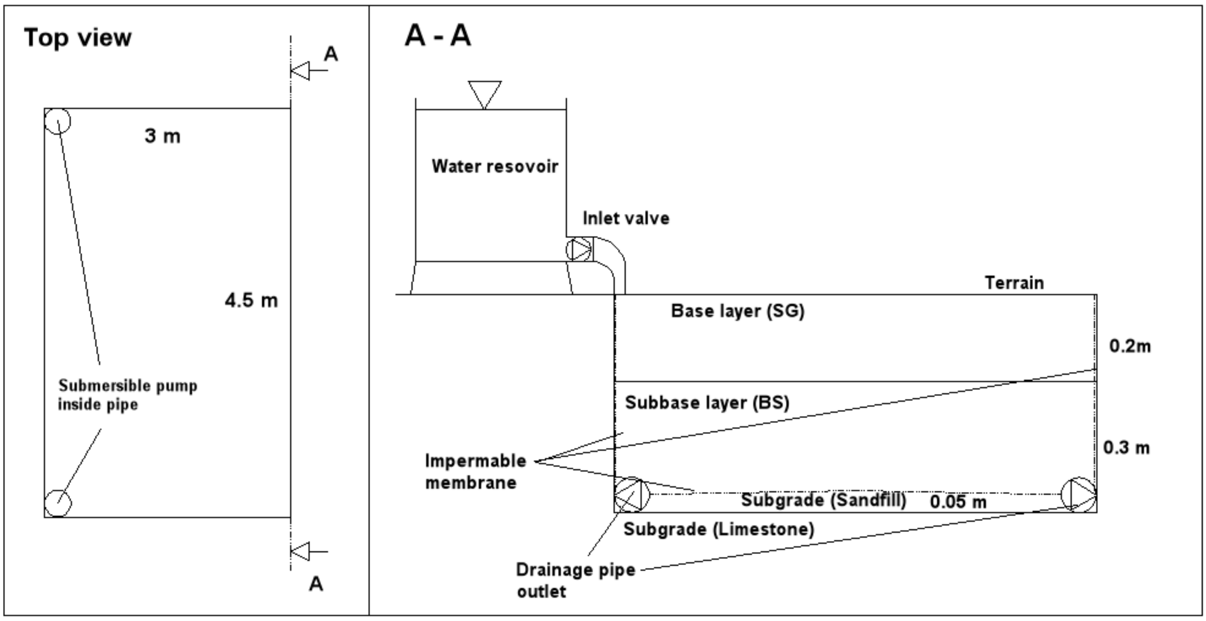

Figure 2: Top view and cross section of test field setup.

Test field preperations

The field was excavated until 60 cm below surface. Subgrade consisted of af firm bedded limestone. A thin layer of sandfill was spread out making a tiny slope from the center of the field towards the ends. An impermable membrane was put down to seal the field. In each side of the field a drainage pipe (80mm diameter) was placed and connected to a well (150mm diameter). The bottoms of the two wells was placed 50 mm below subgrade surface.

30 cm of sand (BL2) was filled into the field and straighten with a wood device. Water was sprayed on the material and hence compacted with a vibratory plate. 20 cm of steady gravel (SG2) was then filled into the field. Water was likewise sprayed on the material and hence compacted.

10 standpipes of 25 mm diamter and 70 cm of length was used to determine the water table. E-moduli measurements were performed next to the standpipes. Standpipe and E-moduli posittions can be seen in Figure 3 and Figure 4.

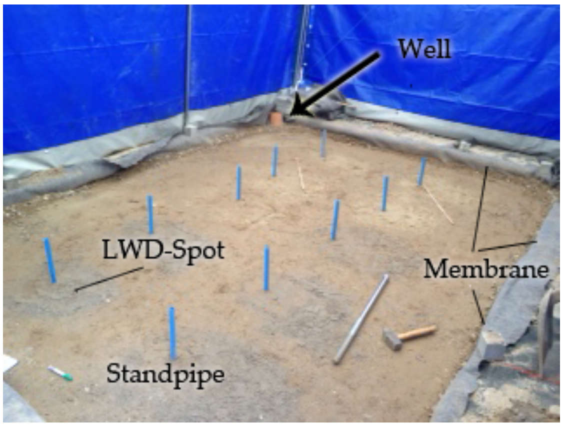

Figure 3: Standpipe positions. LWD measurements were performed next to the standpipes.

During construction the LWD (see later) was used to measure E-moduli for the subgrade, subbase and basecourse at the ten positions for each layer. 15 drops per position was made for the subgrade and 10 drops per position were made for the subbase and base layer at each position. Average E-values for the subgrade, subbase and base layer can be seen in Table 1. Density measurements were performed at the same positions, as for the standpipes, for each layer.

Table 1: Average E-values and standard deviation for ten positions for each layer.

	Subgrade	BL2	SG2
$E_{0,\ average}$ [MPa]	272	40.8	77.8
Std.Dev.[MPa]	131	4.0	5.3

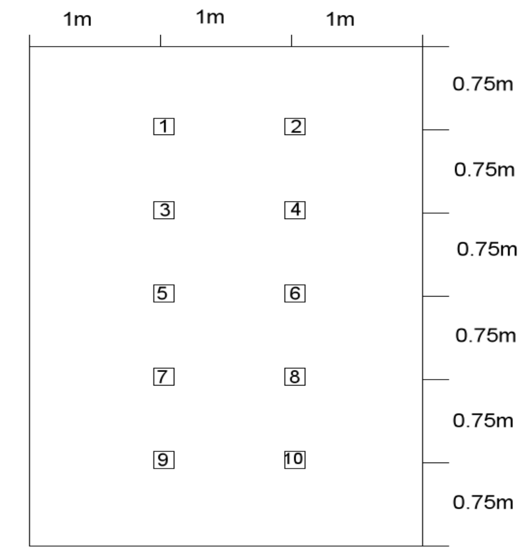

Figure 4: Top view of test field. No. 1 - 10 represents positions of standpipes, E-moduli and density measurements.

Table 2: Water inlet/outlet steps. Average E-values and average water tables a each step.

Step no.	Date water Ingress / outlet	Date E-value	Amount of water Ingessed/total [l]	Average E-value [Mpa]	Ave. water table* [cm]	Water content BS / SG [%]	Notes
0	22/4 - 11.00	25/4 - 08.00	0 / 0	78	40,0	(- / -)	4
1	25/4 - 09.00	25/4 - 10.45	140 / 140	83	40,0	-	4
2	25/4 - 11.00	25/4 - 12.45	140 / 280	81	40,0	-	4
3	25/4 - 13.00	26/4 - 09.00	120 / 400	80	38,8	-	1,2,3
4	26/4 - 10.00	26/4 - 12.00	140 / 540	74	36,0	-	5
5	26/4 - 14.00	27/4 - 08.00	50 / 590	65	21,1	(- / 5,51)	
6	27/4 - 09.00	28/4 - 08.00	50 / 640	61	17,7	(- / 5,6)	2
7	28/4 - 09.00	28/4 - 11.00	50 / 690	57	10,8	(18* / 6,77)	2
8	28/4 - 12.00	28/4 - 14.00	50 / 740	53	4,7	(18* / -)	2
9	28/4 - 15.00	28/4 - 19.00	30 / 770	49	0,8	(18* / -)	2
Fully saturated							
10	--	1/5 - 08.00	0 / 770	50	3,3	(18 / 8,4)	
11	1/5 - 09.00	1/5 - 10.30	30 / 740	52	6,3	(18* / 6,5)	
12	1/5 -11.00	1/5 - 12.00	30 / 710	53	9,3	(18* / 6,4)	
13	1/5 - 11.30	1/5 - 14.00	50 / 660	58	16,6	(18* / 6,2)	
14	1/5 - 14.30	1/5 - 15.30	50 / 610	61	23,3	(18* / 6,6)	
15	2/5 - 08.00	2/5 - 13.00	50 / 560	68	29,2	(12 / 5,32)	
16	2/5 - 14.00	2/5 - 16.00	50 / 510	76	34,8	(- / -)	5
17	2/5 - 16.00	3/5 - 07.30	65 / 445	75	38,0	(- / -)	5
18	4/5 - 08.00	4/5 - 10.00	50 / 395	78	40,0	(- / -)	5
19	5/5 - 08.00	5/5 - 16.00	- / 395	78	40,0	(- / -)	5
20	-	6/5 - 11.00	- / 395	76	40,0	(- / -)	5
21	-	7/5 -11.00	- / 395	78	40,0	(- / -)	5
22	-	8/5 - 08.00	- / 395	79	40,0	(- / -)	5

** Water table below surface. 1: High water table st.pipe no: 1,2 and 9. 2: Ditch/trench overflow. 3 Trench excavated in one side of field (pos. 1 and 2). 4: Water content determination failed. 5: Water content not determined.*

Test procedure

The test series consisted of two main parts. First, a correlation between E-moduli and water table were examined to observe reduction in E-moduli due to partly saturating the construction. Secondly, A correlation between E-moduli and water table when draining were studied. For the saturation process water was let in through the two wells at each side of the field and into the drainage pipes. Inlet was made in steps according to Table 2.

Water inlet was made in controlled steps. On the basis of expected porosity of the BL2 and SG2 layers amount of water needed to cause a raise in water table of ≈ 5cm was calculated. This resulted in 10 steps before complete saturation was obtained. E-moduli was measured on top of the basecourse layer and water tables, at each position, was noted. Then the next step was completed by adding, another specific amount of water cooresponding to the actual step which caused a further rise in water table. Correlations of E-moduli and water tables, at each position, was once again noted. This proces continued until complete saturation was obtained. When complete saturation were reached at step 9 water inlet was stopped.

Water table were sounded with a device with an accuracy of 1cm. Length of standpipes were 70 cm and guided into the construction prepared by a metal rod. Standpipes were lowered until ≈ 30 cm of the pipes were above surface level. E-moduli measurements were not performed until a stable water table was obtained. Water tables could not be measured correctly at depths lower than 40 cm due to the length of standpipes lowered into the field. The water content was obtained using destructive testing at field edges.

For the second part a submersible pump was lowered into the wells and water was pumped out of the field. Corresponding amounts of water, with regard to inlet steps, were endavoured at each step. The water table was sounded simultaniouesly and pumping was stopped when the water table reached a corresponding step for the saturation process in step 1 for easy comparison. When complete drainage were obtained E-moduli measurements were performed once a day for 5 days. (steps 18 to 22).

Materials

Materials used for the field tests were chosen in accordance with the danish standard regulation for base and subbase layers (Berg 2004). For the subbase layer a BL2 sand were used and as base layer a SG2 gravel material were used. Grain size disatributions were made in accordance with DS/EN 933 - 1 and can be seen in Figure 5. Materials were classified in order to obtain the following; Optimum Moisture Content (OMC), Maximum DryDensity (MDD) Solid bedding (e_{min}), loose bedding (e_{max}), Hydraulic Conductivity (κ_T), Permability (K), Uniformity Coefficient (C_U), and Coefficient of Gradation (C_C). Results are shown in Table 3.

The base material contains more fine material than allowed for the higher quality base material SG1. The SG2 is a well graded material having a (C_U) of 25 and hence a very dense bedding can be obtained which will reduce the hydraulic conductivity.

Table 3: Classification parameters.

	BL 2	SG 2
OMC [%]	11	8
MDD [kN/m^3]	17.4	21.2
e_{min} [-]	0.45	0.29
e_{max} [-]	0.78	0.61
SE [-]	82	68
κ_T [m/s]	1.78 * 10^{-4}	6.17 * 10^{-6}
K [m^2]	1.55 * 10^{-5}	5.74 * 10^{-7}
D_{10}	0.25	0.4
D_{30}	0.38	1.2
D_{60}	0.6	10
C_U	2.4	25
C_c	0.96	0.36

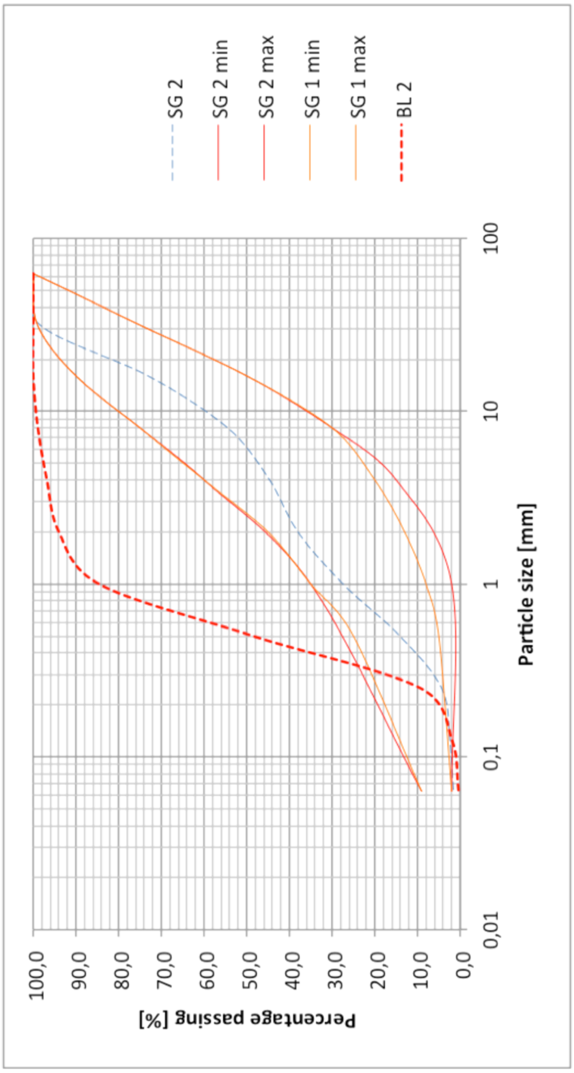

Figure 5: Grain size distribution. "Min" and "max" refers to the danish regulations (Berg 2004). for road base SG1 and SG2 materials.

The base layer was classified as relatively impermable compared to the BL2 subbase layer. Loose and dense bedding (e_{max} and e_{min}) were obtained on dry materials. Since water is added in the field lubricating the particles a more dense bedding could be expected. Permability coefficients are evaluated with pore numbers for the BL2 and SG2 of 0.66 and 0.35 respectively. Pore numbers for the field may differ since heavier compaction was used. Permability conditions may thus differ with regard to lower permability. The well-graded SG2 has a relatively low permability of 10^{-7} compared to the BL2 sand layer of 10^{-5}.

The optimum dry density was obtained with standard proctor laboratory testing in accordance with DS/EN 13286-2 1. ed. 2004 which will not reflect the field conditions when using a vibratory plate.

Compaction

A Primus HS-120 vibratory plate was used for compaction material. The limestone and 0.05 m sandfill subgrade was not compacted The subbase and base layer was compacted with 8 and 6 passes respectively. The weight of the vibratory plate was 120 kg.

A CPN Nuclear Density Gauge was used to evaluate the density of the materials. Measurements were performed with at ten positions shown in Figure 4. The probe was lowered to 15 cm below surface at all positions for each layer/material. The apparatus was callibrated in regard of the surroundings for each layer. To avoid any disturbance the LWD was used to evaluate E-values before the CPN density gaugings. The last drop with the LWD would thereby reflect the density for the material at the specific position.

Testing Equipment

Light Weight Deflectometer

Bearing capacity measurements were performed with a Prima 100 Light Weight Deflectometer (LWD). The setup for these specific tests can be seen in Table 4 and Figure 6.

The device applies an impact load on the surface. The induced surface deflection and the applied force is measured simultaneouesly. The apparatus consists of three main parts. A base with loading plate, sensors and associated electronics. A drop mass (10, 15 or 20kg.) and a upper frame consisting of rubber buffers and guidance rod. A geophone, measuring deflections, is placed in the center of the loading plate. Additional sensors can be used but was not considered essential to these tests. A stepless mechanism is placed on the rod allowing different drop heigths to be used entailing different applied surface pressures. At each test (drop) force impact and deflection data are collected and stored on the appertaining PDA device. Bearing capacity is calculated according to linear-elastic theory of isotrope material in an infinite halfspace according to Boussinesqs equations. Surface moduli values is thus obtained by using Eq. 1 (Vejdirektoratet 2007).

$$E_0 = \frac{f \cdot (1-\upsilon^2) \cdot a \cdot \sigma_0}{d_0} \qquad \textit{Eq. 1}$$

Where E_0 is surface modulus [MPa], f is stress distribution factor (=2 in case of a rigid plate), υ is Poissons Ratio, σ_0 is the surface contact pressure [MPa or kN/m^2], a is the plate radius [mm] and d_0 is the center deflection [μm]. According to (Vejdirektoratet 2007) different contact pressures should be used when performing measurements of surface moduli with the LWD.

- Subbgrade: 10 - 100 kPa
- Subbase: 100 - 200 kPa
- Base: 200 - 300 kPa

These values represents the stresses induced by traffic and can thus be expected in-situ. The specific set-up can be seen in Table 4.

Table 4: Specifications for LWD.

Plate radius [mm]	150
Drop weight [kg]	15
Height of fall [cm]	42.5 / 85
Contact pressure [kPa]	≈ 90 / ≈ 190
Poissons Ratio [-]	0.35
Pulse time [ms]	16 - 20

Figure 6: Prima100 LWD with setup used for these tests. 15 kg drop load, four rubber buffers and 300 mm diameter plate radius. Apparatus developed by Grontmij A/S - DK.

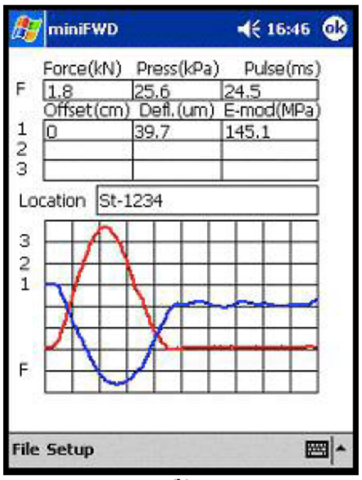

Figure 7: Output force and deflection curves obtained from LWD. Blue trace is deflection and red trace is applied force measured with the geophone and loadcell respectively. Source: (Steinert, Humphrey & Kestler 2006).

To eleminate errors arising from irreversible initial deflections orirginating from the dropped load, a constant deflection level at each drop (load level) was endavoured. Measurements performed during construction of the field was performed by initially discard 5 drops of half falling height (≈90kPa). Hence, average of 5 drops with full falling height was used (≈190kPa). Four rubber buffers was used for giving an approximate load duration time of ≈ 20 ms. One geofone was used placed in the center of deflection. Approximately loading duration time is 15-25ms, but can be adjusted with the use of different rubber buffers.

The output from the LWD test is illustrated in Figure 7. Peak load and peak deflection are thus entered in Eq. 1 and surface E-moduli are obtained.

Results

E-values & Density

E-moduli and density measurements were performed during construction of the field. correlations can be seen in Figure 8. E-moduli was measured at day one when the construction process was finished and once again after 24 hours (day 2) A slightly stronger correlation was obtaied for day 2 measurements. All linear curve fittings is positive meaning that increasing density increases E-moduli as well. The water content for the BL2 was lower than optimum when compacted. This resultet in a poor degree compaction compared to laboratory test. For the SG2 the water content was also lower than optimum and ODD could thus not be obtained. See Table 5.

According to the proctor curve, maximum dry density for the actual field water contents could not be expected to be higher than 17.2 and 20.8 [kN/m^3] for BL2 and SG2, respectively. These lower densities corresponds to a Std. Proctor value of 94% and 93,5%.

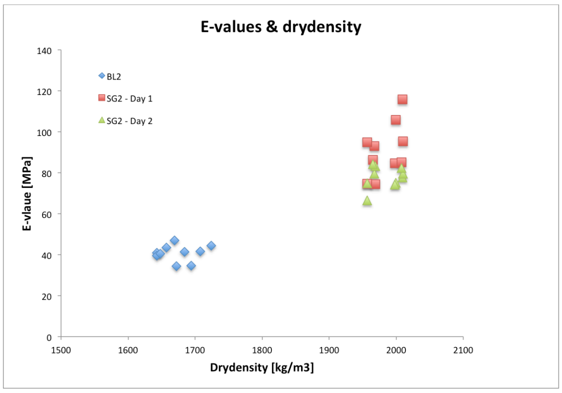

Figure 8: E-moduli and dry density.

Table 5: Compaction control. Reference: Std. Proctor.

	BL2	SG2
Std. Proctor [%]	93	92
w (field ave.) [%]	8,4	6,5
w (opt.) [%]	≈10	≈8,5

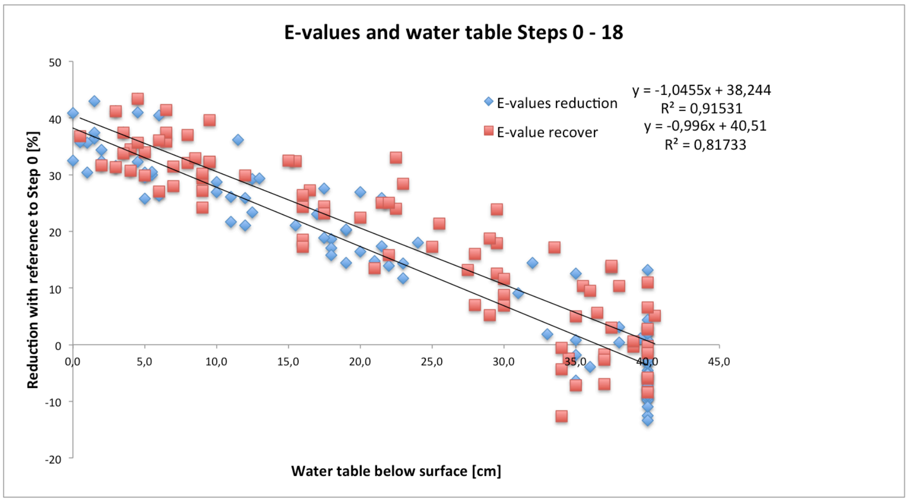

Figure 9: E-value reduction and recovery percentages. Blue scatter represents correlation of E-values when rising the water table. Red scatter is E-vlaues when lowering the water table.

E-values & Water Table

Results for the correlation between water table and E-moduli can be seen in Figure 9. The scatter plot repesents data for every single point at different water tables. Blue scatter represents E-value reduction when rising the water table and red scatter refers to lowering the water table. The scatter may thus be followed from right to left through blue scattter and back from left to right through red scatter. A reduction of approximately 40% in E-moduli was observed when rising the water table 40 cm to the surface of the construction. The E-value reduction showed the highest fit when obtained with a linear approach. When the water table is at the base/subbase interface a reduction in E-moduli of approximately 20 - 25 % could be observed.

Similar results was obtained by (Krarup 1995). When simulating a heavy rainfall and poor drainage positive pore pressure were observed in all unbound layers and E-values was decreased to 60% compared to a drained condition obtained one month later.

As illustrated in Figure 11 the reduction is compared to a drained condition one month later and an intermediate state 16/2-1990 when material was partly saturated. (Krarup 1995) also simulated a rise in ground water table and found that E-values decreased to 40% compared to the initial condition due to the existence of a water table at the subbase/basecourse interface. E-values were by (Krarup 1995) obtained with the Falling Weight Deflectometer (FWD) applying 28 kN (300 mm diamter plate) which resulted in a higher contact pressure than for this study and more wetted material was affected by the impact load decreasing the obtained E-value (Figure 10). The results regarding a reduction in E-values obtained in this study is therefore considered valid.

When considering heavy rainfalls it is of interest to examine any longterm effects when the construction reaches a fully saturated state compared to initial condition to see if the bearing capacity reaches its initial state level.

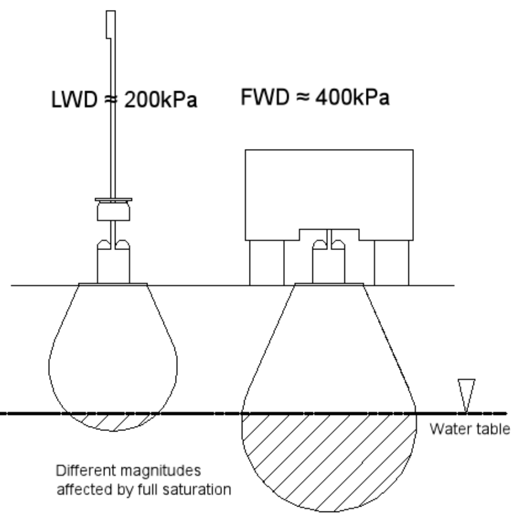

Figure 10: A larger magnitude of soil is affected when a higher load is applied with FWD. Hence, the rise in water table will reduce bearing capacity more for FWD than LWD.

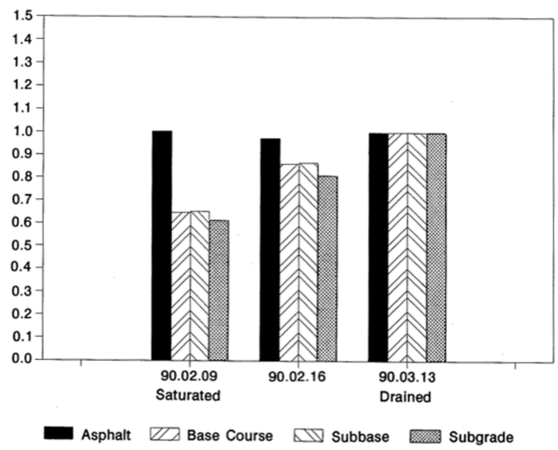

Figure 11: E-values for the different layers when simulating heavy rainfall and poor drainage at different dates obtained by (Krarup 1995).

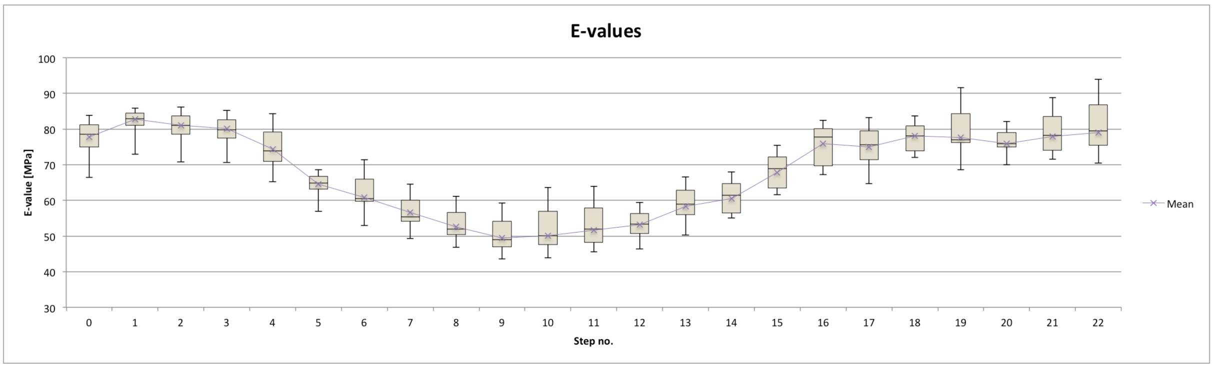

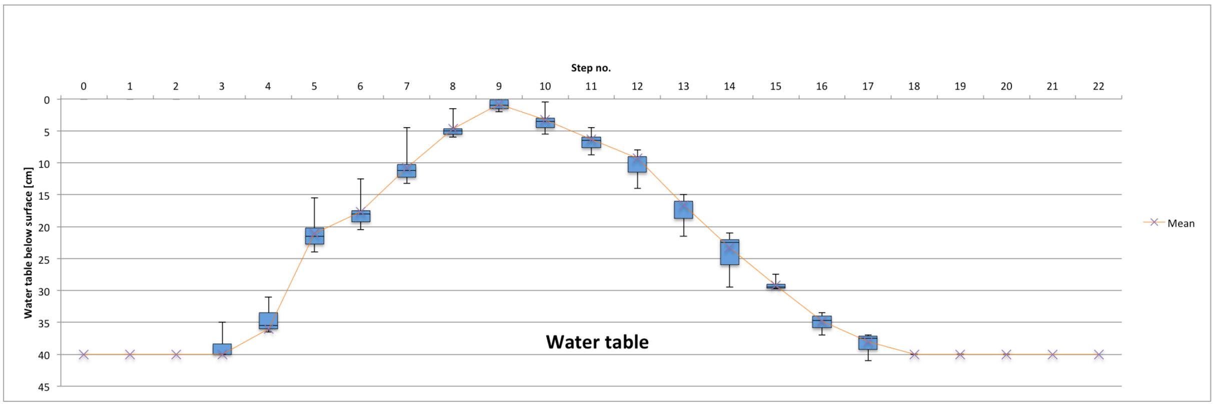

Figure 12: Box and Whisker plots for E-values and water tables for the first twenty-two steps. Values are based on average vlaues for the ten positions.

Box and whisker plots were made for this study for average values for the entire test field. For the first three steps no water table could be observed. For step 3 water table was only observed near the test field sides. At step 5 the water table reaches the subbase/basecourse interface and reduces the basecourse E-values of approximately 20%. When the first ten steps were acomplished a the water table reached surface level and drainage were performed. As presented in Figure 9 the recovering rate is almost similar to the reduction rate but when lowering the water table reaching the initial state of steps 0 - 3 the "recovered" E-value reaches its initial value obtained at step 0. (≈ 78MPa) when water table is lowered to 40cm below surface at step 18. When comparing the initial steps 1 - 3 with steps 18 - 22 of corresponding water tables E-values are decreased by approximately 5-10%. It is quite noticable to observe how average E-values increases when water is let into the construction. (step 0 - step 3) The increase is not considered as a result of initial water ingress but as a result of increasing density when using the LWD.

Every drop compacts the material slightly and the increase will be most distinct at the initial states. 400 liters of water was thus added before any affection could be observed (Table 2 and Figure 11).

When fitting a curve for average basecourse E-values for step 6 - 9 and steps 10 - 13 shows a steeper trend when rising the water table than lowering it. The E-values for the basecourse reduces more rapidly than recovering. Drainage proceeded at a very slow rate and could hence have resulted in a higher water content in the recovering process.

The water content of the materials varied during the test series. A stable level for the SG2 was observed of approximately 6% for partly saturated condition. When water table reached th BL2 layer the water content increased to ≈18% for full saturation and decreased to stable level ≈11% when water table was lowered. OMC for BL2 was found to be 10%. Water content for the SG2 layer increased to approximately 8% when the construction was fully saturated. When lowering the water table drainage of the SG2 layer resulted in a water content of approximately 6%.

E-value reduction can thus be expected to follow a linear trend until a reduction of 40 % is reached. Later, when watertable is lowered E-values recovered linearly with water table.

All E-values obtained with the LWD for the layers are ranging within an interval of ≈10MPa despite the uneven and varying subgrade. The values balances and it can be concluded that fewer points have also been representative for the entire field.

Modelling watertable

When a heavy rainfall and poor drainage conditions are combined water ingressing the road construction will take place and hence completely saturate the construction materials. Since the subbase layer is expected to have a higher permablity than the basecourse one possible way water can be expected to find its way into the construction is illustrated in Figure 13.

When subbase layer is fully saturated it is questionable if the water table will continue

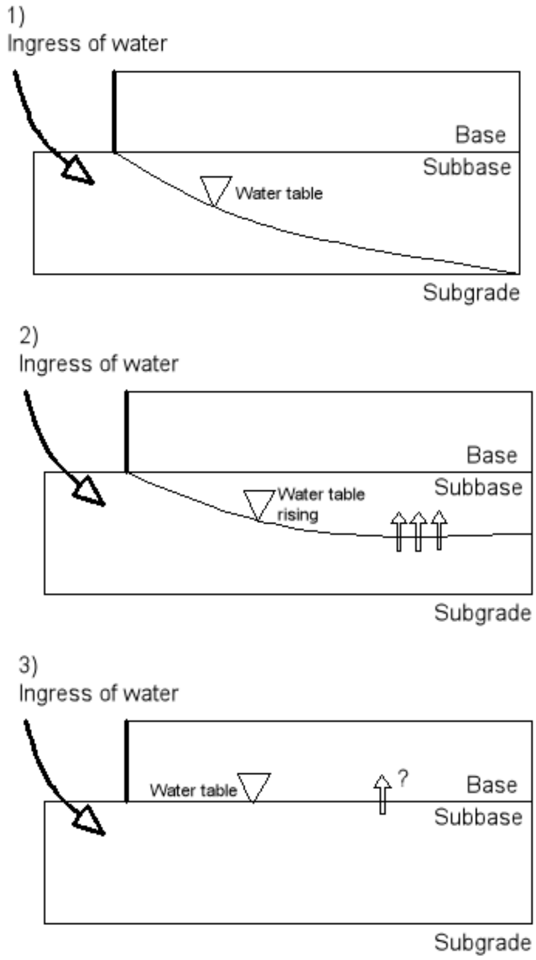

Figure 13: Water table in subbase layer can be expected to rise as consequence of a heavy rainfall.

upwards or if forces of capillarity initially will increase the strength of the baselayer.

As shown in this study E-values will reach a level that is 60% compared to initial values if complete saturation of the unbound layers is obtained.

By setting up a model describing the boundary conditions for a specific site will allow a description of a water table at any given time and position in the unbound layers. The reduction in bearing capacity can be estimated and hence any nescessary precautions can be made (e.g. narrowing the traffic lanes or closure of the road) until a sufficient bearing capacity is achieved.

The complete loss in bearing capacity (≈ 5-10% found in this study) should likewise be implemented in a model and investigated to see if a stable limit is obtainable.

A large scale hydrological Digital Terrain Model (DTM) for Denmark will be finished at september 2013 able to predict where the increased amounts of water is expected to accumulate (Marfelt 2013) These information should be combined with informations of E-moduli variations due to different water tables so that roads suffering from heavy precipitation levels could be mapped and hence precautions during periods of heavy precipitation could be made.

MMOPP Calculations

When bearing capacity of unbound layers reduces due to saturation one way of compensating would be to increase asphalt layer thickness. Based on Boussinesqs equations of linear-elastic theory and Odemarks Method of Equivalent Thickness (MET), which is implemented as the analytical approach in MMOPP, considering maximum allowable stresses on top of each unbound layer, the thickness of each layer is calculated from Eq. 2 (NCC 2001).

$$h_{e1,2} = h_1 \cdot \sqrt[3]{\left(\frac{E_{upper}}{E_{lower}}\right)} \qquad \textit{Eq. 2}$$

where, $h_{e\,1,2}$ is the equivalent height, h_1 is the height of the upper layer, E_{upper} is the E-value of upper layer and E_{lower} is the E-value of lower layer.

Presented in Figure 14 and Figure 15 are calculated asphalt layer thicknesses for three different traffic volume scenarios (low: $N_{Æ,10}$[i] = 50,000, medium: $N_{Æ,10}$ = 500,000, and high: $N_{Æ,10}$ = 5,000,000) and 5 different reduced bearing capacity levels based on the assumption that bearing capacity will reduce linearly to 60% of its origin due to a rising water table inside the construction[ii]. Asphalt layer stiffness is determined to be 2,500MPa.

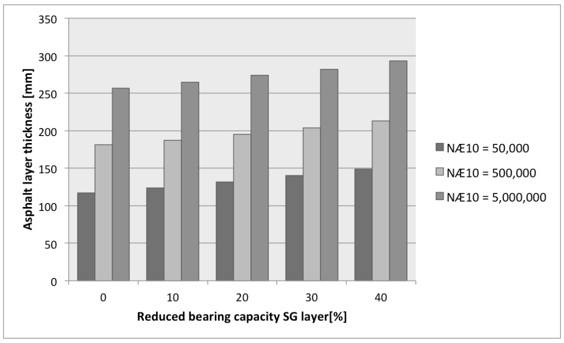

Figure 14: Asphalt layer thickness based on different traffic volume scenarios and different water table levels.

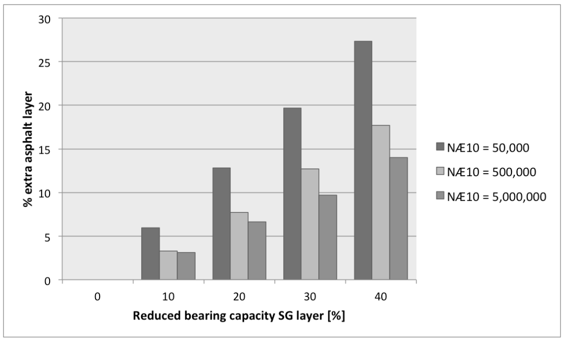

Figure 15: Percentage extra asphalt needed for compensation on the basis of having no water table inside the unbound layers of the road construction and hence no loss of bearing capacity.

[i] $N_{Æ10}$: Equivalent 10 tons axle loads. No. of axle loads causing the same structurel or functional deterioration as the actual traffic loads.

[ii] Results are obtained by assuming a base layer E-value of 300MPa (in accordance with (Vejregelrådet 2007)) reduced linearly to 180MPa (60% of its origin).

Intermediate steps are choosen with reference to water table taking up 0%, 25%, 50%, 75% and 100% of space in the construction. This clearly illustrates that for every of the three traffic volume scenarios reducing bearing capacity of the SG layer will result in increased thickness of the asphalt layer if maximum allowable stresses on top of the reduced SG layer are to be complied. Most remarkable is it for the low volume scenario where ≈ 27 % of extra asphalt would be nescessary to compensate for reduced bearing capacity of the SG layer. Increased asphalt thicknesses for the three scenarios having a water table increased to a 100% are listed below:

Table 6: Increased asphalt layer thickness for the different traffic volume scenarios.

$N_{Æ,10}$	Increased asphalt thickness [mm]
50,000	32
500,000	32
5,000,000	36

Which indicates that approximately 3-4 cm of increased asphalt thickness could be added to compensate for reduced bearing capacity of SG layer when the unbound layers reaches a fully saturated state by a high water table. It could be expected that 5,000 km of public roads in Denmark will suffer from reduced bearing capacity due to a water table inside the unbound layers (Kristiansen 2012). If the approach of increasing asphalt layer thickness is performed it will have a socio-economic cost of ≈ 5 - 10 mia. DKK dependent on type of asphalt material and specific cross sections of roads at exposed areas.

Discussion

Light Weight Deflectometer

When using the LWD for measuring bearing capacity several precautions must be considered. At first, evaluating E-values on an unstabile sand surface a fracture mode can occur along the edge of the rigid contact plate. The magnitude of the fracture is dependent upon stress level and will increase as stress level increases. If this fracture occurs one way to evaluate is to change stress level and thus evaluate the stress dependency. A decrease in E-values when applied stress level is increased could be an indicator of fracture and measurement must be discarded. Secondly, a correlation between density and E-values seems unattainable within the stress levels used for evaluating base and subbase layers. Every drop with the LWD will increase density further and when hammering the spear of the CPN into the layer disturbance may have influenced the results. Additionally, since the spear is a nuclear source and therefore not allowed to be exposed to the surroundings, difficulties when placing the spear into the prepared hole may as well have influenced gaugings (Figure 17).

Finally, using the Prima 100 LWD in tests with fully saturated materials can produce errornous deflection curve. If the water table is located inside the volume affected by the stress distribution the "downward" movement will be reflected when the movement reaches the water table which is incompressible compared to the soil. The result is hence a markedly inverse peak of the deflection curve. This will likely entail erroneous results of E-moduli and caution should be made.

When performing the LWD tests with a high water table did result in false force- and deflection curves as illustrated in Figure 16. E-values reached impractical levels and were thus discarded in the field during the tests. These errornous signals occured when water table reached a level within ≈10 cm below surface and increased when water table was rised further.

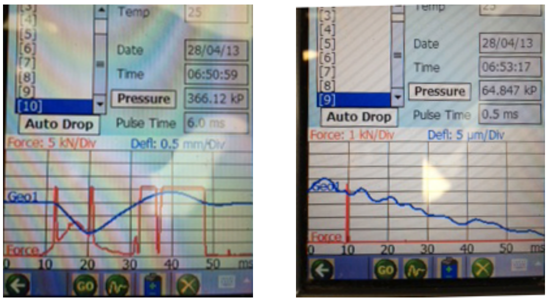

Figure 16: Examples of incorrect deflection signals easily obtained during field tests.

It was still possible to obtain reliable results despite the high water table. Performing tests with a high water table also expected to result in a rearrangement of particles due to positive pore pressure. This could have affected the results. Drainage was observed when having a high water table as illustrated in Figure 18 (left). Lowering the water table thus resulted in a surface displacement as illustrated in Figure 18 (right). Sounding the water table with device used required that the length of the standpipe above surface was subtracted from total length of the pipe. This distance changed during the tests and was adjusted at several steps but might have influenced the correlation.

Figure 17: Example of unprecise CPN nuclear gaunging due to difficulties of lowering the nuclear spear into the prepared hole.

Figure 18: Drainage of layer when performing the LWD tests. (left) Surface displacement due to high water table (right).

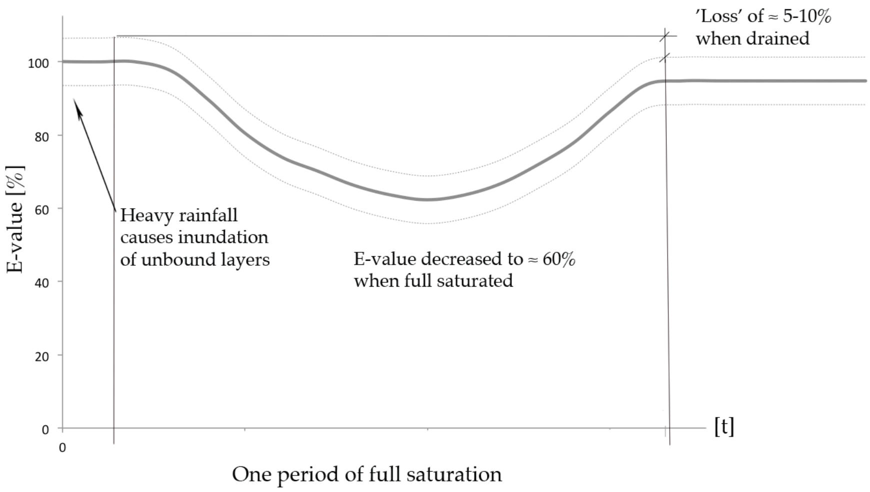

Figure 19: Schematic overview of one period of heavy rainfall affecting the unbound layers and reducing bearing capacity. Solid line represents the average bearing capacity during one cycle of full saturation. Dotted lines represents the deviation in which E-values varied (≈ 10%).

The standpipes were placed just outside the contact area for more precise evaluation of E-values and water table. This might have affected the measurements since the pipe is placed inside the volume of stressed soil. this setup was made for all positions and is therefore treated as a systematic error.

Field Construction

The very firm bedded limestone subgrade made it difficult to obtain an exact slope from the middle of field towards the ends. When BL2 layer was constructed a device was lowered into the layer and when resistance, due to impact with membrane, was met, depth was registrered (Table 7).

Table 7: Layer thickness.

	Average [cm]	Std.Dev. [cm]
BL 2	27,2	1,75

The actual layer thickness varied and especially for a water table at the subbase/basecourse interface could have given errornous results since the water table at some points may have affected the stiffer base layer more than at other positions.

When field was constructed water content was increased by spraying the layers with water just before the compation process was started. Water content was measured using the CPN and was found to be lower than optimum. Small ice lenses were observed when constructing the field. When the BL2 was poured into the field and ice was observed the process stopped and the material was not compacted until the next day but might have affected the relatively low density obtained with the CPN densty gauge.

Conclusion

A test field consisting of a limestone subgrade, a subbase sand, and a gravel basecourse layer were constructed and deflection tests were made by using the Prima 100 light weight deflectometer. Deflection tests were made on top of basecourse layer in order to investigate the reduction in bearing capacity due to a rise in water table.

A correlation between E-values and water table sounded at coincident positions on a construction consisted of sand subbase layer and a gravel base layer on top of a firm bedded limestone subgrade, resulted in a reduction in E-values to 60% of its origin due to a complete saturation (having a water table at the surface of the basecourse layer). The trend was best described with a linear approach and no sifgnificant difference in trend between the subbase and base was observed. The reduction was similar to an earlier study.

The two main results of this study was at first; when lowering the water table the E-values recovers in accordance with a linear approach as well. No significant difference in reduction/recovering was observed.

Secondly, the E-values does not seem to fully recover. A 'loss' of approximately 5-10 % in E-value was observed. This relatively low percentage could have been affected by different influencing factors but the cyclic behaviour of bearing capacity due to fully saturation should be investigated in a future research to see if road constructions will recover, or if a deterioration process should include any recursive effects of heavy precipitation.

When designing by means of simulation using MMOPP a factor concerning the fully saturated state caused by a heavy rainfall should be implemented. A schematic overview is presented in Figure 19. It should be investigated if this effect will deflect and at which rate it could be expected.

The E-values of the subbase and base layer were in average 70 - 85% lower than the subgrade (Table 1). Subgrade E-value is an important input to MMOPP since a varying subgrade E-value entails varying base, subbase, and asphalt layer thickness if the same E-values should be expected on the surface of these layers. Despite the relatively large variation in subgrade E-moduli no markedly deviation could be observed on top of the base course layer.

Increasing asphalt layer thickness would compensate for reduced bearing capacity of the unbound layers. Based on the assumption that bearing capacity reduces linearly to 60% of its origin due to a high water table, approximately 3-4 cm of extra asphalt would be needed to compensate. If this approach is accomplished it will have a socio-economic cost of ≈ 5-10 mia. DKK.

Future research

This study was performed on a construction corresponding to a typical low-volume road. Larger scale tests on constructions corresponding to high volume roads is needed to obtain a higher reliability.

The loss in bearing capacity should be considered in future scenarios by setting up a model describing the hydraulic system of the road construction. This will allow road administrators to take the required precautions when heavy rainfalls, expected to occur at a higher rate than present, will take place.

Combining the hydrological (DTM) with the hydraulic system for the single road construction could be an important step towards preserving the infrastructure for the future.

References

Berg, F. 2004, "Nye Regler for Stabilt Grus og Bundsikring", *Dansk Vejtidsskrift*, vol. 4, pp. 22-25.

Brodersen, R. 2013, *Effects of Climatic Changes to the Accelerated Deterioration of Road Constructions. - litterature review*, Master Thesis edn.

Krarup, J. 1995, *Bearing capacity and water: part 3: measured pavement performance.*, Danish Road Institute. Institute of Roads, Transport and Town Planning, -Technical University of Denmark. Report no. 75, Danish Road Directorate. Notat 253.

Kristiansen, J., Riishede 2012, "Klimaændringerne og Konsekvenserne for det Kommunale Vejnet", *Trafik og Veje*, .

Marfelt, B. 2013, "**Hydrologisk højdemodel viser hvor skaderne sker ved skybrud**", *Ing.dk*, [Online], vol. April, no. 18, pp. May 7th. Available from: http://ing.dk/artikel/hydrologisk-hoejdemodel-viser-hvor-skaderne-sker-ved-skybrud-157974.

NCC 2001, *Vejbygning. materialer, befæstelser, belægninger*, 3. Edition edn, NCC Danmark A/S, Boisen og Nielsen A/S.

Steinert, B.C., Humphrey, D.N. & Kestler, A.M. 2006, "Portable Falling Weight Deflectometers for Tracking Seasonal Stiffness Variations in Asphalt Surfaced Roads", *TRB 2006 Annual Meeting CD-ROM*, , pp. found at: http://docs.trb.org/prp/06-2738.pdf date: 24. sept. 2012.

Vejdirektoratet 2007, "Måling af Overflademodul med Minifaldlod. pr VI 90 - 4:2007", vol. Januar.

Part two - Appendices

Appendix A IPCC Scenarios

The IPCC Special Report on Emission Scenarios (SRES) defines four main scenarios for the future development of emission based on human activity. The groups are based on the following scenarios and illustrated in Figure A—1 (Nakicenovic et al. 2000).

A1: Scenarios

The A1 scenarios are of a more integrated world. The A1 family of scenarios is characterized by:

- Rapid economic growth.
- A global population that reaches 9 billion in 2050 and then gradually declines.
- The quick spread of new and efficient technologies.
- A convergent world - income and way of life converge between regions. Extensive social and cultural interactions worldwide.

A2 Scenarios

The A2 scenarios are of a more divided world. The A2 family of scenarios is characterized by:

- A world of independently operating, self-reliant nations.
- Continuously increasing population.
- Regionally oriented economic development.

B1 Scenarios

The B1 scenarios are of a world more integrated, and more ecologically friendly. The B1 scenarios are characterized by:

- Rapid economic growth as in A1, but with rapid changes towards a service and information economy.
- Population rising to 9 billion in 2050 and then declining as in A1.
- Reductions in material intensity and the introduction of clean and resource efficient technologies.
- An emphasis on global solutions to economic, social and environmental stability.

B2 - Scenarios

The B2 scenarios are of a world more divided, but more ecologically friendly. The B2 scenarios are characterized by:

- Continuously increasing population, but at a slower rate than in A2.
- Emphasis on local rather than global solutions to economic, social and environmental stability.
- Intermediate levels of economic development.
- Less rapid and more fragmented technological change than in A1 and B1.

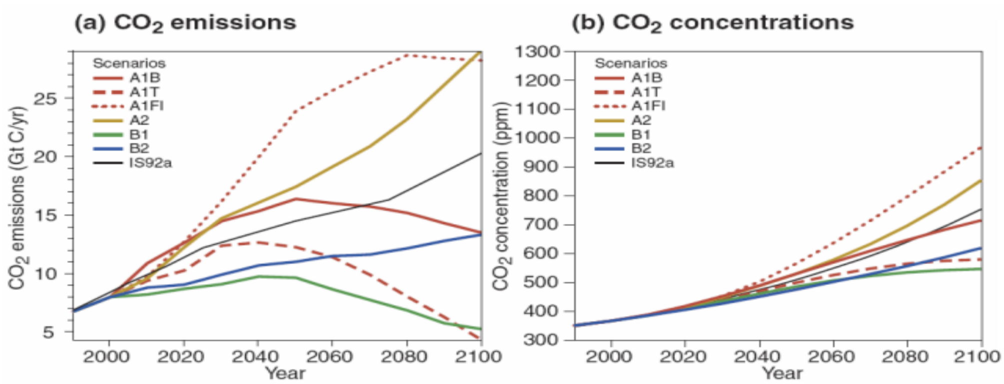

Figure A—1: CO2-emissions due to the different above listed scenarios(Jørgensen 2008).

Appendix B Bearing Capacity

The structural performance of the road is based on its bearing capacity and related to the mechanical behaviour of the material. When a moving wheel passes on the surface every soil element in the construction are affected by the stress regime shown in Figure B—1.

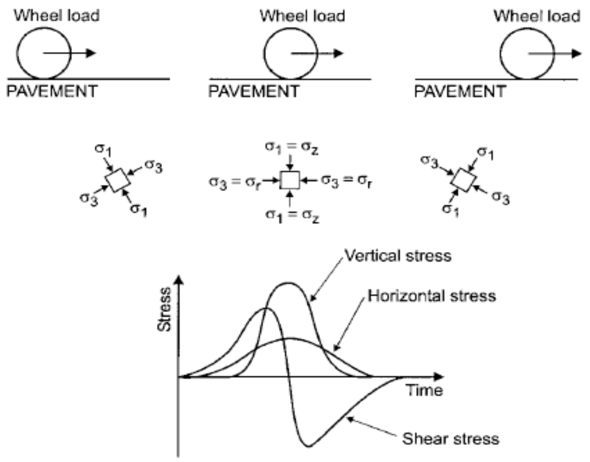

Figure B—1: Stress regime in a soil element due to a single wheel load (Lekarp, Isaccson 2000).

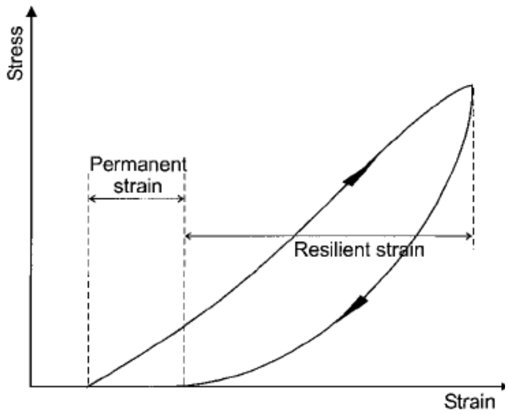

Figure B—2: Hysteresis loop outlining the resilient and permanent strain response of unbound materials subjected to loading (Lekarp, Isacsson & Dawson 2000).

Every element in layer is subjected to vertical- , horisontal- and shear stresses. Since the vertical and horisontal stresses are positive and that the shear stresses are reversed the axes of principal stresses will rotate, as a wheel passes the surface. This stress regime leads to a deformation of the material, which can be deduced to a result of three mechanisms:

1) Consolidation (dilatation)
2) Distortion
3) Attrition

The first comes from a change in shape and compressibility. Distortion is caused by bending, sliding and rolling of particles and attrition occurs when the particles undergo stresses that exceeds the strenght of the particles thus leading to breakage of the particles (Lekarp, Isaccson 2000).

Deformation characteristics

The deformation of a unbound granular soil specimen can be characterized as either resilient (elastic) or permanent (plastic) as shown in Figure B—2.

Elastic Theory

The theory of elasticity is based on Hooke's Law and applied when bearing capacity is determined. When subjecting a cube to a uniform stress (σ_z) it will show a change in length (ε_z). The ratio between the stress and strain is a constant expressed as the Coefficient of Elasticity or E-modul (E).

$$E \cdot \varepsilon_z = \sigma_z \qquad \textit{Eq. B-1}$$

or

$$E = \frac{\sigma_z}{\varepsilon_z} \qquad \textit{Eq. B-2}$$

Another important parameter is Poissons Ration, ν, which is the nummerical ratio between vertical and horisontal displacement (Eq. B-3).

$$\nu = \left| \frac{\varepsilon_x}{\varepsilon_z} \right| \qquad \textit{Eq. B-3}$$

The parameters are illustrated in Figure B—3.

Figure B—3: Elastic parameters for uniaxial stress. From (Ullidtz 1998).

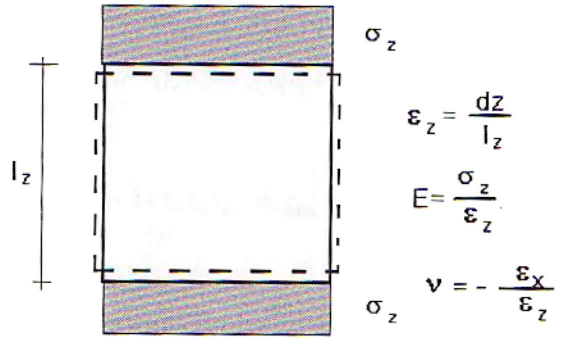

Poissons Ratio is dependent on the single material. For most granular materials a value of 0.35 can be used.

The E-modulus of a soil is a difficult parameter to determine since it depends on many factors such as water content, stress state and density. But also the loading time when obtaining the modulus is of importance. Considering the stress-strain relationship for a given soil several moduli can be obtained as shown in Figure B—4.

Figure B—4: Different obtainable slopes for describing soil E-moduli. From (Briaud 2001).

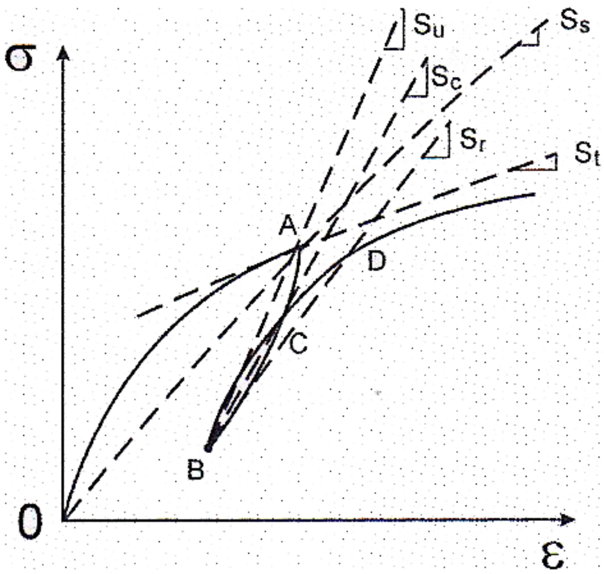

The solid line describes the stress-strian relationship for a single reloading cycle from the origin (O) to point A, back to point B and returns through C and D when loading is resumed. Dotted lines are different obtainable slopes of the curves. If a slope is drawn from the origin (O) to the point A, the secant slope S_S is obtained and hence the Secant Modulus can be calculated from it. This E-modulus is useful when the movement due to any initial loading is wanted. If a slope is drawn as the tangent to the considered point one would obtain the tangent slope S_t. The tangential modulus E_t could hence be calculated and is considered useful when an incremental movement due to an incremental loading is wanted. The unloading slope from point A to B indicates the unloading slope S_u and is useful for pavement design. The unloading modulus E_u is calculated from it and is useful when calculating the rebound of a pavement after a truck tire loading. This value represents the resilient modulus and will describe the reversible strain under repeated loads. A slope drawn from point B to D would represent the reloading curve. The reloading moduus E_r could be obtained from this slope and could be used to calculate the movement of the pavement under reloading by the same truck load S_c refers to the cyclic slope and are drawn from point B through C. The cyclic modulus E_c can be calculated from this and used when predicting movement due to cyclic loading (Briaud 2001).

Boussinesqs Equations

In 1885 Boussinesq developed equations for calculating the stresses, strains and displacements in a homogeneus, isotropic, linear elastic, semi infinite space with modulus E, Poisson Ratio ν, loaded by a point P, perpendicular to the surface.

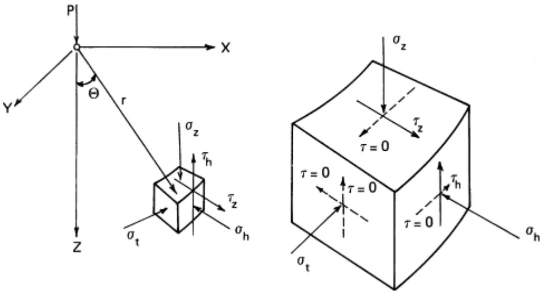

Figure B—5: Stress distribution under a vertical point load at the surface. After Boussinesq. Source: www.sciencedirect.com.

$$a)\ \delta_z = \frac{3P}{2\pi z^2}\cos^5\theta$$

$$b)\ \sigma_h = \frac{P}{2\pi z^2}\left[3\cos^3\theta\sin^2\theta - (1-2v)\frac{\cos^2\theta}{1+\cos\theta}\right]$$

$$c)\ \sigma_z = -(1-2v)\frac{P}{2\pi z^2}\left[\cos^3\theta - \frac{\cos^2\theta}{1+\cos\theta}\right]$$

$$d)\ \tau_{hz} = \frac{3P}{2\pi z^2} - \cos^4\theta\sin\theta$$

Boussinesqs equations for calculating stresses and displacements under a point load P perpendicular to load surface.

From the equations it can be noticed that the vertical stress and the major principal stress are independent of elastic parameters. The modulus does, in other words, not affect the stresses (Ullidtz 1998).

If the distance from the point load is known, the vertical normal stress (σ_{zz}) in an arbitrarily point under the surface can, according to Boussinesq, be calculated from Eq. B-4.

$$\sigma_{zz} = \frac{3P}{2\pi h^2}\cdot\frac{1}{\left[1+\left(\frac{r}{h}\right)^2\right]^{\left(\frac{5}{2}\right)}} \qquad \textit{Eq. B-4}$$

where, P is the point load, r is the perpendicular horizontal distance and h is the depth at which the stresses are requested. The design load for pavements is presumed as represented by a uniformely distributed load of a circular elastic plate with radius (a) as represented in Eq. B-5.

$$P = \sigma_0 \cdot 2\cdot\pi\cdot r\cdot dr \qquad \textit{Eq. B-5}$$

where, P is the tire load, σ_0 is the contact pressure between tire and surface[1], r is smallest radius for the circle representing the tire. If the point load (P) of Eq. B-4 is replced by the design load in Eq. B-5 the equation reduces to:

$$\sigma_{zz} = \sigma_0 \cdot \left(\frac{1}{\left[1+\left(\frac{a}{h}\right)^2\right]^{\left(\frac{3}{2}\right)}}\right) \qquad \textit{Eq. B-6}$$

where, a is tire radius and σ_0 is the contact pressure between the road surface and tirepressure.

Odemarks Method

A road construction does not consist of a semi-infinite halfspace as assumed in the equations of Boussinesq. The construction is made up of more layers each having specific characteristics. To calculate stresses and strains in a layered construction The Method of Equivalent Thickness (MET) can be used. The principle is to convert the layers into one homogeneus layer allowing Boussinesqs equations to be used.

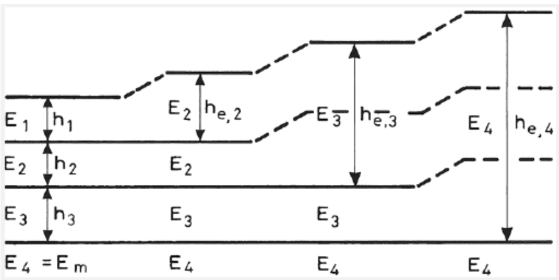

Figure B—6: The theoretical transformation approached with MET. At first, the upper layer is transformed corresponding to the second layer's E-modul. Thereafter the second layer is tranasformed into the third layers E-value, etc. Source: (Bolet 2010).

A precondition for using MET is that E-moduli will decrease from top to bottom. With the purpose of calculating the normal stresses by using Eq. B-6 the following can be used to determine the increased equivalent thickness of the upper layer (Bolet 2010).

1 0.7 or 0.9 MPa. If 0.7 is used the wheel radius can be determined to be 165mm and if 0.09 is used the wheel radius is reduced to 157mm.

$$h_e = f \cdot h \cdot \sqrt[3]{\left(\frac{E_{upper}}{E_{lower}}\right)} \qquad \textit{Eq. B-7}$$

where, h_e is the equivalent heigth, f is a factor of correction taking into account linear-elastic assumptions and E refers to the specific layers elastic stiffness. Using these equations will allow to calculate the stresses on top of each layer of the construction due to a wheel load on the surface.

When designing in accordance with the dansish design guideline (Vejregelrådet 2007) maximum allowable stresses on top of each unbound layer is considered. Eq. B-8 shows the requirement set in the danish regulation for road design.

$$\sigma_N = 0.086 MPa \left(\frac{E}{160}\right)^{1.06} \cdot \left(\frac{N_{Æ10}}{10^6}\right)^{-0.25} \qquad \textit{Eq. B-8}$$

Where σ_N and $N_{Æ10}$ refers to the maximum permissible stresses on top of the unbound layers and the equivalent 10 tons axels respectively. E refers to the examined layers E modulus and thus regarding a specific permissible stress rate in the light of a specific obtained E modulus/moduli for the considered surface. The foundation of this equation is based on three internal reports from The Asphalt Industri Research Laboratory and is written by J.M. Kirk in 1971. The first article examine the possibility of using theory of elasticity to determine stresses of the unbound layers according to the AASHO road tests (Busch 2009).

Plate load test

The modulus may be obtained in the field using plate load test. The generel formula, derived on the basis of Boussinesqs equations, for obtianing the surface modulus is shown in Eq. B-9.

$$E_0 = f \frac{(1-\nu^2)\cdot\sigma_0\cdot a}{d_0} \qquad \textit{Eq. B-9}$$

Where, E_0 is the surface modulus, f i a distribution factor (= 2 in the case of a rigid plate), ν is Poissons Ratio, σ_0 is the applied surface stress [MPa or kN/m^2], a is radius of plate used [mm] and d_0 is deflection measured [μm]. (Vejdirektoratet 2007).

Unbound materias show non-linear behaviour. The E-modulus obtained can be expected to vary if different stress levels are applied due to the non-linearity between stress and deflection. Taking into consideration this non-linearity the surface modulus can be described using Eq. B-10.

$$E_0 = C_0 \left(\frac{\sigma_0}{100kPa}\right)^n \qquad \textit{Eq. B-10}$$

Where, E_0 is the surface modulus, C_0 is the surface modulus at at contact pressure of 100kPa chosen as a convinient reference (≈ 1atm.) σ_0 is applied surface stress and n describes the materials non-linearity. For cohesive materias, n-values are negative and for friction based materials n-values can be expected positive. (Vejdirektoratet 2007).

Plastic theory

If the strain is not fully recovered a irecoverable strain is obtained. This can be due to the mechanisms listed above. For granular materials this deformation will occur momentaneouesly with the applied load and can be denoted as compaction. The copaction properties can be investigated in the laboratory by the Proctor compaction tests. The compaction process will be very dependent upon water content since water will act as a lubricant, and hence reduce friction, and will allow the particles to 'pack' even further.

California Bearing Ratio (CBR) - Value

Since the typical road construction consists of several layers with varying properties, the design of road constructions are based upon theory of elsticity and additionally, road constructions will not deteriorate due to a plastic failure but rather as a consequence of a fatigue failure or by an accumulation of small permanent deformations of the layers or the subgrade.

The CBR - value is obtained by lowering a piston into a soil specimen of controlled velocity which will resut in a plastic deformation of the soil. The CBR - value is thus a measure of the specific soils resistance against plastic deformation. The following empirical relation can be used between the E-value and CBR - value (Thagesen 2009).

$$E = 10 \cdot CBR \qquad \textit{Eq. B-11}$$

The value obtained will be highly dependent upon water content and density of the material. Fully saturated conditions of the unbound materials can be expected due to high water table or periods of heavy rainfall it is often steted that CBR - values (if used) should be obtained on soil specimens prepared by a minimum of 4 days of complete wetting (Thagesen 2009).

Viscous properties

When a saturated soil specimen is subjected to loading positive pore pressure can occur. Excessive pore pressure is drained and entails a permanent strain development. For sand and gravel the permanent strains are primarily obtained as a consequence of consolidation or distortion mechanism.

Effective Stresses

A main geotechnical consideration is the distinction between total and effective stresses as presented in Eq. B-12.

$$\sigma' = \sigma - u \qquad \textit{Eq. B-12}$$

where,

σ: total stresses

σ': effective stresses

u: pore pressure

The equation states that the total stresses σ are reduced due to the influence of pore pressure Adding water influences the effective stresses in two ways depending on the degree of saturation.

- **Negative pore pressure (suction)**
- **Positive pore pressure**

The relation between matric suction and degree of saturation is illustrated in Figure B—7.

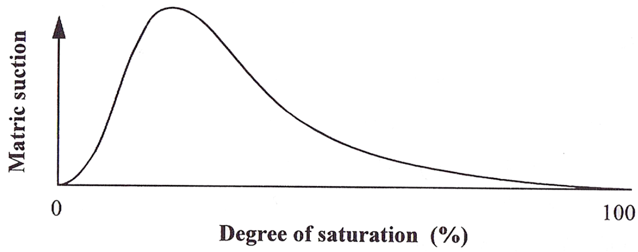

Figure B—7: Suction as a function of the percentage of saturation. From (Kolisoja 1997)

If the material is dry no suction due to capillary forces exists. When degree of saturation increases the matric suction will increase as well until the degree of saturation reaches a point where the surface tension between air bubbles and water will at this stage only produce slightly negative pore pressures thus reducing the effective stresses.

The Soil Water Characteristic Curve (SWCC)

To provide a relationship between the matric suction and the water content, the SWCC can be used. An example is shown in Figure B—8.

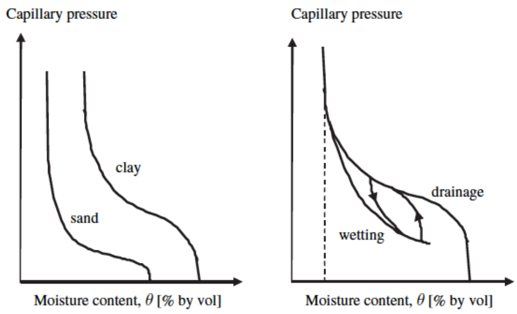

Figure B—8: Typical characteristic curves for sand and clay. Soil water characteristic curve showing drainage, wetting. (left) dotted line represents the residual water. From (Dawson 2008).

Saturating the materials above a specific value will thus lead to a signigficant decrease in the capillary effects of the specific soil. Since clayey materials will contain more water than the coarser-grained the irreducible water level will be smaller for the coarse-grained material (left figure).

When subjecting the specific soil specimen to wetting drying cycles it can be observed that drainage from a saturated level will result in higher capillary pressures than if the same material is wetted from a dry state. This is presented in Figure B—8 (right) and is caused by hysteresis. If the wetting or drying process is interrupted between the two endpoints of saturation the 'scanning' curves are followed (Dawson 2008).

To describe the relationship between moisture content for a specific soil and the matric suction the van Genuchten Model shown in Eq. B-13 can be used:

$$\Theta = n\left[\frac{1}{1+(\alpha\psi)^{N}}\right]^{M} \qquad \text{Eq. B-13}$$

where, α, N and M constants determined based on experiments. ψ in an air entry value which is the matric suction at which air starts entering the largest pores in the soil. Another, later developed model by Fredlund and Xing (1994) can be used considering the pore size distribution. (Eq. B-14). (Dawson 2008).

$$\theta = n\left[\frac{1}{\ln\left(e+\left(\frac{\psi}{\alpha}\right)^{N}\right)}\right]^{M} \qquad \text{Eq. B-14}$$

where,α, N and M are different parameters than those of Eq. B-13, but has to be determined experimentally, n is the porosity and ψ: matric potential in metres. Two SWCC of typical coarse and fine-grained materials can be seen in Figure B—9.

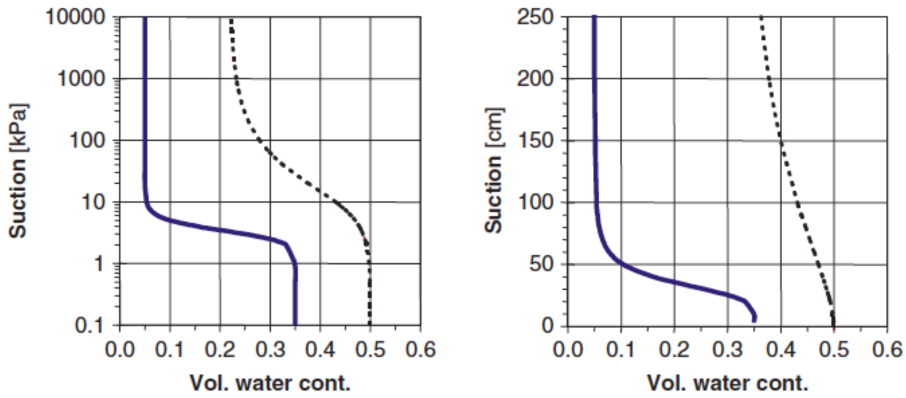

Figure B—9: SWCC for fine (dotted)- and coarse-grained (solid line) material. From (Dawson 2008).

Capillary rise (negative pore pressure)

Bearing capacity variations can be expected for a road construction due to capillary forces when the material are subjected to different levels of saturation. The capillay rise can be estimated by the following relation: (Ovesen, Fuglsang & Bagge 2009).

$$h_c \cdot d_{10} \cdot e = \text{c} \qquad \text{Eq. B-15}$$

Where, h_c is the capillary rise, d_{10} is the 10% fractile of the grain size distribution, *e* is the pore number and c is a constant ranging from 0.1 - 0.5 cm^2.

Positive Pore Pressure

Positive pore pressure can occur in saturated material when exposed to external loading. According to Eq. B-12, the effective stresses will be reduced due to a positive pore pressure.

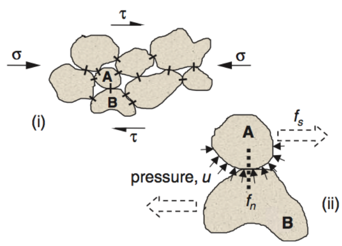

Figure B—10: Schematic inter-particle forces. 1: an assembly of particles subjected to stresses. 2: when water is added, interparticle force fn is reduced. From (Dawson 2008).

Shear Strength

As shown in Figure B—10 the effective stresses will be reduced as pore pressure builds up. The shear strenght will decrease as well. Figure B—11 shows the Mohr-Coloumb failure envelope.

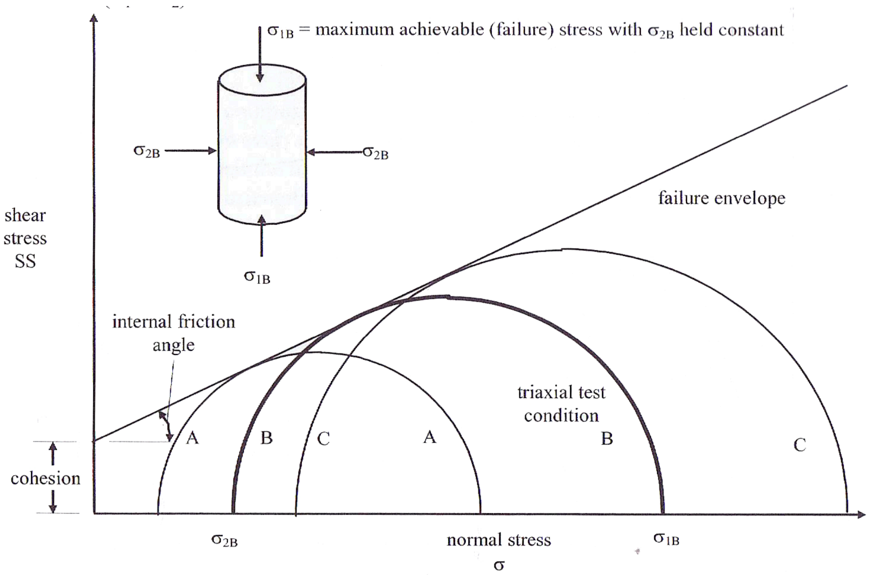

Figure B—11: The Mohr-Culoumb failure criterion. From [Lay_2009]

When stresses are reduced to effective stresses the highest principal stress is reduced and the slope of the Mohr-Coulomb failure envelope reduces. (Eq. B-16).

$$\tau_f = c' + \sigma'_f \tan(\varphi') \qquad \textit{Eq. B-16}$$

Stiffnes is similarly affected since it is beeing approximately proportional to the square root of the intergranular stress (Lay 2009: p.178). And is affected due to frictional effects. (Dawson 2008: p.19).

When negative pore pressure exists in a soil specimen an increase in effective stresses can be expected and hence an increase in the coefficient of elasticity. On the other hand, when positive pore pressure exists in a soil specimen the stresses reduces and hence the coefficient of elasticity (E) reduces as well. This further entail that the layers thickness' increases when designing based on Method of Equivalent Thickness' for the case of having a positive pore pressure and reduces when having a negative.

Appendix C Mathematical Modelling Of Pavement Performance (MMOPP)

In June 2011 a revised manual for the use of software Mathematical Modelling Of Pavement Performance (MMOPP) was presented by (Vejregel Arbejdsgruppe p.21 2011). MMOPP is attached to the danish procurement regulation for road design. (Vejregelrådet 2007). The program is capable of designing flexible, semi-flexible or simi-rigid and concrete pavements in terms of an analytical approach and simulate the deterioration progress of flexible pavements.

Design by Simulation

The simulation of a road construction and pavement is made mathematically by letting a wheel pass a stretch of road with a given length under different speed and climatic conditions. The calculations are made in terms of the specific period of year. This allows for incorporation of a homogenues procedures with the specific amount of traffic allowing a recursiv effect, of earlier years deterioration, to be considered. The simulation of the deterioration process is based upon six different models. This appendix considers the relevant model due to climatic changes. The six different models used in the software are listed a) - f). The underlined *Climatic Model* is enhanced below.

a) Construction model. Determines the properties of the specific layers, height and the surface of the pavement.

b) Loading model. Determines the correlation between the geometry of the surface and the impact caused by the movements of the wheel.

c) Climatic model. Determines the correlation between the deformational mechanisms of the materials and the climate.

d) Model of response. describes how the impact on the surface is distributed through the construction. This model is based on Boussinesq's and Odemarks assumptions.

e) Structural deterioration (cracking). Determines the correlation between the dynamic effects and the deterioration of the asphalt layer.

f) Model of permanent deformations. (roughness and rutting). Determines the correlation between the dynamic effects and permanent defomations.

Climatic Model

The Climatic Model (CM) is based upon two sub-models that determines the materials bearing capacity in terms of E-moduli for different periods of year and calculates the the depth of frost impact for the winther period.

E-modul Model

Simple tablefunctions are used for determine the E-moduli of the materials during the different periods of year.

The climatic parameters used are based upon simple modified climatic parameters from Skåne, Sweden. Parameters are listed in Table C-1.

Table C-1: Modified climatic parameters from Skåne, Sweden. Used in MMOPP. (Vejregel Arbejdsgruppe p.21 2011).

Period	Day	Temp	E_1	E_2	E_3	E_m
-	-	°C	-	-	-	-
Winter	49	-2	4	4.2	10	20
Winter (thaw)	10	1	3.7	0.3	10	20
Spring (thaw)	15	1	3.7	0.7	0.7	0.6
Late spring	46	4	3.1	1.0	0.8	0.8
Summer	143	20	1.0	1.0	1.0	1.0
Heat wave	10	50	0.3	1.0	1.0	1.0
Autumn	92	7	2.6	1.0	1.0	1.0

The E-moduli values used for input in MMOPP is based upon the conditions for the summerperiod. (factor 1.0 for each layer).

Model Determinig the Impact of Frost

Impact of frost depth impact is based upon a model expressed in regulations from Switzerland. The model is shown in Eq. C-1.

$$\text{Frost impact depth} = 45mm \cdot \text{days with degees below freezing}^{0.5} + \text{thickness of construction (mm)}/2 \quad \textit{Eq. C-1}$$

The days with degees below freezing is are calculated based on time series for the years 1873 - 2003 registered by DMI at Tranebjerg (Station 27080).

The 24 previous hours maximum and minimum values are are registered and based on the assumption that average max and min value for these time intervals represents the daily average values of min and max the daily average is calculated. Additionaly, accumulated days of degrees below freezing are thus calculated for periods with freezing temperatures and the highest number of days with degrees below freezing for each single year are thus saved as representing the number of days below freezing for the year considered.

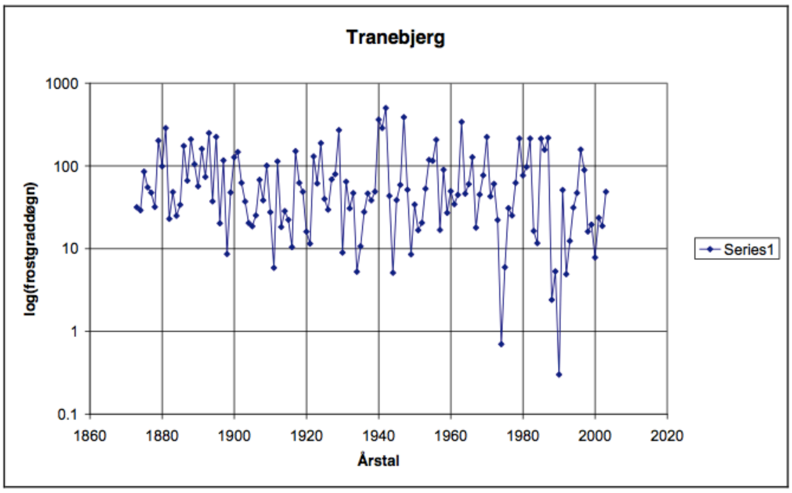

Figure C—1: Days with degrees below freezing. (Vejregel Arbejdsgruppe p.21 2011).

The result is presented in Figure C—1. The days of degrees below freezing can be described by logaritmic normal distribution with average 1.64 (43.9 °C x days) and standard deviation 0.53 (sdf factor 3.39)

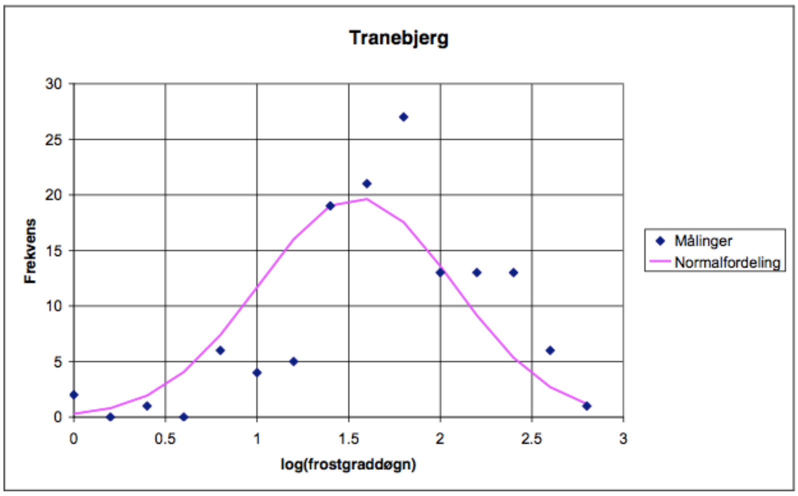

Figure C—2:Distribution of days with degrees below freezing. (Vejregel Arbejdsgruppe p.21 2011).

For every year the program will pick a stochastic value of days with degrees below freezing baed on the logaritmic normal distribution and hence, calculate the depth of frost impact based on Eq. C-1.

Appendix D TRVK-Väg

Kapitel 4: Bärförmåga, stadga och beständighet

See the following pages.

Excerpts from the swedish design guideline for climatic zones and stiffness parameters for the unbound layers.

Source:
TRVK Väg TRV 2011:072 TDOK 2011:264. Trafikverket, published 2011-06-15. Found at http://publikationswebbutik.vv.se/shopping/ShowItem____5343.aspx, Date: 2011-03-08.

TRVK Väg

Trafikverkets tekniska krav Vägkonstruktion

TRV 2011:072

TDOK 2011:264

Anläggningsstyrning

4 Bärförmåga, stadga och beständighet

4.1 Allmänt

Vägöverbyggnad ska konstrueras så att kraven på ingående delars dimensionerande tekniska livslängd, enligt IFS 2009:2 Bilaga A, uppnås.

Vägöverbyggnad ska dimensioneras enligt någon nedanstående dimensioneringsklasser, DK.

4.1.1 Nybyggnad

DK 1 – Tabellmetod enligt VVMB 302, maximal trafikbelastning 500 000 standardaxlar, under dimensioneringsperioden.

DK 2 – Empirisk/mekanistisk dimensionering

DK 3 – Avancerade mekanistiska modeller och laboratorie provning

4.1.2 Underhåll/förstärkning

DK 1 – Index metoden (kan även användas för kalla och halvvarma beläggningsmassor vid nybyggnad) enligt VVMB 302, maximal trafikbelastning 500 000 standardaxlar, under dimensioneringsperioden.

DK 2 – Empirisk/mekanistisk dimensionering

DK 3 – Avancerade mekanistiska modeller och laboratorie provning

4.2 Klimat

Överbyggnad i DK 1 och 2 ska dimensioneras för aktuell klimatzon. Denna framgår av VVFS 2004:31 ”Vägverkets föreskrifter om bärförmåga, stadga och beständighet hos byggnadsverk vid byggande av vägar och gator”, se illustration 4.2-1 nedan.

Vid tveksamheter ska högre klimatzon väljas.

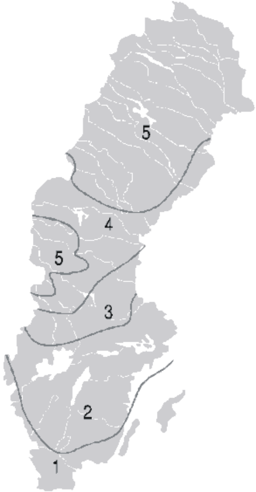

Illustration 4.2-1 Illustration av klimatzoner

Flexibla överbyggnader ska konstrueras för klimatperioder med längd enligt tabell 4.2-1.

Tabell 4.2-1 Klimatperiodens längd DK 2 [antal dygn under året]

	Klimatzon				
	1	2	3	4	5
Vinter	49	80	121	151	166
Tjällossningsvinter	10	10			
Tjällossning	15	31	45	61	91
Senvår	46	15			
Sommar	153	153	123	77	47
Höst	92	76	76	76	61

Bitumenbundna lager ska dimensioneras för beläggningstemperaturer enligt tabell 4.2-1.

Tabell 4.2-2 Temperatur i bitumenbunden beläggning, DK 2 [^{o}C]

	Klimatzon				
	1	2	3	4	5
Vinter	-1,9	-1,9	-3,6	-5,1	-7
Tjällossningsvinter	1	1			
Tjällossning	1	2,3	4,5	6,5	7,5
Senvår	4	3			
Sommar	19,8	18,1	17,2	18,1	16,4
Höst	6,9	3,8	3,8	3,8	3,2

Överbyggnad i DK 3 kan dimensioneras med klimatdata och beläggningstemperaturdata från mätningar.

4.5.4 Obundna lager, underhåll och bärighetsförbättring

4.5.4.1 Obundna överbyggnadsmaterial, nyare material

Styvhetsmodulerna i tabell 4.5-8 – 4.5-10. avser obundna överbyggnadsmaterial som uppfyller materialkrav för nyare material enligt TRVMB 120 ”Inventering av befintlig väg”.

Tabell 4.5-8 Styvhetsmoduler, Ms, (MPa) för obundna överbyggnadsmaterial.

Dräneringsgrad 1	Bärlager	Förstärkningslager		Skyddslager
		Okrossat	Krossat	
Vinter	1000	1000	450	1000
Tjällossningsvinter	150	1000	450	1000
Tjällossning	300	160	450	70
Senvår	450	240	450	85
Sommar	450	240	450	100
Höst	450	240	450	100

Tabell 4.5-9 Styvhetsmoduler, Ms, (MPa) för obundna överbyggnadsmaterial.

Dräneringsgrad 2	Bärlager	Förstärkningslager		Skyddslager
		Okrossat	Krossat	
Vinter	1000	1000	450	1000
Tjällossningsvinter	150	1000	450	1000
Tjällossning	300	160	450	70
Senvår	450	240	450	85
Sommar	450	240	450	85
Höst	450	240	450	85

Tabell 4.5-10 Styvhetsmoduler, Ms, (MPa) för obundna överbyggnadsmaterial.

Dräneringsgrad 3	Bärlager	Förstärkningslager		Skyddslager
		Okrossat	Krossat	
Vinter	1000	1000	450	1000
Tjällossningsvinter	150	1000	450	1000
Tjällossning	300	160	450	70
Senvår	450	160	450	70
Sommar	450	160	450	70
Höst	450	160	450	70

4.5.4.2 Övriga obundna överbyggnadsmaterial

Styvhetsmodulerna i tabell 4.5-11 – 4.5-13 avser obundna överbyggnadsmaterial som uppfyller materialkrav för äldre material enligt TRVMB 120 ”Inventering av befintlig väg”.

Tabell 4.5-11 Styvhetsmoduler, Ms, (MPa) för äldre obundna överbyggnadsmaterial.

Dräneringsgrad 1	Bärlager	Förstärkningslager
Vinter	1000	1000
Tjällossningsvinter	100	1000
Tjällossning	200	100
Senvår	300	125
Sommar	300	150
Höst	300	150

Tabell 4.5-12 Styvhetsmoduler, Ms, (MPa) för äldre obundna överbyggnadsmaterial.

Dräneringsgrad 2	Bärlager	Förstärkningslager
Vinter	1000	1000
Tjällossningsvinter	100	1000
Tjällossning	200	100
Senvår	300	125
Sommar	300	125
Höst	300	125

Tabell 4.5-13 Styvhetsmoduler, Ms, (MPa) för äldre obundna överbyggnadsmaterial.

Dräneringsgrad 3	Bärlager	Förstärkningslager
Vinter	1000	1000
Tjällossningsvinter	100	1000
Tjällossning	200	100
Senvår	300	100
Sommar	300	100
Höst	300	100

4.5.5 Undergrundsmaterial

4.5.5.1 Undergrundsmaterial, nybyggnad

Tabell 4.5-14 Styvhetsmoduler, Ms, (MPa) för material i underbyggnad och undergrund

	Materialtyp 2	3	4	5
Vinter	1000	1000	1000	1000
Tjällossningsvinter	1000	1000	1000	1000
Tjällossning	70	35	30	10
Senvår	85	50	40	20
Sommar	100	100	50	45
Höst	100	100	50	45

4.5.5.1.1 Underindelning av materialtyp 6 och 7

Styvhetsegenskaper för materialtyp 6 och 7 ska väljas efter särskild utredning.

4.5.5.1.2 Underindelning av materialtyp 4B samt materialtyp 5

Materialtyp 4B och 5A underindelas för bärighetsberäkning i följande klasser baserat på den odränerade skjuvhållfastheten hos leran. Särskild vikt måste läggas vid kontroll av leran eller silten vid utförandet så att inte skjuvhållfastheten som förutsattes vid dimensioneringen underskrids.

Tabell 4.5-15 Styvhetsmoduler Ms (MPa) för leror och silter

	Odränerad skjuv-hållfasthet c_u [kPa]	Styvhetsmodul Ms [MPa]
4B Fast lera, 5A Silt	> 75	Se Tabell 4.5-14
4C Medelfast lera, 5C	40-75	25 - 35
4D Lös lera, 5D	20-40	15 - 20
4E Mycket lös lera, 5E	20-10	10 - 15
4F Extremt lös lera, 5F	< 10	Särskild utredning

4.5.5.2 Undergrundsmaterial och övrigt överbyggnadsmaterial, underhåll och bärighetsförbättring

Tabell 4.5-16 Styvhetsmoduler, Ms, (MPa) för material i underbyggnad och undergrund, Dräneringsgrad 1.

Dräneringsgrad 1	Materialtyp 2	3	4	5
Vinter	1000	1000	1000	1000
Tjällossningsvinter	1000	1000	1000	1000
Tjällossning	70	35	30	10
Senvår	85	50	40	20
Sommar	100	100	50	45
Höst	100	100	50	45

Dessa värden ska även tillämpas på obundna överbyggnadsmaterial som inte kan klassas enligt 4.5.4.

Styvhetsegenskaper för materialtyp 6 och 7 ska väljas efter särskild utredning

Tabell 4.5-17 Styvhetsmoduler, Ms, (MPa) för material i underbyggnad och undergrund, Dräneringsgrad 2.

Dräneringsgrad 2	Materialtyp			
	2	3	4	5
Vinter	1000	1000	1000	1000
Tjällossningsvinter	1000	1000	1000	1000
Tjällossning	70	35	30	10
Senvår	85	50	40	20
Sommar	85	50	50	20
Höst	85	50	50	20

Dessa värden ska även tillämpas på obundna överbyggnadsmaterial som inte kan klassas enligt 4.5.4.

Styvhetsegenskaper för materialtyp 6 och 7 ska väljas efter särskild utredning.

Tabell 4.5-18 Styvhetsmoduler, Ms, (MPa) för material i underbyggnad och undergrund, Dräneringsgrad 3.

Dräneringsgrad 3	Materialtyp			
	2	3	4	5
Vinter	1000	1000	1000	1000
Tjällossningsvinter	1000	1000	1000	1000
Tjällossning	70	35	30	10
Senvår	70	35	30	10
Sommar	70	35	30	10
Höst	70	35	30	10

Dessa värden ska även tillämpas på obundna överbyggnadsmaterial som inte kan klassas enligt 4.5.4.

Styvhetsegenskaper för materialtyp 6 och 7 ska väljas efter särskild utredning

4.5.5.3 Material i undergrund och underbyggnad av materialtyp 1

Tabell 4.5-19 Styvhetsmoduler, Ms, (MPa) för material i underbyggnad och undergrund. Materialtyp 1, samtliga årstider och dräneringsgrader.

Fast berg M1a	Bergunderbyggnad M1b och M1c	Bergbank, äldre grovfraktion tjocklek ≥ 0,7 m	tjocklek < 0,7 m
1000	Se tabell i 4-20	300	200

Vid byggande av bergunderbyggnadskonstruktionerna M1b eller M1c på materialtyp 4B med underindelning, samt 5A med underindelning, ska lagret av sprängsten underindelas beräkningsmässigt i lika tjocka lager med varierande styvhet, se avsnitt 4.4.2.6.

Tabell 4.5-20 Styvhetsmoduler för sprängsten, Ms, (MPa) för beräkning av underbyggnadskonstruktionerna M1b och M1c, samtliga årstider och dräneringsgrader.

S1	S2	S3	S4
450	250	100	25

4.5.5.4 Materialegenskaper för särskilda underlag

Här anges materialegenskaper som kan användas vid beräkning av bärighet och tjällyftning för vägöverbyggnad. Om dessa egenskaper inte anses vara korrekta ska de egenskaper man avser att använda visas med hjälp av en särskild utredning.

Tabell 4.5-21 Styvhetsmoduler, Ms, (MPa) för särskilda material, samtliga årstider och dräneringsgrader.

	Styvhetsmodul
Lättklinker	40
Cellplast EPS[2)]	3[1)]
Cellplast XPS[2)]	10
Skumbetong, ρ_d=400 kg/m^3	800
Skumbetong, ρ_d=500 kg/m^3	1000
Skumbetong, ρ_d=600 kg/m^3	1250

[1)] Vanligen används dock en 10 cm tjock betongplatta ovan EPS-fyllning.

[2)] Finns dock i olika styvhetsklasser beroende på användning, kontakta leverantörer för materialegenskaper.

4.5.6 Övriga bundna lager

4.5.6.1 Bitumenindränkt makadam

Bitumenindränkt makadamlager delas upp i två skikt, ett övre 20 mm tjockt bitumenrikt skikt och ett undre bitumenfattigt skikt. Det bitumenrika skiktets styvhetsmodul sätts till 25 % av värdet för det

TRAFIKVERKET

Trafikverket, 781 87 Borlänge. Besöksadress: Röda vägen 1.
Telefon: 0771-921 921, Texttelefon: 0243-795 90

Appendix E Field Tests

The following appendix presents pictures taken during the field test series. The appendix is divided into 3 subsections concerning the construction of the field, the field testing equipment used, and the conduction of the tests. Captions include remarks of special considerations linked to the illustrations.

Construction of Test Field

Figure E—1: Test field before excavation.

Figure E—2: Excavated test field. Subgrade consisted of a firm bedded limestone. The field was excavated until 60 cm below surface. A metal frame was placed at the top edge to avoid for any collapse of the sourroundings.

Figure E—3: A tent was raised in order to control the the amount of water in the field. No rain or sunny periods would hence disturb the test series markedly.

Figure E—4: The subgrade was prepared by using a wood device for making a slope towards each side of the field.

Figure E—5: A geotextile was used to seal the test field in order to aviod leakage in the membrane. Saturated sand was used on the sides to paste the geotextile.

Figure E—6: The membrane was enrolled on the geoxtextile surface.

Figure E—7: Unrolled membrane ready for construction materials. The slope of the subgrade was tested by pouring water in the middle of the membrane and hence observe its flow. The tests showed that all water ended up near the edges. This was done in order to allow easier drainage of the construction.

Figure E—8: Construction of wells and drainage pipes. Subbase sand was used to make a slope of approximately 0.3 percentage towards the well. This was made in each side of the field.

Figure E—9: At each well the subgrade was excavated until 50 mm below subgrade surface. This was made in order to allow for easier drainage of the construction.

Figure E—10: When subbase was constructed the material was gently put down around the wells avoiding any disturbance of the wells and drainage pipes.

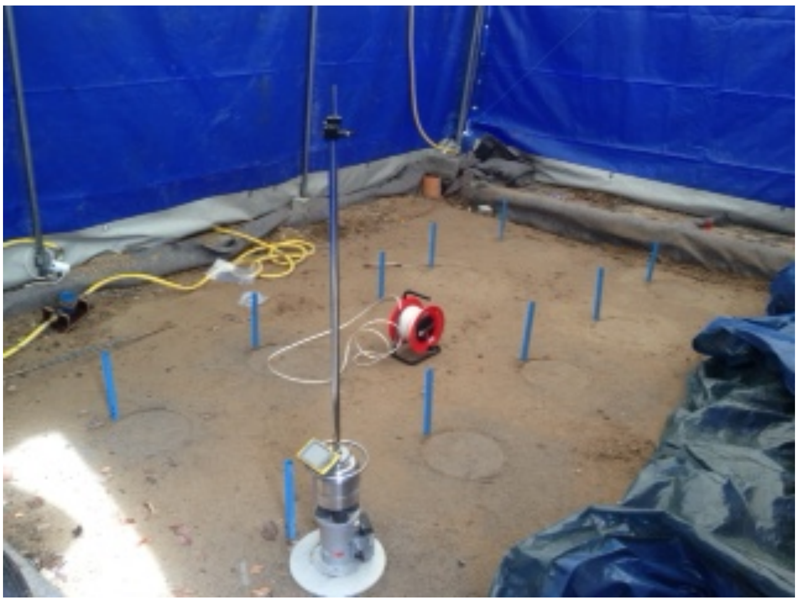

Figure E—11: SG2 material on top of sand layer finished the construction field. The LWD-tests were performed at the ten positions next to the ten standpipes. The device for sounding the water table was used at every position making it possible to correlate water table and E-moduli. The device is placed in the middle of the figure.

Figure E—12: By using a hammer and a metal device the ten positions were prepared by hammering the metal device into the construction so that standpipes could be easily lowered into the construction afterwords. This was done after the compaction process but before any LWD measurements were made.

Figure E—13: Water tanks used for rising the water table in the field. Hoses were connected to each of the two wells. This allowed the amount of water added at each step to be precisely determined. The flowmeter connected to the tank was used to note amount of water and was compared to the markings on the water tank showing good correlation.

Figure E—14: A tarpaulin was used to cover the field when waiting for a stable water table. This arrangement minimize the loss of water which could be expected due to evatransporation.

Figure E—15: The electric driven submersible pump used for lowering the water table. Equal amounts of water was pumped at each well and the pump was thus moved. The pump was connected to a flowmeter and values obtained using this device was compared with a bucket having a volume of ten litres. A high correlation was obtained.

Testing Equipment

Figure E—16: LWD-setup with a 15 kg drop weigth and 300mm diameter plate resulting in a contact pressure of ≈ 190 kPa when using full drop height (85cm).

Figure E—17: CPN nuclear density gauge.

Figure E—18: Vibratory plate. Specifications are given in table E-1.

Table E-1

Model no.	*HS - 120*
Shock Strenght	*3000 kg*
Maximum shock freq.	*5488 V.P.M.*
Move Speed	*0 - 30 M*
Flet Measurement	*670 x 480 mm*
Diesel Engine	*GX 160*
Power	*5.5HP*
Rotation Speed	*3600 R/MIN*
Weight	*120 kg*

Test Conduction

Figure E—19: Pouring water into the wells sometimes resulted in an overflow next to the well and paralel with the drainage pipes. This might have disturbed the expectance of a water table in the subbase layer due to increasing water content in the base layer.

Figure E—20: A trench was excavated, until ≈ 15 cm below surface, between step 3 and 4. This allowed following the water table precisely when it reached the base layer.

Figure E—21: Further compaction was obtained when using the LWD. length of standpipes above surface level was thus corrected severel times throughout the tests.

Figure E—22: When water table was close to surface a free water table in positions of LWD measurements could be observed close to field edges. Inlet was stopped at this stage. When water table was stabilized the free water table was drained and LWD measurements could be performed.

Figure E—23: With a high water table the dropped weight from the LWD caused a drainage of the baselayer. The geophone is placed in the middle of the contact plate and was sorrounded by water. The presence of water could have affected geophone measurements.

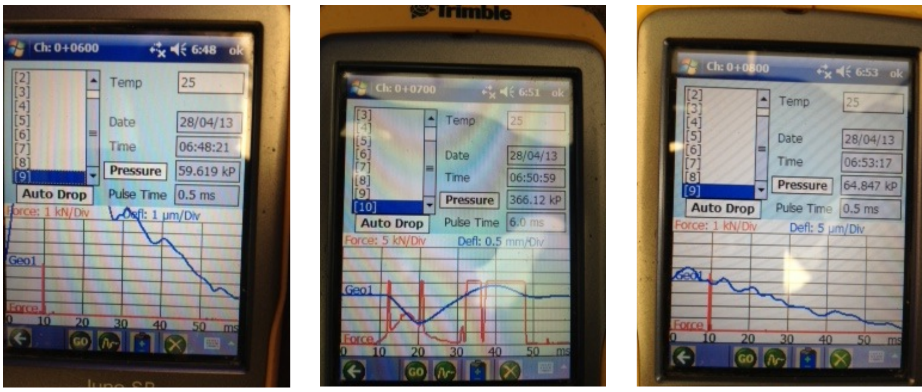

Figure E—24: Examples of different erronous force and deflection curves. These curves caused an impractical obtained E-moduli and could easily be deleted during the field tests. They were only obtained when having a high water table.

Appendix F Grain Size Distribution

References
AAU test manual based on DS/CEN ISO/TS 17892-4. DS/EN 933-1.

Preparations
Materials were collected and dried for 24 hours. Sample sizes were based on estimated D_{90} (Table F-1).

Table F-1: Sample size in regard of D_{90}.

D_{90} [mm]	Sample size [g]
0.5	50
1.0	100
4.0	150
6.0	350
8.0	600
16.0	2,500
22.4	5,000
31.5	10,000
45.0	20,000
63.0	40,000
75.0	56,000

Sample sizes choosen:

BL 2: 2,500 g

SG 2: 10,000 g

Results

BL 2

Sample	sk	280					
	Ws + sk	2900				Limits DS/EN 933-1	
Sieve [mm]	sk + Ws	sk	Ws	Pass. [g]	Pass. [%]	Sieve [mm]	
Sample size				2620,0		90	No larger
63	-	-	-		100,0	63	Max. 15% larger
31,5					100,0		
16	123,2	114,2	9	2619,1	100,0		
8	149,5	121,9	27,6	2591,5	98,9		
4	178,3	123,1	55,2	2536,3	96,8		
2	194,9	121,1	73,8	2462,5	94,0		
1	422,4	176	246,4	2216,1	84,6		
0,5	1116,6	169,74	946,86	1269,2	48,4		
0,25	1195,6	170,4	1025,2	244,0	9,3		
0,125	364,3	170,4	193,9	50,1	1,9		
0,063	209,3	168,9	40,4	9,7	0,4	0,063	Max 5% smaller
Rest	293,7	284	9,7	0,0			
			2619,1				

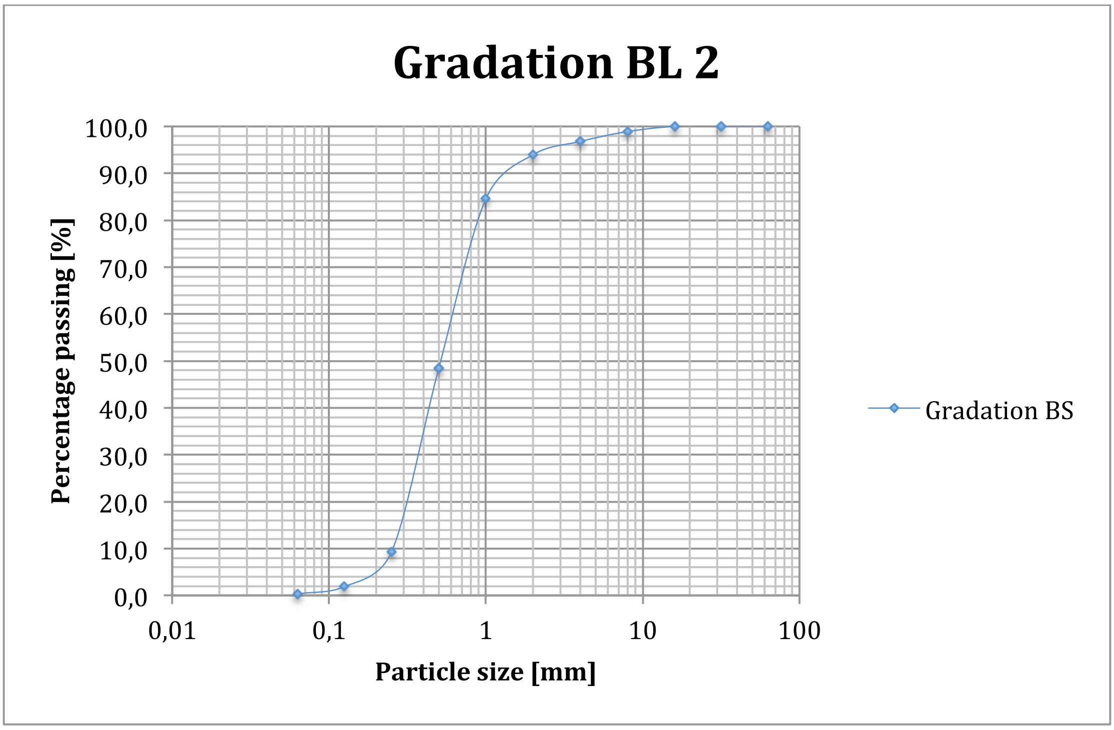

Figure F—1: Grain size distribution for BL 2.

SG 2

Prøve	sk	1920						
	Ws + sk	12360						
Sieve [mm]	sk + Ws	sk	Ws	Pass. [g]	Pass. [%]	Limits DS/EN 933-1		
Sample size				10440,0	100,0	Sieve [mm]	min	max
63	-	-	-	10449,6	99,9	63	100	100
31,5	293,3	114,3	179	10270,6	98,4	31,5	75	99
16	2926	286,9	2639,1	7631,5	73,1	16	50	90
8	2141	194,6	1946,4	5685,1	54,5	8	30	75
4	1218	194,4	1023,6	4661,5	44,7	4	15	60
2	862,8	168,4	694,4	3967,1	38,0	1	2	35
1	1349,6	246,5	1103,1	2864,0	27,4	0,063	2	9
0,5	1561	169,1	1391,9	1472,1	14,1			
0,25	1189	170,2	1018,8	453,3	4,3	63	100	100
0,125	321	121,8	199,2	254,1	2,4	31,5	75	99
0,063	212	122,9	89,1	165,0	1,6	16	50	90
Rest	286	121	165			8	30	75
			10449,6			4	20	60
						2	13	45
						1	8	35
						0,5	5	25
						0,063	2	9

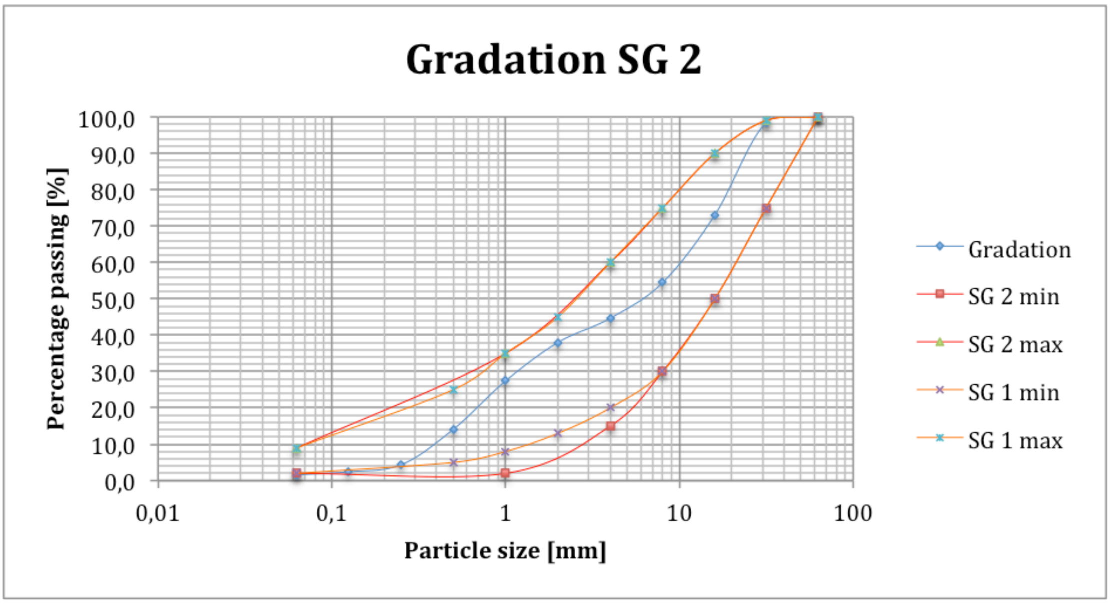

Figure F—2: Grain size distribution for SG2. SG1 and SG2 limits, in accordance with DS/EN 933-1 (Berg 2004) are also plotted.

Appendix G Sand Equivalent

References
DS/CEN ISO/TS 933-8:2001

Subbase sand (BL2)

BL	Part #1	Part #2
Mass [g]	120.21	120.25
h1 [mm]	105	105
h2	87	86
(h2/h1)*100	82.9	81.9
Sand equivalent	**SE = 82**	

Specification requirement according DS/CEN ISO/TS 933-8:2001

BL 1: at least 40

BL 2 : at least 30

Steady Gravel (SG2)

SG	Part #1	Part #2
Mass [g]	125.14	125,23
h1 [mm]	126	128
h2	86	86
(h2/h1)*100	67,2	68,3
Sand equivalent	**SE = 68**	

Specification requirement according DS/CEN ISO/TS 933-8:2001

SG 1: at least 34

SG 2: at least 30

Appendix H Proctor Tests

Tests for laboratory reference density and water content has been carried out in order to determine optimimum moisture content for the materials.

The tests are based on standard proctor compaction procedure.

References

DS/EN 13286-2 1. ed. 2004 - 11 - 01. Unbound and hydralically bound mixtures -- Part 2: Test methods for laboratory reference density and water content -- Proctor compaction.

Preperations

Specimen size and proctor mould are choosen according to Table H-1.

Table H-1: Proctor mould preperations for different sample sizes dependent of gradation. DS/EN 13286-2.1.

Percentage passing test sieves			**Preperation clause**	**Mass of sample [kg]**	**Proctor Mould**
16 mm	31.5 mm	63 mm			
100	-	-	6.4	15	A
				40	B
75 to 100	100	-	6.5.1	40	B
< 100	75 to 100	100	6.5.2	40	B
-	< 75	75 to 100	6.5.3	200	C

BL2:
Preparation 6.4
Mass of sample: 15 kg.
Proctor mould A

SG 2
Preparation 6.4
Mass of Sample: 15 kg.
Proctor mould A

Table H-2: Mass, diameter, height of fall, number of layers and blows per layer for the single proctor mould. DS/EN 13286-2.1.

Type of test	Characteristics of test	Symbol	Dimension	Proctor mould		
				A	B	C
Proctor test	Mass of rammer	m_R	kg	2,5	2,5	15,0
	Diameter of rammer	d_2	mm.	50	50	125,0
	Height of fall	h_2	mm.	305	305	600
	Number of layers	-	-	3	3	3
	Number of blows per layer	-	-	25	56	22

BL 2:
Mass: 2.5 kg.
Diameter: 50 mm.
Height of fall: 305.
Number of layers: 3
Number of blows per layer: 25.

SG 2
Mass: 2.5 kg.
Diameter: 50 mm.
Height of fall: 305.
Number of layers: 3
Number of blows per layer: 25.

Formulas

Water content

$$w = \frac{W_W}{W_S} \cdot 100\% = \frac{(W + sk) - (W_S + sk)}{(W + sk) - sk} \cdot 100\%$$

Dry specimen

$$W_t = \frac{W_W}{1 + {}^{w}\!/_{100}}$$

Dry density

$$\gamma_d = \frac{W_S}{V} \left[{}^{t}\!/_{m^3} \right]$$

Correction of discarded material ≥ 16 mm. (SG 2)

$$\gamma_{d,korr} = \frac{100}{\frac{s}{\gamma_s} + \frac{100 - s}{\gamma_d}}$$

Equipment

Volume of proctor mould

h=118mm

d=102mm

$\Rightarrow$ V=964211mm^3 $\Rightarrow$ 0.0009642m^3

Percentage discarded material

43,8% (SG2)

0% (BL2)

Test Results

BL 2

BL 2																
Tørrumvægt																
Forsøg nr	1,00	2,00	3,00	4,00	5,00	7,00	8,00	9,00	10,00	11,00	12,00	13,00	14,00	15,00	16,00	17,00
cyl + w	9400,00	9420,00	9440,00	9460,00	9500,00	9500,00	9510,00	9520,00	9530,00	9520,00	9530,00	9530,00	9520,00	9500,00	9510,00	9510,00
cyl	7700,00	7700,00	7700,00	7700,00	7700,00	7700,00	7700,00	7700,00	7700,00	7700,00	7700,00	7700,00	7700,00	7700,00	7700,00	7700,00
W	1700,00	1720,00	1740,00	1760,00	1800,00	1800,00	1810,00	1820,00	1830,00	1820,00	1830,00	1830,00	1820,00	1800,00	1810,00	1810,00
Ws	1600,26	1608,98	1619,78	1630,93	1649,16	1640,22	1658,33	1658,45	1659,04	1643,75	1635,73	1633,53	1585,20	1566,39	1564,94	1556,28
gamma d	1,69	1,70	1,71	1,73	1,75	1,74	1,75	1,75	1,76	1,74	1,73	1,73	1,68	1,66	1,66	1,65
	16,93	17,03	17,14	17,26	17,45	17,36	17,55	17,55	17,56	17,39	17,31	17,29	16,77	16,58	16,56	16,47
Vandindhold																
sk	3,17	3,18	3,07	3,05	3,09	3,08	3,15	3,09	3,10	3,10	3,20	3,10	3,10	3,10	3,20	3,20
sk + W	91,80	77,70	105,40	80,50	116,10	80,70	99,70	88,80	113,50	125,40	107,30	110,20	124,60	124,73	107,20	112,50
sk + Ws	86,60	72,89	98,33	74,82	106,63	73,81	90,68	80,50	101,78	112,27	93,87	96,30	108,15	107,68	93,12	93,12
Ww	5,20	4,81	7,07	5,68	9,47	6,89	9,02	8,30	11,72	13,13	13,43	13,90	16,45	17,05	14,08	19,38
Ws	83,43	69,71	95,26	71,77	103,54	70,73	87,53	77,41	98,68	109,17	90,67	93,20	105,05	104,58	89,92	89,92
w [%]	6,23	6,90	7,42	7,91	9,15	9,74	9,15	9,74	10,31	10,72	11,88	12,03	14,81	14,91	15,66	16,30

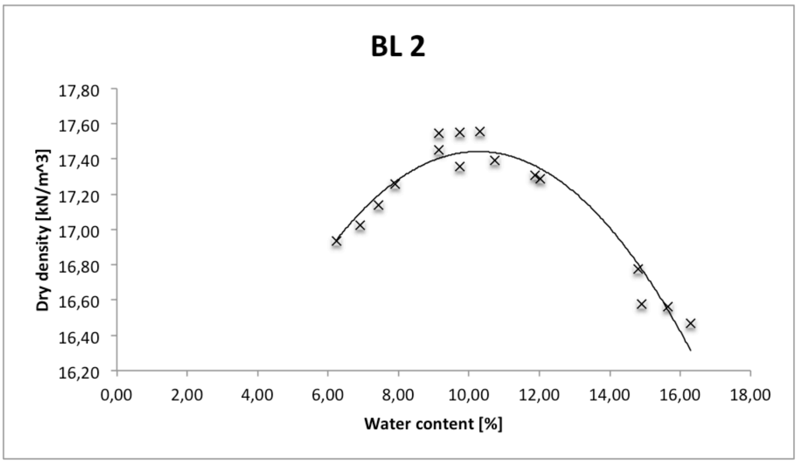

Optimum moisture content of 10%. MAximum drydensity 17.4 kN/m^3

SG 2

SG 2							
Tørrumvægt							
Forsøg nr	1,00	2,00	3,00	4,00	5,00	6,00	7,00
cyl + w	9700,00	9750,00	9820,00	9860,00	9830,00	9810,00	9760,00
cyl	7700,00	7700,00	7700,00	7700,00	7700,00	7700,00	7700,00
W	2000,00	2050,00	2120,00	2160,00	2130,00	2110,00	2060,00
Ws	1895,84	1935,46	1979,11	1991,34	1954,00	1927,59	1877,74
gamma d	2,01	2,05	2,09	2,11	2,07	2,04	1,99
gamma d korr	20,08	20,50	20,96	21,09	20,70	20,42	19,89
Vandindhold							
sk	4,22	4,26	4,25	4,24	4,22	4,25	4,65
sk + W	120,77	136,17	138,47	136,28	186,36	201,36	204,48
sk + Ws	114,70	128,80	129,55	125,97	171,31	184,32	186,80
Ww	6,07	7,37	8,92	10,31	15,05	17,04	17,68
Ws	110,48	124,54	125,30	121,73	167,09	180,07	182,15
w [%]	5,49	5,92	7,12	8,47	9,01	9,46	9,71

Test	**γ_d [kN/m^3] Correction**
1,00	**20,20**
2,00	**20,52**
3,00	**20,98**
4,00	**21,31**
5,00	**20,59**
6,00	**20,22**
7,00	**19,86**

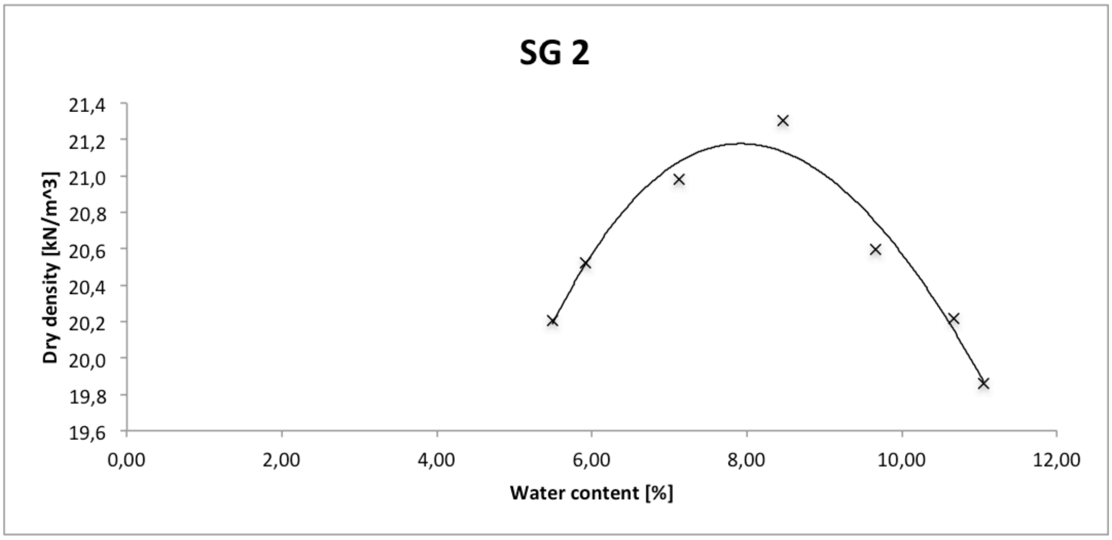

Optimnum moisture content 8 %. Maximum drydensity 21,2 kN/m^3.

Appendix I Loose/Dense Bedding

The test was based on (Danish Geotechnical Society 2001).

Preperations

Relative density. estimated: 2,65

Large Cylinder used

Diameter: 7.00 cm

Height': 14.40

Area: 38.48 cm^2

Volume: 554 cm^3

Solid bedding impacts:

Layer	Impacts
1	5
2	10
3	20
4	40
5	80

Formulas

Relative Compactness

$$I_D = \frac{e_{\max} - e_{insitu}}{e_{\max} - e_{\min}}$$

$$e_{insitu} = (1+w) \cdot \frac{d_s}{\gamma} \cdot \gamma_w - 1$$

$$e = \frac{d_s \cdot \rho_w \cdot V}{W_s} - 1$$

Results

BL 2

Loose Bedding

Test nr.	*1*	*2*	*3*
Area [cm^2]	38,48	38,48	38,48
h [cm]	14,40	14,40	14,40
V [cm^3]	554,00	554,00	554,00
Cyl + Ws [g]	2411,44	2410,64	2410,61
Cyl. [g]	1585,82	1585,82	1585,82
Ws [g]	825,62	824,82	824,79
e	0,7782	0,7799	0,7800
e - ave.			**0,78**

Dense Bedding

Test nr.	*1*	*2*	*3*
Area [cm^2]	38,48	38,48	38,48
h [cm]	12,36	12,92	12,28
V [cm^3]	475,61	497,16	472,34
Cyl + Ws [g]	2456,52	2488,67	2452,10
Cyl. [g]	1585,82	1585,82	1585,82
Ws [g]	870,70	902,85	866,28
e	0,4475	0,4592	0,4449
e-ave.			**0,45**

SG 2
Loose Bedding

Test nr.	*1*	*2*	*3*
Area [cm^2]	38,48	38,48	38,48
h [cm]	14,40	14,40	14,40
V [cm^3]	554,00	554,00	554,00
Cyl + Ws [g]	2509,32	2499,09	2487,95
Cyl. [g]	1585,82	1585,82	1585,82
Ws [g]	923,50	913,27	902,13
e	0,5897	0,6075	0,6274
e - ave.			**0,61**

Dense Bedding

Test nr.	*1*	*2*	*3*
Area [cm^2]	38,48	38,48	38,48
h [cm]	13,50	13,68	12,74
V [cm^3]	519,48	526,41	490,24
Cyl + Ws [g]	2662,03	2658,55	2590,15
Cyl. [g]	1585,82	1585,82	1585,82
Ws [g]	1076,21	1072,73	1004,33
e	0,2791	0,3004	0,2935
e-ave.			**0,29**

Appendix J Permability

Tests series were performed on both materials (BL 2 and SG 2). Determining:

- Hydraulic Conductivity
- Coefficient of Permability

Tests were performed in a falling head apparatus. See Figure J—1.

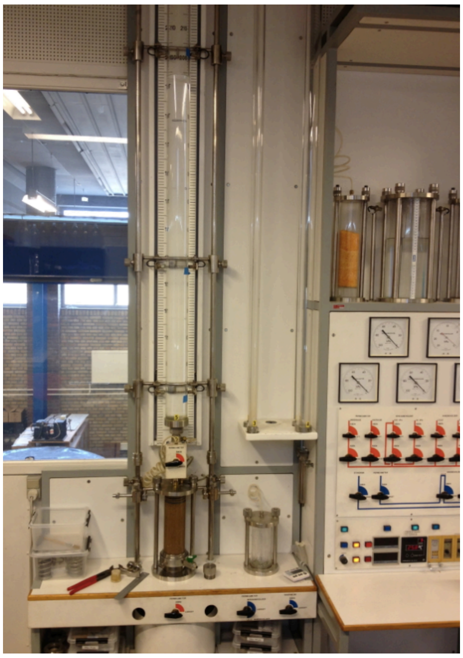

Figure J—1: Falling head test apparatus.

Preparations

To initiate the conditions for the as-built road construction, material were compacted into the permeater apparatus using the equipment as for determining the loose and dense bedding. Test specimen preperations were performed on natural moistured material for increasing density.

- BL 2: 5 layers with 5 impacts per layer. 1/2 fall of height
- SG 2: 10 layers with 5 impacts per layer. 1/2 fall of height

Theory

In a saturated soil Darcy's Law can be applied for stationary laminar flow. Darcy's Law is shown in Eq. J-1.

$$Q = k_T \cdot A \cdot \frac{\Delta h}{L} \qquad \textit{Eq. J-1}$$

Where,

Q: The total discharge [m^3/s]

k_T: Hydraulic conductivity at temperatur T [m(s]

L: Lenght of test specimen

A: Cross sectional area of test specimen [m^2]

Δh: Pressure drop [m]

Sketch of equipment is illustrated in Figure J—2.

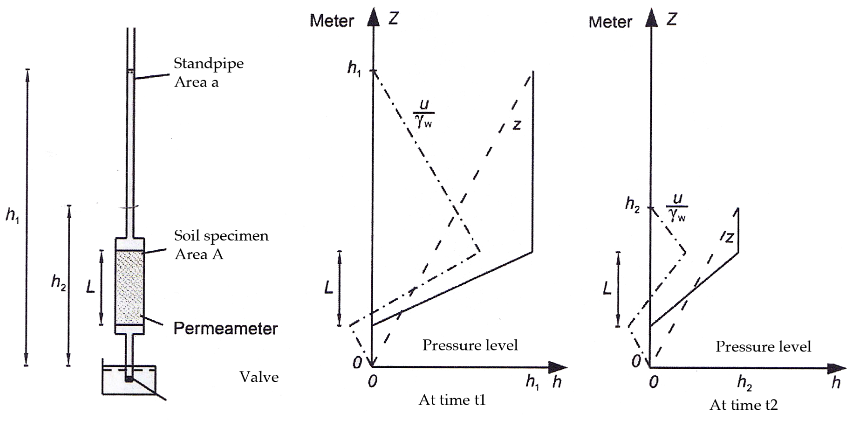

Figure J—2: Schematic overview of the falling head test.

Water level was kept constant by an overflow installation at the bottom of the apparatus. The test was started when the valve beneath the permeater is opened. Water level will drop and a parallel water flow is observed through the soil speciemen.

Usually Darcy's Law is written as:

$$v = k_T \cdot i \qquad \textit{Eq. J-2}$$

Where,

$v = \frac{Q}{A}$ fluid flow rate through the medium [m/s]

$i = \frac{\Delta h}{L}$, gradient [-]

At time t, the equation of contuniuty is given by

$$-\frac{dh}{dt} \cdot a = A \cdot v \qquad \textit{Eq. J-3}$$

where,

a: cross-sectional area of standpipe [m^2]

Solving Eq. J-3 with the boundary conditions of $h = h_1$ for $t = 0$ gives:

$$\ln(h) = -\frac{A}{a} \cdot \frac{k_T}{L} \cdot t + \ln(h_1) \quad \text{or} \quad k_T = \frac{a}{A} \cdot \frac{L}{t} \cdot \ln\left(\frac{h_1}{h}\right) \qquad \textit{Eq. J-4}$$

When performing the tests it is relevant to find the pressure level at 1/2 t_2, given that $t_1 = 0$

Hence,

$$h = \sqrt{h_1 \cdot h_2}, \text{ as } t = \tfrac{1}{2} t_2 \qquad \textit{Eq. J-5}$$

Results

BL 2

	No.
Permeater	A
Filter	100
Spring	Hard
Relative density (estimated)	2.65
Time for saturation	1 hour

Permability

Standpipe no.	5	5	5
Standpipe diameter, d [cm]	7.0	7.0	7.0
Standpipe area nominel, a [cm^2]	38.48	38.48	38.48
Pressure level height, h_1 [cm]	200	200	200
Pressure level height, h_2	80	80	80
Pressure level height $(h_1 * h_2)^{0.5}$ [cm]	126.49	126.49	126.49
Specimen lenght, L [cm]	20.1	20.1	20.1
Temperatur upper, T_u [°C]	24.8	25.0	24.0
Temperature lower, T_l [°C]	24.9	25.9	23.9
Flowtime, t1 [s]	505	541	574

Flowtime, t2 [s]	509	548	581
Hydraulic Conductivity $\kappa_T = \frac{a}{A} \cdot \frac{L}{t_1 + t_2} \cdot \ln\left(\frac{h_1}{h_2}\right) \cdot 10^{-2}$	**1,81632 * 10^{-4}**	**1,69123 * 10^{-4}**	**1,59458 * 10^{-4}**
Temperature	26	25.7	25.3
Kinematic viscosity	0.9228	0.91671	0.90859
Permability $K = \kappa_T \cdot \frac{\upsilon_T}{g}$	**1,70682 * 10^{-5}**	**1,48857 * 10^{-5}**	**1,47538 * 10^{-5}**

Water content and pore space

Permeater diameter nominel, D [cm]	7.0
Permeater area nominel, A [cm^2]	38.48
Specimen volume, V [cm^3]	773.45
sk [no.]	1a
sk [g]	840.3
sk + Ws [g]	2362.4
Ws	1522.1
sk + W [g]	2071.3
W [g]	1231
Water content [g]	291.1
Water content [%]	23.6
Porenumber $e = (1+w) \cdot \frac{d_s \cdot \rho_w \cdot V}{m_{soil}} - 1$	**0.66**

Saturation

$S_W = \frac{w \cdot d_s}{e}$ **, [-]**	**0.95**

SG 2

	No.
Permeater	A
Filter	100
Spring	Hard

Relative density (estimated)	2.65
Time for saturation	2.5 hours

Permability

Standpipe no.	2	2	2	2	2	2
Standpipe diameter, d [cm]	1.0	1.0	1.0	1.0	1.0	1.0
Standpipe area nominel, a [cm^2]	0.79	0.79	0.79	0.79	0.79	0.79
Pressure level height, h_1 [cm]	200	200	200	200	200	200
Pressure level height, h_2	80	80	80	80	80	80
Pressure level height $(h_1 * h_2)^{0.5}$ [cm]	126.49	126.49	126.49	126.49	126.49	126.49
Specimen lenght, L [cm]	20.8	20.75	20.75	20.75	20.75	20.75
Temperatur upper, T_u [°C]	23.7	23.6	23.7	23.7	23.6	23.7
Temperature lower, T_l [°C]	22.9	22.9	23.0	23.0	23.0	22.9
Flowtime, t1 [s]	358	349	279	315	316	271
Flowtime, t2 [s]	364	354	298	325	332	272
Hydraulic Conductivity $\kappa_T = \frac{a}{A} \cdot \frac{L}{t_1 + t_2} \cdot \ln\left(\frac{h_1}{h_2}\right) \cdot 10^{-2}$	**$5.41*10^{-6}$**	**$5.55*10^{-6}$**	**$6.77*10^{-6}$**	**$6.10*10^{-6}$**	**$6.02*10^{-6}$**	**$7.19*10^{-6}$**
Temperature	25.3	25.3	25.4	25.7	25.7	25.7
Kinematic viscosity	0.90859	0.90859	0.91062	0.91671	0.91671	0.91671
Permability $K = \kappa_T \cdot \frac{\upsilon_T}{g}$	**$5.00*10^{-7}$**	**$5.14*10^{-7}$**	**$6.27*10^{-7}$**	**$5.69*10^{-7}$**	**$5.62*10^{-7}$**	**$6.71*10^{-7}$**

Water content and pore space

Permeater diameter nominel, D [cm]	7.0
Permeater area nominel, A [cm^2]	38.48
Specimen volume, V [cm^3]	269.36
sk [no.]	1x
sk [g]	1495.2
sk + Ws [g]	3275.2
Ws	1780
sk + W [g]	3044.3
W [g]	1549.1
Water content [g]	230.9
Water content [%]	13
Porenumber	**0.35**

$e = (1+w) \cdot \frac{d_s \cdot \rho_w \cdot V}{m_{soil}} - 1$	

Saturation

$S_W = \frac{w \cdot d_s}{e}$ **, [-]**	**0.98**

Conversion for other temperatures

Eq. J-6 can be used to correct the hydraulic conductivity for other temperatures

$$\kappa_{20^\circ C} = \kappa_T \cdot \frac{\upsilon_T}{\upsilon_{20^\circ C}} \qquad \textit{Eq. J-6}$$

Where,

υ_T : kinematic viscosity at T [m^2/s]

$\upsilon_{20^\circ C}$: kinematic viscosity at 20°C [m^2/s]

If temperature conditions differs significantly, hydraulic conductivity should thus be corrected.

Discussion

The compaction of the test specimens were performed with the equipment used as determining loose and dense bedding of soil. It is very questinable whether this proces equals in situ density. Since the larger particles was not discarded from the test material problems concerning a relatively large pore space should be considered. This is most significant when testing the steady gravel SG 2, though. Tiny air bubbles inside test specimen were observed when performing the tests (Figure J—3). 6 test series were performed on the steady gravel to increase the level of reliability.

Figure J—3: Tiny airbubbles was observed when performing the falling head test with SG2.

Turbulent flow was avoided by requiring a flow time of $t_1$and t_2 of at least 2 min each.

A consistently larger t_2 than t_1 was observed throughout the tests. This may have been as a result from difficulties when reading water level in the standpipe due to broken photocells. This should not be considered as problematic in terms of obtaining a reliable result.

The relative density was estimated to 2.65, which could have influenced the results. Errors, if any, due to this fixed value, should be seen as a systemic error.

The pore numbers were desired to match the in-situ conditions. Laboratory testings were made in order to find loose and dense bedding of the materials. Results were found to be:

Table J-1: Loose and dense bedding.

	Loose e_{max} [-]	Dense e_{min} [-]
BL 2	0.78	0.45
SG 2	0.61	0.29

Pore numbers for the materials when performing hydraulic conductivity and permabilty testings were determined to be

- BL 2: 0.66
- SG 2 0.35,

which is quite large for the BL 2 material. Material was thus tested at a relatively loose bedding due to testing equipment that could not withstand any further compaction impacts. The values obtained in this test is considered as representative to reflect the in-situ conditions, though.

The bedding for the SG 2 material was tested at a relatively dense bedding, which therefore reflects in-situ conditions.

Conclusion

Falling Head tests were performed on sand subbase layer and steady gravel base layer. The hydraulic conductivity and permability for the materials were found to be in average:

Hydraulic conductivity:

- Subbase sand (BL2): $1.78*10^{-4}$
- Base steady gravel (SG2): $6.17*10^{-6}$

Permability

- Subbase sand (BL2): $1.55*10^{-5}$
- Base staedy gravel (SG2): $5.74*10^{-7}$

The permability and hydraulic conductivity is thus approximately 27 ~29 times higher, respectively, for the subbase sand than for the base material.

Appendix K Socio-economic Costs

This appendix presents a calculation of the socio-economic costs related to a reduced bearing capacity when the unbound layers of a road construction are affected by a water table. The calculations are based on the approach of increasing the thickness of the stiffer asphalt layer reducing the stresses on the surface of the base layer to an acceptable level.

Design was made on the basis of maximum allowable stresses.

Calculations are based upon three different traffic volumes:

a) $\mathbf{N_{Æ,10} = 5 * 10^4}$

b) $\mathbf{N_{Æ,10} = 5 * 10^5}$

c) $\mathbf{N_{Æ,10} = 5 * 10^6}$

At each traffic volume 5 scenarios based on reduced bearing capacity due to a water table inside the constructions are calculated:

1) **Water table covers 0% of unbound layers (no reduction in SG2 bearing capacity)**
2) **Water table covers 25% of unbound layers (≈10% reduction in SG2 bearing capacity)**
3) **Water table covers 50% of unbound layers (≈20% reduction in SG2 bearing capacity)**
4) **Water table covers 75% of unbound layers (≈30% reduction in SG2 bearing capacity)**
5) **Water table covers 100% of unbound layers, fully saturated. (≈40% reduction in SG2 bearing** capacity)

Maximum allowable stresses

SG2 layer E-values are estimated to be 300MPa. Reduces linearly to 60% (180MPa) when layer is complete saturated.

Maximum allowable stresses are calculated according to Eq. K-1 (Vejregelrådet 2007) and listed in Table K-1.

$$\sigma_z = 0.086 \cdot \left(\frac{E}{160}\right)^{1.06} \cdot \left(\frac{N_{Æ10}}{10^6}\right)^{-0.25} \qquad \textit{Eq. K-1}$$

where,

σ_z is the maximum allowable stresses

E is the E-value for the specific layer (reduces for different water tables)

$N_{Æ,10}$ is the traffic volume for the design period. (situation a), b), and c))

Table K-1: Maximum allowable stresses for different traffic volumes and levels of water table.

	1)	2)	3)	4)	5)
a)	0,354	0,317	0,280	0,243	0,206
b)	0,199	0,178	0,157	0,136	0,116
c)	0,112	0,100	0,088	0,077	0,065

Equivalent thickness

Asphalt layer equivalent thickness in regard of a reduced SG2 bearing capacity calculated on the basis of Eq. K-2 (NCC 2001) can be seen in Table K-2.

$$\sigma_{zz,h} = \sigma_{zz,0} \cdot \left(1 - \frac{1}{\sqrt{\left(1+\left(\frac{a}{h_e}\right)^2\right)^3}}\right) \qquad \textit{Eq. K-2}$$

where,

$\sigma_{zz,h}$ is the maximum allowable stresses calculated with Eq. K-1.

$\sigma_{zz,0}$ is the contact pressure at the surface (0.70 MPa)

a is contact pressure radius (165mm)

h_e is the equivalent height.

Table K-2: Equivalent thickness for different traffic volumes and levels of water table.

	1)	2)	3)	4)	5)
a)	213	235	259	287	322
b)	330	354	384	419	460
c)	469	501	539	580	636

Asphalt layer thickness

The finite asphalt layer thickness are calculated from Eq. K-3 (NCC 2001)and listed in Table K-3.

$$h_{e1,2} = f \cdot h_1 \cdot \sqrt[3]{\left(\frac{E_{upper}}{E_{lower}}\right)} \qquad \textit{Eq. K-3}$$

where,

$h_{e\,1,2}$ is the equivalent height calculated from Eq. K-2

f is a factor of correction (= 0.9)

h_1 is the height of the asphalt layer

E_{upper} is the E-value of upper layer (asphalt)

E_{lower} is the E-value of lower layer (SG).

Table K-3: Calculated asphalt layer thickness.

	1)	2)	3)	4)	5)
a)	117	124	132	140	149
b)	181	187	195	204	213
c)	257	265	274	282	293

The nescessary increased asphalt thicknesses are listed in table Table K-4.

Table K-4: Nescessary extra asfalt thickness for the three traffic volume scenarios.

$N_{Æ,10}$		Increased asphalt thickness [mm]
50,000	a)	32
500,000	b)	32
5,000,000	c)	36

The extra asphalt thickness needed to compensate for reduced bearing capacity of SG layer can thus be calculated to be ≈ 3-4 cm.

Socio-economic costs estimate

According to (Kristiansen 2012) 20,000 road sections or what equals 5,000 km of public roads will suffer from a high water table in the future. Different standard asphalt mixtures and unit prices are listed in Table K-5.

Table K-5: Different asphalt mixtures and unit prices including delivery and construction. (V&S PRISDATA 2013).

V & S Prisdata

Beskrivelse	*	Enhed	Mængde	Enhedspris
33 mm GAB 0, 80 kg/m2	TE	m2	5.000	95,96
37 mm GAB 0, 90 kg/m2	TE	m2	5.000	106,43
48 mm GAB 0, 115 kg/m2	TE	m2	5.000	131,88
48 mm GAB I, 115 kg/m2, 50 - 500 m2	TE	m2	100	239,87
48 mm GAB I, 115 kg/m2, 1.000 - 20.000m2	TE	m2	5.000	118,36
56 mm GAB I, 135 kg/m2, 1.000 - 20.000m2	TE	m2	5.000	134,87
75 mm GAB II, 180 kg/m2	TE	m2	5.000	175,65
33 mm AB, 80 + 10 kg/m2	TE	m2	20.000	130,24
30 mm AB, 70 + 10 kg/m2	TE	m2	20.000	117,4
38 mm AB, 90 + 10 kg/m2	TE	m2	20.000	143,08
33 mm SMA, 80 + 10 kg/m2	TE	m2	20.000	145
30 mm SMA, 70 + 10 kg/m2	TE	m2	20.000	129,25
38 mm SMA, 90 + 10 kg/m2	TE	m2	20.000	158,7

Based on the standard cross-section of 8 meter and data obtained at Table K-5 a cost between 5 - 10,000,000,000 DKK can be expected depending on the asphalt mixture used and the specific road sites.

List of References - Appendices

Berg, F. 2004, "Nye Regler for Stabilt Grus og Bundsikring", *Dansk Vejtidsskrift,* vol. 4, pp. 22-25.

Bolet, L. 2010, *Vejbefæstelser. Design og Dimensionering,* Udgave til review edn.

Briaud, J.L. 2001, "Introduction to Soil Moduli", *Geotechnical News. BiTech Publishers Ltd, Richmond, B.C., Canada,* vol. June 2001.

Busch, C. 2009, "Dansk Analytisk Belægningsdimensionering - Kriterier og Historik. Vejregel Arbejdsgruppe P. 21", , ed. U.D. Jakobsen, , 5. november.

Danish Geotechnical Society 2001, "Klassifikationsforsøg. Relativ Lejringstæthed" in *Laboratoriehåndbogen. DGF-Bulletin 15*, eds. W. Lund P., J. Horn & H. Jacobsen J., Dansk Geoteknisk Forening, PRINFO AALBORG - HANDELSTRYKKERIET, pp. 34-36.

Dawson, A. 2008, *Water in road structures: movement, drainage & effects,* Springer.

Jørgensen, A., K. 2008, 6. maj 2008-last update, *Fremtidens Klima* [Homepage of DMI], [Online]. Available: http://www.dmi.dk/dmi/fremtidens_klima-2.pdf [2013, 03/08].

Kolisoja, P. 1997, *Resilient Deformation Characteristics of Granular Materials,* Tampere University of Technology.

Kristiansen, J., Riishede 2012, "Klimaændringerne og Konsekvenserne for det Kommunale Vejnet", *Trafik og Veje,* .

Lekarp, F., Isacsson, U. & Dawson, A. 2000, "State of the Art. II: Permanent Strain Response of Unbound Aggregates", *Journal of Transportation Engineering,* vol. 126, no. 1, pp. 76-83.

Lekarp, F. & Isaccson, U. 2000, "State of the Art. I: Resilient Response of Unbound Aggregates", *Journal of Transportation Engineering,* vol. 126, no. 1, pp. 66.

Nakicenovic, N., Alcamo, J., Davis, G., de Vries, B., Fenhann, J., Gaffin, S., Gregory, K., Grubler, A., Jung, T.Y. & Kram, T. 2000, *Special report on emissions scenarios: a special report of Working Group III of the Intergovernmental Panel on Climate Change,* .

NCC 2001, *Vejbygning. materialer, befæstelser, belægninger,* 3. Edition edn, NCC Danmark A/S, Boisen og Nielsen A/S.

Ovesen, N.K., Fuglsang, L. & Bagge, G. 2009, *Lærebog i Geoteknik,* 1. edition edn, Polyteknisk Forlag, 2800 Lyngby.

Thagesen, B. 2009, *Veje og Stier,* 4.th edn, Polyteknisk Forlag, 2800 Lyngby.

Ullidtz, P. 1998, *Modelling Flexible Pavement Response and Performance,* 1. edition edn, Polyteknisk Forlag, 2800 Lyngby.

V&S PRISDATA 2013, "V&S - Anlæg database - 2013" in , ed. Byggecentrum,.

Vejdirektoratet 2007, "Måling af Overflademodul med Minifaldlod. pr VI 90 - 4:2007", vol. Januar.

Vejregel Arbejdsgruppe p.21 2011, "MMOPP DIMENSIONERINGSPROGRAM FOR VEJBEFÆSTELSER", *ANLÆGSPLANLÆGNING,* .

Vejregelrådet 2007, *Vejregel. Dimensionering af Befæstelser og Forstærkningsbelægninger.*, København: Vejdirektoratet.